Prifysgol Abertawe
Swansea University

Department of Chemical Engineering

Swansea University

Investigating Water Treatment Procedures with a Focus on Novel Porous Silicon

By

Chialuka Ikokwu

Submitted in fulfilment of the requirements for the degree of

MASTER OF PHILOSOPHY (MPhil)

February 2025

Abstract

Membrane processes for seawater desalination offer solutions to global water challenges, but factors such as high energy consumption and membrane fouling limit their capacity to provide fresh water worldwide.

This work investigated the use of nanofiltration to desalinate seawater, with specific reference to the removal of monovalent and divalent ions. Nanofiltration was found capable of removing 85% of calcium and 93% of magnesium from seawater. However, one limitation of the process is its inability to effectively remove monovalent ions such as Na.

Electrodialysis as a means of seawater desalination was also investigated in this study. It achieved over 90% ion exchange in seawater within 75 minutes of operation. However, it has high energy requirements and is unable to remove organics from seawater.

Surface modification of the NF membrane with oxygen plasma was found to improve hydrophilicity and flux while trading off performance in rejection. Ammonia plasma treatment for 50 seconds showed hydrophobic recovery after some time.

Metal-assisted etching was used to create pores in a silicon wafer. Filtration results showed that water was able to pass through these pores, presenting a new approach to water desalination.

DECLARATION

This work has not previously been accepted in substance for any degree and is not being concurrently submitted in candidature for any degree.

Signed 

Date 21/09/2025

STATEMENT 1

This thesis is the result of my own investigations, except where otherwise stated.

Other sources are acknowledged by footnotes giving explicit references. A bibliography is appended.

Signed 

Date 21/09/2025

STATEMENT 2

I hereby give consent for my thesis, if accepted, to be available for photocopying and for inter-library loan, and for the title and summary to be made available to outside organisations.

Signed [redacted]

Date 21/09/2025

Table of Contents

Acknowledgements

My special and heartfelt thanks go to Almighty God, on whose wings I have flown over these years.

To my dear mother, Mrs. Theresa Ikokwu, and my siblings Ral, Kachi, Zitenwa, Ify, and Kamdi, for all their prayers and support during this journey.

To my wife, Onyii, whom God placed by my side to undertake this journey with me.

To Professor Owen Guy, my supervisor, for his firm support, guidance, assistance, and encouragement, even in trying times throughout this work.

To Dr. Darren Oatley-Radcliffe, my second supervisor, who provided significant technical support during this work.

To my pastors—Rev. Nches Iredu, Dr. Solomon Ilouno, Dcn., and Dr. (Mrs.) Chika James, Pastor Tunji Lawal, and Liz Ejiama—for all your spiritual support, prayers, and warm wishes, even in trying times.

Finally, to all my friends and colleagues within and outside the department who provided any form of support, thank you very much.

List of Figures

Abbreviations

NF	Nanofiltration
RO	Reverse Osmosis
MSF	Multi-Stage Flash
MED	Multiple Effect Distillation
VCD	Vapour Compression Distillation
ED	Electrodialysis
FTIR	Fourier Transform Infrared Spectroscopy
AAS	Atomic Absorption Spectroscopy
TFC	Thin Film Composite
PA	Polyamide
SEM	Scanning Electron Microscopy
DI	Deionised Water

CHAPTER ONE

1 Introduction

About 70% of the Earth's surface is covered by water [1]. This amounts to 1 x 10^9 km^3 of water [2]. An estimated 97% of the water on the Earth's surface is seawater, while 3% is freshwater. 68.7% of freshwater is locked in glaciers and icecaps, 30.1% is groundwater, and less than 1.2% is available as surface water. Of the available surface water, 69.0% is found as ground ice and permafrost. Lakes make up 20.9%, 3.8% is available in the soil as soil moisture, 2.6% as swamps and marshes, 0.49% is found as rivers, 0.26% in living things, while 3.0% is atmospheric moisture [3]. There is, however, an immense quantity of fresh water available under the surface of the earth, but that is economically difficult to access efficiently.

According to the United Nations World Water Development Report (2024) [4], water scarcity continues to worsen globally. As of 2025, nearly two-thirds of the world's population live in regions experiencing water stress, a significant increase from one-third in earlier decades. This intensifying demand for water underscores the urgent need for sustainable water treatment technologies, such as desalination.

For this reason, many countries of the world suffer from a natural freshwater shortage. Rising population growth rate has led to a significant increase in demand for fresh water. This trend is expected to increase with increasing human activities such as enhanced standards of living, the expansion of industrial and agricultural activities, as well as rapid urbanisation. Sources of fresh water from groundwater and rivers are currently being increasingly depleted at a high rate in many countries of the world [4].

Water is a global economic and social commodity [5]. It is the primary basis for sustaining all life and life's activities.

Reports indicate that the worldwide population has tripled over the last century, whereas the reported water use, or the withdrawals of water, significantly increased by more than six times. This trend suggests that the increase in water consumption is mostly driven by improved global living standards and industrialisation. Many regions of the world have inadequate freshwater

sources to meet the ever-growing demand for water. There is also the challenge of sufficient surface and groundwater sources to even meet existing water demand [6].

To mitigate the challenge of water shortage, researchers have explored salt waters from the oceans as well as other brackish water sources. However, seawater is unsuitable for human consumption, agricultural, and industrial purposes, because of its high salinity. Procedures and processes that convert saline waters into freshwater are being developed.

Desalination is a technology that many countries depend on for the purpose of generating fresh water to meet their freshwater requirements. In some Middle East countries like the United Arab Emirates, Saudi Arabia, and Kuwait, desalination has grown to become a reliable and important source of fresh water [7]. Research reports further show that an estimated over 75 million people globally source fresh water from desalination of seawater or brackish water [8]. This shows that desalination is a growing procedure in water treatment.

The International Desalination Association, one of the world's leading desalination firms, contracted and installed a total of 17,348 units in 10,350 desalination plants in 2002, according to the association's 2004 report [9]. Those desalination plants produce 37.75 million cubic metres per day of fresh water from salt water. Brackish and seawater accounted for 40% and 60% of the desalinated global sources of water in 2001 [10]. Saudi Arabia, the USA, UAE, Spain, and Kuwait are the leading five countries in desalination.

In 2007, desalination accounted for a total of 47.6 million cubic metres of fresh water per day. This figure increased to 53 million cubic metres per day in 2008. In 2011, the global desalination capacity had reached 65.2 million cubic metres. The year 2012 witnessed another increase to 74.8 million cubic metres of water[11]. In 2002, desalination procedures such as Multi Stage Flash accounted for 36.5% of seawater and brackish water desalination capacity, while reverse osmosis accounted for 47.2% [12].

This introductory chapter provides an overview of water desalination techniques around the world, as well as an update on recent approaches and advancements.

1.1. Seawater Desalination Technology

Sea water desalination is a process that removes dissolved salts from seawater. The process separates seawater into two streams: a concentrated stream and a freshwater stream containing a low concentration of dissolved salts. The concentrated brine contains a high concentration of dissolved salts.

Over the years, diverse desalination technologies have been developed and explored. These procedures can be classified into two types: thermal and membrane processes. Thermal processes involve a change in water phase as a means of desalination. This includes evaporation of seawater under suitable temperatures and pressures and condensation as fresh water. Processes such as solar distillation (use of solar stills), Multi-Stage Flash (MSF) distillation, Multi-Effect Distillation/Evaporation (MED), Thermal Vapor Compression (TVC), and Mechanical Vapor Compression (MVC) are examples of thermal desalination techniques. Membrane processes, on the other hand, involve the use of a physical barrier, such as a porous membrane, to separate the salt from seawater to produce fresh water [13]. Membrane processes include Microfiltration (MF), Ultrafiltration (UF), Nanofiltration (NF), Reverse Osmosis (RO), and electrodialysis (ED).

Some hybrid processes involve a combination of thermal and membrane desalination, either in single units or in a series of steps, to achieve desalination. Such processes may include Membrane Distillation (MD), microfiltration with RO, or RO combined with membrane distillation or multi-effect distillation.

1.1.1. Multiple Effect Distillation

The Multiple Effect Distillation (MED) process involves the use of various evaporators known as effects. The technique is based on the principle of reducing the standard pressure in the various pressures. In this process, the seawater feed undergoes multiple evaporation without supplying additional heat after the first effect. The feed seawater is allowed to enter the first evaporator and is heated to evaporation, usually by steam from a normal dual-purpose power plant. This involves spraying the seawater onto the surface of the effect tubes to enhance evaporation. The evaporated water (as steam) steam flows into the tubes of the next effect, heating, and the cycle is repeated. MED principle allows each stage to reuse the energy from the previous stage, with successively lower temperatures and pressures as the process goes on.

At the last effect, the produced steam finally condenses on a conventional shell and tubes heat exchanger, known as distillate condenser is cooled by seawater. Some of the warm seawater at the outlet of the condenser is then used as make-up of the unit, as the boiler feed, while the remainder is disposed of into the sea. The concentrated brine and distillate are collected from the cells. until the last one is finally collected. They are eventually extracted by centrifugal pumps. The steam economy in the MED plant steam economy is dependent on the number of effects available in the process.

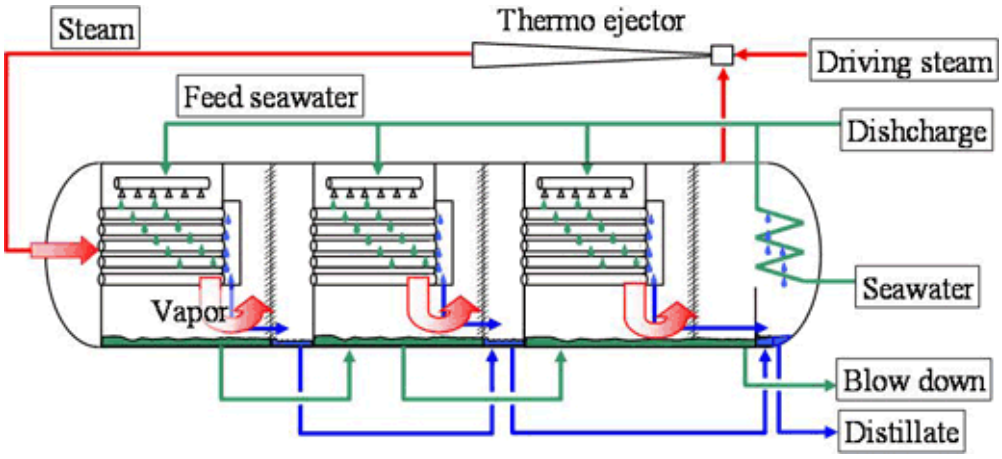

Figure 1. Schematic diagram of the MED process for seawater desalination [14].

In the MED process, not all the seawater that is fed into the first effect is evaporated. The un-evaporated portion is subsequently fed into the second effect with a tube bundle. The tube bundle is again heated by the vapours emanating from the first effect. Condensation of the vapour to fresh water takes place, and heat is released. The released heat is recycled into the system to evaporate the feed seawater in the next effect. The entire process of evaporation and condensation is then repeated from one effect to another at a subsequent lower pressure and temperature. This process continues for several evaporators in the system. There can be between 4 to 21 effects in a system [14].

The Top Brine Temperature, which is the maximum permissible operating temperature for the first effect, is usually 70^0C. This reduces the risk of scaling in plants [15]. However, more area is needed for effective heat transfer within the tubes.

Multi-effect distillation plants can have submerged, vertical, or horizontal tubes. Some of the advantages of MED include reduced scaling potentials and low thermal energy requirements. Additionally, the MED process may not require very large plant sizes and consequently, reduced operating costs.

1.1.2. Multi-Stage Flash Distillation (MSF)

The MSF process distils water by flashing part of it into steam in multiple stages. This technique relies on the principle of flash evaporation, which involves evaporating seawater by reducing pressure rather than increasing temperature. An MSF plant

contains a series of chambers known as stages. Each stage includes a heat exchanger and a condensate collector. There is a hot end and a cold end, while intermediate stages have intermediate temperatures. The stages operate at distinct pressures that correspond to the boiling points of water at those stage temperatures. The hot end contains a component called the brine heater.

Normally, feedwater at the cold inlet is pumped through the heat exchangers in the stages, where it is heated by low-pressure steam supplied from a gas turbine with a heat recovery steam apparatus [16,17] or by extraction steam from a steam turbine power plant [18]. The feed seawater in the brine heater flows into the tube compartment of the heat exchanger in the upper portion of the evaporator. These heat exchangers are typically arranged across the width of the evaporator. The evaporator contains multiple stages, with some modern large plants having between 19 and 28 stages [19–21].

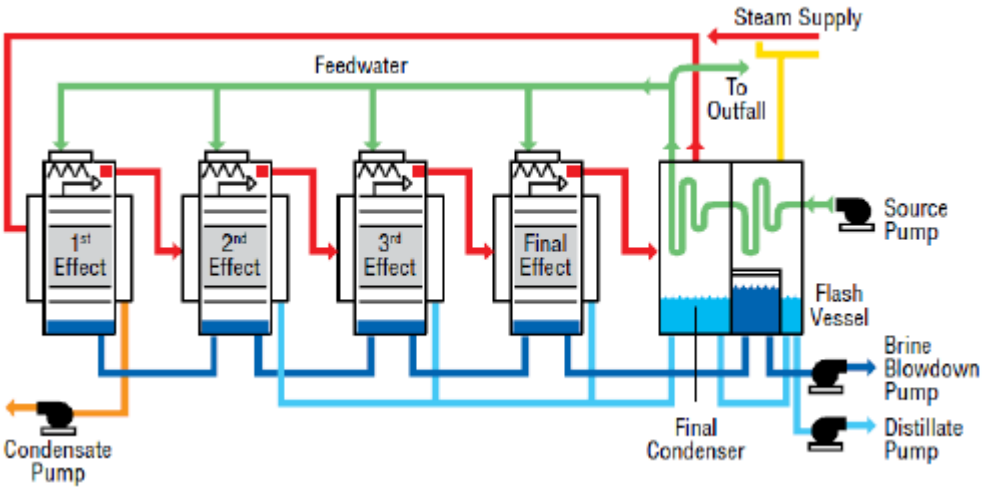

Figure 2: Schematic diagram of MSF distillation for desalination of seawater [23].

Like the MED, top brine temperature (TBT) is essential for the efficiency of the system. TBT of 90–120°C has been widely reported for operating MSF plants. Scale control methods also depend on the operating TBT [22–34]. Higher operating temperature increases the efficiency of the system, but it also increases the risk of scale formation with attendant rapid corrosion of metal surfaces in contact with seawater.

As the feed seawater enters the flash chamber, it gains heat and boils quickly and vigorously due to flashing. This process continues until the feed temperature reaches the boiling point in the flash chamber [35,36].

The unflashed, colder seawater is used to cool and condense the flashed steam in the condenser tubes, producing the distillate. The heat released from condensation is

recycled into the tubes to heat the incoming brine. The distillate is collected stage by stage, while the concentrated brine is pumped into a storage tank.

Reports indicate that the TDS of desalinated seawater from the MSF process is typically 2-10mg/l.

Moreover, the number of stages in a plant influences the freshwater production rate as well as the plant economics. Increasing the number of stages provides more heat transfer area, which improves the plant efficiency. However, this increases the capital cost of running the MSF plant.

MSF technology dates back to the 1950s. Since then, significant progress has been made in its development and improvement. A five-stage MSF plant was constructed in 1953 by the US Navy, with a daily water production capacity of 189 m^3. Another four-unit plant, with a daily capacity of 2,271 m^3 per unit, was installed in Kuwait [9]. Saudi Arabia has the largest MSF plant, with a daily water output of 815,120 m^3, operated by the Saline Water Conversion Corporation's Al-Jubail facility.

1.1.3. Vapour Compression Distillation (VCD)

In the VCD procedure, heat generation occurs through the compression of vapour, rather than direct heat from a boiler. Rapid compression of vapour causes an increase in temperature. This principle operates by reducing the boiling point of the water by reducing the pressure. A mechanical compressor (mechanically driven) and a steam jet can be used to compress the feed seawater for vapour compression, generating sufficient heat for its evaporation. Some of the compressed and heated vapour is then recycled into a low-pressure chamber, through a series of tubes, where evaporation of the seawater occurs.

Technical modifications led to diverse configurations in VCD units to enable the required heat exchange for the seawater evaporation. The compressor in the evaporator creates a vacuum such that the vapour taken from the evaporator is compressed and then condensed inside a tube bundle. Seawater is sprayed on the outside of the heated tube bundle where it boils and partially evaporates, producing more vapour.

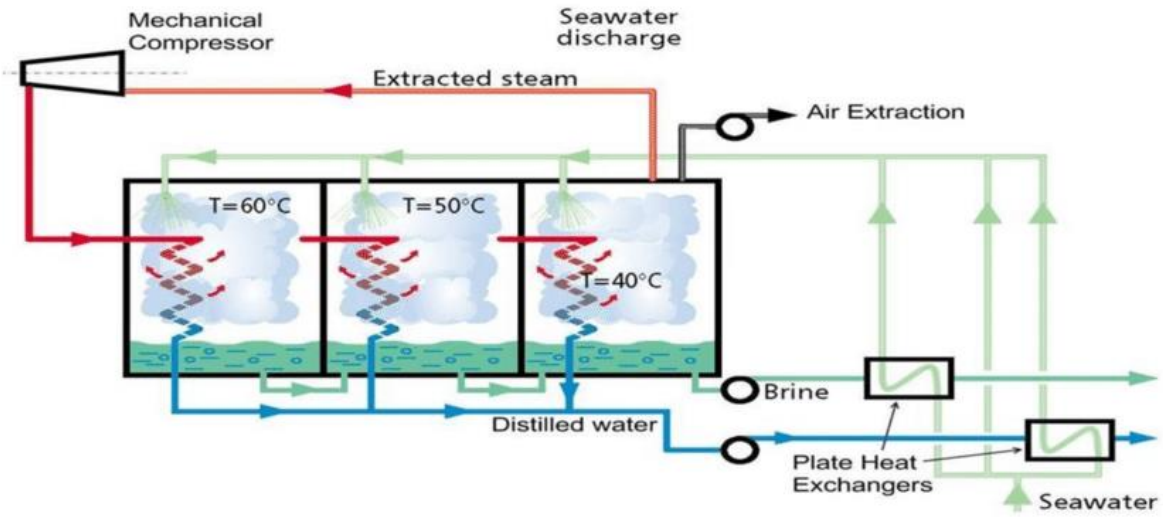

Figure 3: Schematic Diagram of Vapour Compression Distillation for seawater desalination [37]

The steam-jet type of VCD unit, called a thermocompressor, extracts water vapour is extracted from the evaporator by a venturi orifice at the steam jet, creating a lower ambient pressure. The extracted water vapor is compressed by the steam jet. This mixture is condensed on the tube walls to provide the thermal energy, heat of condensation, to evaporate the seawater being applied on the other side of the tube walls in the evaporator.

Low-temperature VCD distillation is quite simple, efficient, and reliable. It only requires power to run. For increased efficiency, a high-capacity compressor that allows operation at low temperatures below 70°C is used. This reduces the risk of scale corrosion and the formation of scale. The VCD process is generally used for small-scale desalination units. The maximum daily desalination capacity could be 3000 m^3 of water. The larger unit's power consumption is about 8 kWh/m^3 of product water. This technology is often employed for resorts, industries, and drilling sites where fresh water is not readily available [37].

1.1.4. Freeze Desalination

Freeze desalination is a process that separates pure water from a saline solution by freezing. Salt and water behave differently upon freezing because salt cannot fit into the crystalline structure of ice. This method involves freezing seawater under controlled

conditions to form ice crystals. The freezing process isolates the dissolved salts from the ice crystals.

The freeze desalination process consists of heat removal from the seawater feed, resulting in cooling, partial formation of ice crystals, separation of ice from seawater, melting of the ice, refrigeration, and heat rejection. When the water is frozen, the resulting ice crystals are usually pumped as a slurry to the washer, where they are washed and rinsed to remove salts adhering to the ice. In the washer, a small volume of product water is made to flow in the opposite direction to the crystals, ensuring effective washing. This is followed by melting the ice to produce freshwater.

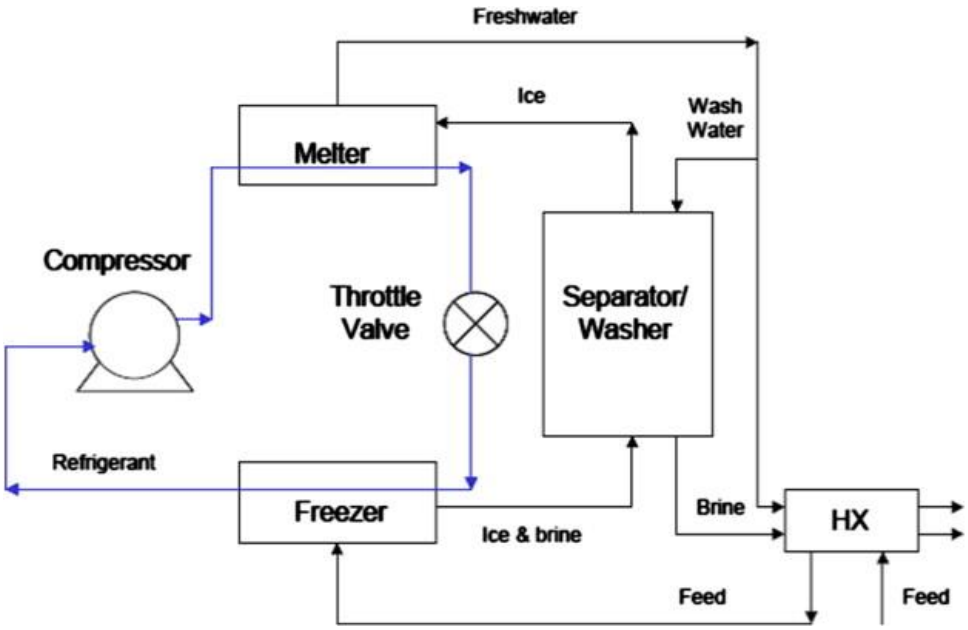

Figure 4: Schematic diagram showing Freeze Desalination process [38]

The heat removed during the freezing process is typically recycled to the melter for melting the ice. This is achieved by releasing the refrigerant into the melter, which transfers heat to the ice. The freezer is normally designed to produce a large quantity of isolated ice crystals rather than crystals that clump together. Lumping of ice crystals traps brine between them; therefore, the freezer is designed to minimise this effect. The size of the crystals formed is also important, as fine crystals are difficult to wash.

Freeze desalination processes have been developed to pilot-plant status over the years. These include the triple point, secondary refrigerant, indirect, eutectic, and hydrate

processes [38]. Advantages of freezing include lower theoretical energy requirements, minimal potential corrosion, and reduced scaling or precipitation. One disadvantage of freezing is the handling of ice and water mixtures, which is mechanically complicated to move and process. Only a small number of plants have been built over the years. However, the process has not been commercialised successfully to produce substantial quantities of freshwater for use. In 1985, an experimental solar-powered freeze desalination unit was constructed in Saudi Arabia [39].

1.1.5. Solar Evaporation

This process utilizes direct solar energy for desalinating seawater. It is based on the principle of evaporating seawater using solar heat. This is followed by condensing the water vapour on a cool surface. The condensate is then collected as product water.

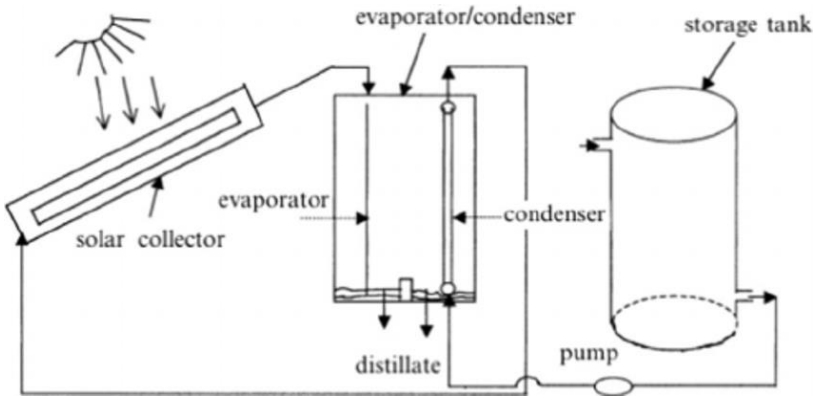

Figure 5 : Schematic diagram of solar evaporation desalination [40]

The greenhouse solar still is an example of this procedure. In this process, the saline water is heated in a basin on the floor. The generated water vapour condenses on the sloping glass roof that covers the basin and is collected off as fresh water [40]. To increase still efficiency further, modifications have been made. One drawback of this process is that it requires a large area for the collection of solar energy. For instance, 25 hectares of land are required for a daily capacity of l000 m^3 of product water. This leads to high capital cost. There is also the risk of vulnerability to weather-related damage to the facility. Additional energy is also required to pump the water to and from the facility. This leads to increased operational costs.

1.1.6. Membrane technology

A membrane is a thin film of porous material capable of allowing water molecules to pass through while retaining larger, unwanted molecules such as salts, bacteria, viruses, and metals.

Membrane technologies are used to separate dissolved solids from water. Membranes can be synthesised from a wide range of polymers, such as nylon, cellulose acetate, or non-polymeric materials such as composites, ceramics, and metals.

Membrane processes offer several advantages over traditional separation techniques. These include relatively low capital and operating costs, low energy consumption, high selectivity, operation at constant temperatures without phase change, modular construction, and continuous automatic operation.

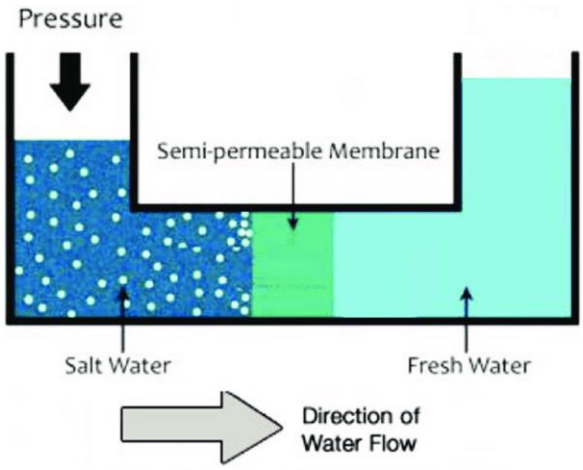

Figure 6: Schematic diagram of the membrane desalination process [41]

Membrane processes can be classified as either pressure-driven or electrically driven. Pressure-driven processes require the application of pressure across the membrane, whereas electrically driven processes rely on an electric potential difference as the driving force for separation. Electrodialysis and bipolar membrane separation are examples of electrically driven processes. Pressure-driven membrane processes include microfiltration (MF), ultrafiltration (UF), nanofiltration (NF), and reverse osmosis (RO). Table 1 summarises the types of membranes and their typical performance.

Membrane Type	**Pore Size**	**Materials Rejected**	**% Efficiency**
Microfiltration	0.1-3µm	Microorganisms, turbidity	90 - 99.9

Ultrafiltration	0.01-0.1µm	Microorganisms, turbidity, TOC	85 - 99
Nanofiltration	1-10nm	colour hardness, organic content	85 - 98
Reverse Osmosis	0.1nm	radionuclides, pesticides	95 – 99.5

Table 1: Types of membranes and their performances [41]

Microfiltration removes particles with a minimum size of 0.1-3µm. Its operating pressure is about 0.3 – 5 bar. Research shows that it has 99.9% efficiency in removing turbidity, bacteria/protozoa.

Ultrafiltration removes smaller particle-sized (0.01–0.1µm) materials from seawater, including turbidity, bacteria/protozoa, and Total Organic Carbon (TOC), at over 95% efficiency. UF is also used to remove some viruses from water. Operational pressure ranges from about 0.3 to 5 bar.

Nanofiltration removes even smaller particles than microfiltration (MF) and ultrafiltration (UF). It operates at pressures above 5 bar and can reach up to 40 bar. Besides turbidity and bacteria, NF is also used to eliminate sulfate, colour, hardness, and synthetic organic contaminants in water with over 97% efficiency. The smallest particles it removes range between 200 and 400 Daltons.

Reverse osmosis utilizes the pressure difference between saltwater and pure water to remove particles from seawater. It effectively removes Total Dissolved Solids (TDS), nitrates, radionuclides, and pesticides (i.e., much smaller particles in the size range of 50-200 Daltons). It can operate at pressures up to 50 bars. Figure 7 illustrates the main separation features of the membrane processes.

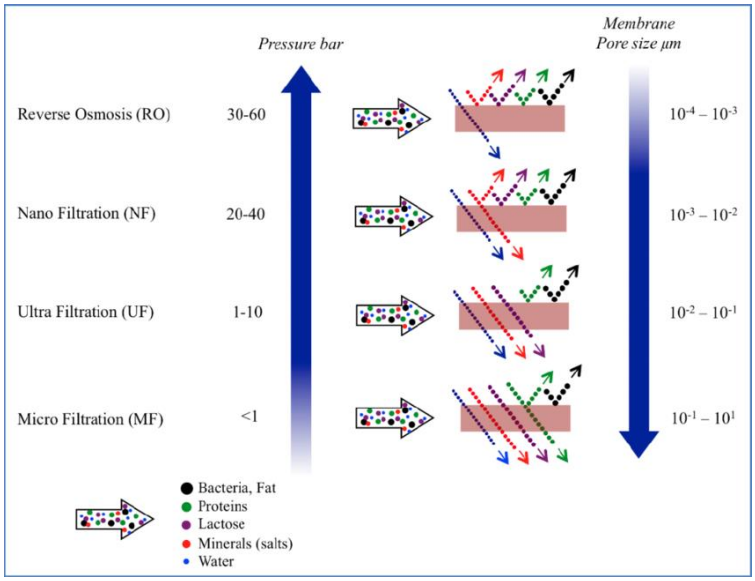

Figure 7: The separation features of different membrane desalination techniques [41].

1.1.6.1. Membrane Materials

Membranes are typically made from synthetic polymers. Advances in technology have led to new polymers and production methods used in membrane desalination [42, 43]. A membrane's performance mainly depends on the materials it is composed of. The composition also influences specific performance features such as salt rejection, fouling tendency, mechanical strength, and reactivity. Thin film composite (TFC) polyamide (PA) and cellulose acetate (CA) membranes are commonly used for reverse osmosis and forward osmosis [44]. Despite efforts to select the best membrane materials and fabrication techniques based on the process's goals and requirements, achieving optimal performance can still be challenging. This is because the intrinsic properties of the materials used can impair separation efficiency [45]. For example, polymeric membranes may react with oxidants used in drinking water treatment. Consequently, such membranes are not recommended for use with chlorinated feed water. Additionally, the conflicting effects of polymer chain stiffness and inter-chain spacing contribute to the selectivity-flux trade-off in membranes [46, 47,48].

Furthermore, membranes with greater strength tend to withstand larger transmembrane pressure levels. This allows for greater flexibility in operation and the use of higher pressures during operation. Surface charge also plays a vital role in membrane filtration, as membranes with a particular surface charge reject substances such as microbial contaminants or particulate matter with opposite charges due to the electrostatic attraction phenomenon.

Ultrafiltration and microfiltration membranes are manufactured from a wide range of materials such as cellulose acetate, polyvinylidene fluoride, polyacrylonitrile, polypropylene, polysulfone, polyethersulfone, or other polymers.

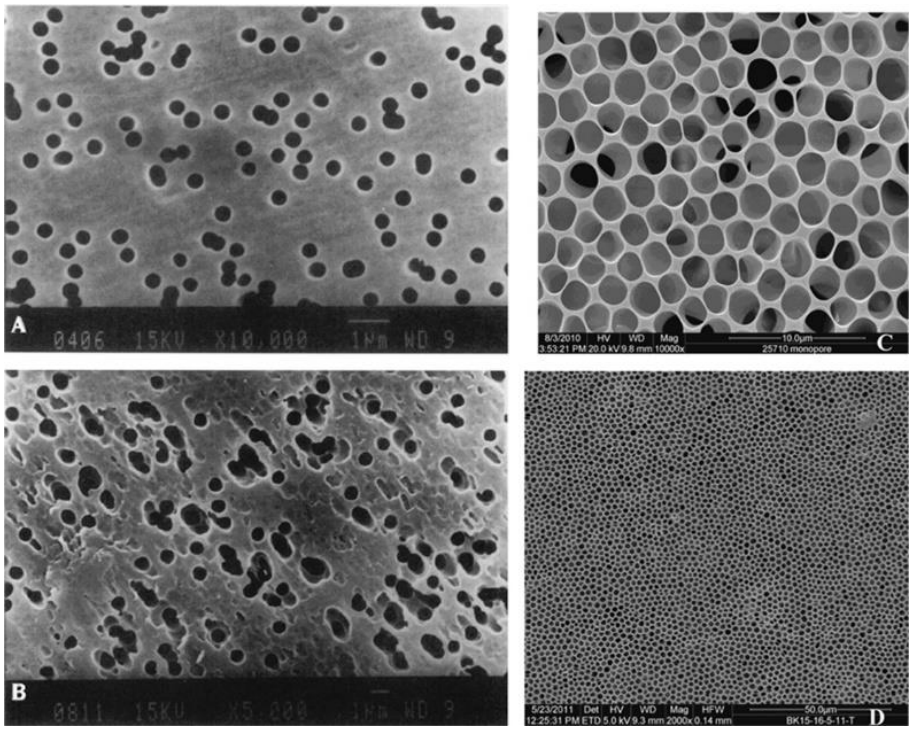

Figure 8 SEM images showing porous structure of polysulfone microporous membranes [45]

These materials exhibit distinct properties related to surface charge, degree of hydrophobicity, pH, and oxidant tolerance, as well as strength and flexibility. Other membrane materials, such as ceramic composites and thin-film nanocomposites, are also increasingly used, depending on operational conditions and feedwater characteristics. Cellulose membranes are susceptible to biodegradation and must be operated within a narrow pH range of 4 to 8. However, they do possess some resistance to continuous low-level oxidants. Chlorine doses of 0.5 mg/L or less may control biodegradation and biological fouling without damaging the membrane. Polyamide membranes, by contrast, can be used under a wide range of pH conditions and are not subject to biodegradation. Although these membranes have very limited tolerance for strong oxidants, they are compatible with weaker oxidants such as chloramines.

Generally, membranes dedicated to desalination are designed and formulated to achieve high throughput and selectivity while exhibiting high mechanical integrity and resistance towards fouling at minimum processing costs [42].

Different strategies have, over the years, been established to enhance membrane resistance to fouling, especially for pressure-driven processes. These measures help in achieving low operational energy, enhance the reliability of the process, as well as minimise the environmental impacts of the desalination process [49]. Recent research findings show that smoothing the membrane surface, increasing the hydrophobicity of the surface as well as introducing strong electrostatic repulsion between the membrane surface and charged contaminant particles improve membrane resistance to fouling [50,51]. Application of membranes with these properties showed resistance to adhesion of bacteria and protein molecules, which subsequently reduced the need for membrane cleaning and the use of biocides in water treatment.

1.1.6.2. Membrane Backwashing

Backwashing is a cleaning process designed to remove contaminants from membranes. During this process, the flow direction is reversed for about 30 seconds to 3 minutes. The direction and force of flow dislodges the foulants at the surface of the membrane and washes accumulated solids through the discharge line. This process is known to improve membrane productivity as a result of the volume of filtrate used during the backwash.

1.1.6.3. Chemical Cleaning

This is the major means of cleaning nanofiltration and reverse osmosis membranes, although it can also be applied to ultra- and microfiltration membranes. Chemical cleaning is used to remove any contaminant that is not removed by backwashing, particularly inorganic and organic scaling and fouling. It also removes foulants that have accumulated gradually over time. Different varieties of chemicals can be used for chemical cleaning, with each chemical used to remove specific forms of contamination. For instance, citric acid may be used to dissolve inorganic fouling where whereas strong bases can be used to remove organic contaminants. Surfactants and detergents can also be used to remove organics and particulate fouling, especially those that are difficult to dissolve. Strong chlorine solution can also be used to remove biofouling. Combinations of different chemicals may also be used to optimise the process, especially if fouling involves different types and degrees of contaminants.

1.1.7. Recent Developments in Membrane Technology

To improve desalination techniques using membranes, a number of developments have been made in the membrane industry. Most significant among them is the modification of membranes for better productivity. This is carried out through the incorporation of additives with desired functionalities or surface modification of the membrane. The current common goal of membrane modification is to provide enhanced membrane properties, particularly in terms of product water quality, permeability, and antifouling properties, through facile and straightforward methods that present the ease of synthesis, reproducibility, and, most importantly, high potential to be upscaled or mass-produced for practical application.

1.1.7.1. Nanocomposite Membranes

This involves the introduction of nano-materials into polymeric membranes. Nanomaterials, when incorporated into membranes, provide the latter with new advantageous properties that macroscale materials do not offer. For instance, nanomaterials are able to tackle contaminants that occur in low concentrations. Nanomaterials can be introduced as additives into the membrane matrix by incorporation during the formation of the material or by coating the nanoparticles on the membrane through a process known as chemical bonding or self-assembly [52]. Interactions between the surface of the nanomaterials and the polymers produce the desired properties in the membranes. More so, the type and size of nanomaterials incorporated into the polymer matrix play a vital role in the permeability and structure of the resultant membrane. The structure and permeability of the resultant membrane are a function of the type, size, and concentration of the nanoparticles used in doping the polymer [53].

Over the last decade, there has been a focus on the incorporation of a wide range of metal/metal oxide nanoparticles dope into the polymeric matrix [54]. Incorporation of nanoparticles such as silica, silver, titanium dioxide, and zeolite has been reported. These metal/metal oxide dopants often possess desirable characteristics such as photocatalytic, antimicrobial, as well as super-hydrophilic qualities. The interaction between silver nanoparticles and phosphorus/sulphur is known to have bactericidal effects by damaging the bacterial proteins, an effect desirable in combating biofouling in membrane systems. Titanium dioxide, which possesses super-hydrophilicity and photocatalytic qualities, is also known to improve the hydrophilicity of the membrane as well as combat biofouling [50]. Emerging fullerene-based

nanomaterials possess good mechanical strength, flexibility in functionality modification, ability to tailor size and electron affinity has great potential in membrane technology [55].

Carbon-based nanomaterials have also been reportedly used to dope the membrane matrix for improved system performance. Defect-free carbon-based nanomaterials possess a hydrophobic surface on their interior, which enables an almost frictionless flow [56]. Furthermore, modified carbon-based nanomaterials and graphene oxide are attached to the membrane to enhance its hydrophilicity and roughness [57]. Carbon-based nanomaterials are able to filter out dissolved ions while letting water pass through, which is one of their most important structural advantages [58]. Carbon-based nanomaterials also possess small diameters, which can be controlled which allowing the membrane to be modified in a way that fluid can be selectively desalinated [59]. Graphene-based nanomaterials have reportedly demonstrated potential for producing ultra-fast, environmentally friendly, and energy-efficient membranes. Numerous computational studies have predicted that nanoporous graphene could outperform the commercial water desalination membrane, where it can work under lower pressures and provide well-defined channels that can filter salty water at a faster rate than RO membranes [60].

The development of Aquaporin-based membranes over the last three to five years presents an interesting dimension to membrane desalination technology, as aquaporin is known to transport water molecules at a high rate. Aquaporin-based membranes are notable for their high selectivity, high permeability, defect-free, and mechanical strength, which enables them to withstand high operating pressures, defect-free, chemically and biologically stable for long-term use [61,62].

1.1.7.2. Thin Film Nanocomposites

Thin film composites (TFC) are generally synthesised by the polymerisation reaction of m-phenylenediamine (MPD) and trimesoyl chloride (TMC) on a nanoporous substrate layer. This technology was developed by John Codette in 1981 [63] and has been used for fantastic reverse osmosis desalination. The resultant membrane demonstrated certain desirable qualities such as good salt rejection, good water flux, and production of very pure water from highly contaminated water sources, as well as good mechanical strength and good tolerance to a wide range of feed pH [64]. However, its hydrophobic aromatic groups and high degree of cross-linking at the selective layer inhibit water flux. This consequently increases desalination cost.

In tackling this pitfall, recent proposals exist to increase water permeability and anti-fouling qualities by structurally modifying the chemistry of the active layer. The addition of poly(m-aminostyrene-co-vinyl alcohol) into the aqueous phase during the membrane fabrication process showed a considerable water flux increase due to the hydrophilic and flexible poly(vinyl alcohol) with the resultant membrane [65].

Another new approach to modification of thin film composite membranes is the incorporation of functional nanoparticles with super-hydrophilic and anti-microbial qualities into the thin film composite matrix. The resultant membranes, thin film nanocomposite membranes, showed improved rejection and flux qualities.

Further studies reveal that the incorporation of inorganic additives enhances the diffusion properties of the resulting membrane and increases its hydrophilicity, thereby improving its resistance to fouling. The additives enhance film formation by increasing the diffusion rate of monomers to the interface, expanding the wet zone on top of the support layer, and capturing by-products while regulating reaction pH (buffer agent) [66,67,68].

1.1.7.3. Mixed Matrix Membranes

This category of modified membrane is synthesised through the direct incorporation of inorganic fillers into the polymeric membrane matrix. Mixed matrix membranes are easier to fabricate than TFNs, as the nanofillers are typically added to the polymer dopant, an operation followed by the production of flat sheet or hollow fibre membranes by the phase inversion technique. Cellulose acetate/polyethylene glycol (PEG) RO membrane embedded with fused silica particles (FSP) has been reported using this technique [69]. An increase in permeation flux and rejection was achieved through the application of this technique. The increase in permeation flux was mainly due to the hydrophilic nature of FSP, in which the doping of FSP changed the permeate mobility and also the polymer chain segmental motion, and subsequently increased the free volume of the resultant membrane. However, the electrostatic interactions between the FSP and dense membrane prevented the formation of undesired voids and hence increased the salt rejection.

New approaches involve the use of detonation nanodiamond (DND), a carbon-based nanomaterial that can aid hydrophobic membranes for water vapour flux in membrane distillation processes [70].

1.1.8. Economics of Desalination

The large-scale production of fresh water from seawater is largely dependent on technical and economic standpoints, as well as the performance of the procedures in specific situations. Technical parameters such as the characteristics of the feed seawater, product water quality, energy source, energy consumption, plant size, reliability of the plant, concentrate disposal, space requirements, operation, and maintenance aspects are considered in setting up a desalination plant. Furthermore, capital energy, labour, chemicals, materials, and consumables costs are factors to consider in putting up an economic analysis of a process [71,72,73].

Joint generation of electricity and useful heat for desalination is essential from an economic standpoint.

Over the years, the broadening of the desalination market as a result of expanding fresh water sources has led to increased interest from many organisations and companies in the business. Consequently, the improvement of desalination technologies to significantly reduce the costs has been achieved over the last decades. Water price in the US is at US$0.50/$m^3$ [74] for large-scale seawater reverse osmosis plants, and for specific local conditions, and below US$1.00/$m^3$ for the Multistage Flash technique. Technological maturity, system integration, and competition combined to cause the reduction of desalination costs in the last 20 years.

Subsequent technological improvements in membrane design and procedures have also driven down the cost of desalinating salt water by half over the last two decades. For instance, some processes witnessed a decrease in the energy requirement for the production of 1m^3 of fresh water from brackish water by over 64% [75].

Electrodialysis reversal (EDR) technology can also be used to desalinate brackish water at low cost. In Barcelona, the Spanish capital, there is a very large-scale brackish water desalination EDR plant, with a total daily capacity of 200,000 m^3. Typically, EDR is selected over RO for systems that have a particular water chemistry issue, such as a high sulfate-to-chloride ratio in the raw water.

The prices of membranes have significantly dropped in the last decades. Prices of thermal processes are also falling as a result of improvements in materials, process innovation, and increasing competition. Also, as technological advancements lead to a reduction in equipment costs, the overall plant operating costs are expected to decrease.

The water production cost analysis takes into account the capital and operating, and maintenance costs. Production capacity, plant life, and direct and indirect capital costs are also parameters considered when working out cost analysis. The operating and maintenance costs are made up of labour, materials, parts, consumables, electricity, chemicals, seawater costs, etc.

1.2. Research Gaps

Recent advancements in membrane-based desalination, particularly in the areas of nanofiltration (NF) and electrodialysis (ED), have significantly improved process efficiency and selectivity. However, challenges remain in enhancing membrane performance under high salinity conditions while maintaining energy efficiency and minimising fouling. Studies highlight the potential of surface modification, including plasma treatments, in improving membrane hydrophilicity and antifouling properties. However, limited research exists on directly comparing oxygen and ammonia plasma treatments on NF membranes for seawater desalination. Furthermore, while electrodialysis is well-established for treating brackish water, its comparative performance versus modified NF membranes in high-salinity conditions remains underexplored. This study addresses these gaps by systematically evaluating the performance of plasma-modified NF membranes and ED for synthetic seawater desalination, with a focus on energy consumption, ion rejection, and membrane stability.

1.3. Objectives of this Work

Water scarcity is one of the greatest global challenges of recent times, with one-third of the world's population living in countries where there is water stress. To mitigate this problem, several water treatment procedures have been developed, while others are being developed. Many of those methods are geared towards the conversion of seawater to fresh water, since seawater is the most abundant water resource on the planet. Enormous potential exists for seawater desalination to reliably produce enough potable water to support large populations of the world where there are risks of severe water shortage.

However, despite the major advancements in desalination technologies, desalination of seawater poses a huge challenge to the water industry because it is still more energy-intensive when compared to other conventional freshwater treatment techniques. There are various processes and technologies for the desalination of water.

Membrane processes have been developed over the years as a technique for seawater desalination. However, issues such as the cost of membrane materials, energy input, and

fouling are factors militating against its wide usage. Processes and design methodologies exist for optimising membrane operation performance, aimed at mitigating these challenges.

Despite the significant advancements in desalination technologies, key gaps remain unaddressed. First, there is limited comparative data on the performance of nanofiltration (NF) and electrodialysis (ED) for high-salinity seawater, particularly in terms of energy efficiency and ion rejection. Moreover, while surface modification of membranes using plasma treatment has shown promise, there is minimal research comparing the effects of ammonia plasma and oxygen plasma treatments on NF membranes.

Finally, the potential use of porous silicon membranes in desalination has not been extensively explored for cost-effectiveness or scalability. This study addresses these specific gaps through a combination of experimental evaluations and novel membrane modifications. These objectives will be achieved specifically through the following

1. Investigate Nanofiltration (NF) for Seawater Desalination:
    - Examine the effectiveness of NF membranes in removing divalent ions, specifically calcium and magnesium, from both synthetic and real seawater.
2. Compare Nanofiltration and Electrodialysis (ED) Techniques:
3. Evaluate the comparative ion rejection and water flux performance of nanofiltration (NF) and electrodialysis (ED) using synthetic seawater solutions.
4. Enhance NF Membrane Performance through Surface Modification:
    - Develop and apply surface modification techniques, specifically comparing oxygen and ammonia plasma treatments, to improve NF membrane hydrophilicity and antifouling properties. This objective addresses the limited research on the direct comparison of these plasma treatments and their impact on membrane performance in seawater desalination.
5. Explore Low-Cost, Earth-Abundant, Silicon-Based Microfiltration:
    - Investigate the feasibility of utilizing silicon-based materials for microfiltration in desalination processes. This objective seeks to develop cost-effective and scalable alternatives to current membrane materials, contributing to the reduction of overall desalination costs.
6. Provide a Comparative Analysis of Desalination Processes:
    - Conduct a comprehensive evaluation of the processes above, highlighting their efficiencies, costs, and practical applications. This analysis aims to offer

insights into the most viable desalination strategies, considering current technological advancements and economic factors.

1.4. Purpose of the Study:

This research aims to develop innovative desalination methods capable of reducing seawater salinity from approximately 35,000 mg/L to 70–100 mg/L, effectively removing divalent ions, hardness, and organic contaminants.

CHAPTER TWO

2.1. Overview of Nanofiltration Technology

Although NF membranes have been in use for over 28 years, their significance has grown notably in the past two decades [76]. Their properties lie between those of ultrafiltration (UF) and reverse osmosis (RO) membranes and are therefore sometimes referred to as "loose," "leaky," or low-pressure RO membranes [76]. NF membranes offer the advantage of providing high water flux at low operating pressures while maintaining high salt and organic matter rejection, typically exceeding 90% [77].

Since the late 1970s, NF membrane processes have gradually gained acceptance in industrial applications, serving as viable alternatives to traditional separation methods, including extraction, evaporation, and distillation. The first industrial systems using NF membranes were installed in 1978, employing tubular membranes for the separation of dyes and brighteners. The benefits of nanofiltration include ease of operation, reliability, comparatively low energy consumption, and high pollutant removal efficiency [76].

NF membranes typically possess a pore size of around 1 nm, corresponding to a molecular weight cut-off (MWCO) of 300–500 Da [77]. When NF membranes come into contact with an aqueous solution, they are slightly charged due to the dissociation of surface functional groups or the adsorption of charged solutes onto the membrane. For example, NF (typically polymeric) membranes contain carboxylic and sulfonic acid groups that ionise and result in a charged surface in aqueous feed solutions. NF membranes are used for the separation of inorganic salts and small organic molecules. Compared to RO membranes, NF membranes generally have lower rejection of monovalent ions, higher rejection of divalent ions, and higher flux. Numerous review papers [78,79] have investigated various aspects of NF technology.

NF membranes are manufactured using two primary preparation techniques [80]:

- Polymer phase inversion, resulting in a homogeneous asymmetric membrane.
- Interfacial polymerisation of a thin-film composite layer on top of a substrate, ultrafiltration membrane, or other porous material.

Cellulose acetate and sulfonated polysulfone are two common materials used to make homogeneous asymmetric NF membranes. Thin-film composite NF membranes are usually produced by reacting crosslinked polyamide polymers with carboxylic or other charged "pendant" groups. Typical substrate materials for thin-film composite membranes include

polysulfone (PS), polyethersulfone (PES), polyvinylidene fluoride (PVDF), polyacrylonitrile (PAN), and polyether ether ketone (PEEK).

Recent advancements in NF technology have been able to produce membranes that are exceptionally stable in low or high pH, at very high temperatures, or in organic solvent media through the incorporation of new materials into the membrane matrix. These materials used for innovative membranes are highly crosslinked to allow long-term stability and practical membrane life in aggressive environments. Recent studies reinforce the importance of membrane surface properties in determining nanofiltration (NF) performance, particularly regarding permeability, selectivity, and resistance to fouling. For example, Zhang et al. highlighted how thin-film nanocomposite membranes (TFNMs), enhanced with nanomaterials such as graphene oxide and metal–organic frameworks (MOFs), significantly improve water permeability and reduce biofouling [81]. Similarly, Lee and Kim reviewed multiple fouling mitigation strategies, confirming the benefits of improving membrane hydrophilicity through plasma treatment, polymer blending, and surface grafting [82].

In addition, Chen et al. demonstrated that incorporating zwitterionic functional groups into the active layer of polyamide membranes improved both anti-fouling behaviour and chlorine resistance under real-world wastewater conditions [83]. Al-Gamal et al. investigated plasma-treated NF membranes and reported a 25–40% improvement in flux recovery ratio and reduced organic fouling compared to unmodified membranes [84]. Patel et al. explored the effects of surface roughness and hydrophilicity on ion rejection efficiency, showing that smoother, more hydrophilic surfaces enhanced divalent ion selectivity without compromising flux [85]. These findings collectively support the growing consensus that tailoring surface chemistry and morphology is critical to advancing NF membrane performance in desalination and wastewater reuse.

NF membranes generally have a slightly charged surface and are mostly negatively charged at neutral pH. This surface charge plays a vital role in the ion transport mechanisms and separation properties of NF membranes.

Industrial applications of NF membranes are common in the food and dairy, chemical processing, pulp and paper, electronics, and textile industries. The primary application of NF membranes remains in water treatment, particularly for water softening.

Most commercial NF membranes are hydrophobic. While these membranes maintain good water permeability through their selective layers, surface modification techniques such as

plasma or chemical treatment are often employed to enhance hydrophilicity. Increasing surface hydrophilicity has been shown to reduce membrane fouling and improve long-term water flux stability. Also, while many NF membranes are made from polyamide, other materials such as cellulose acetate, polyethersulfone, and ceramic supports are used depending on the feed solution, cleaning requirements, and durability demands.

2.2. Separation mechanisms in NF membranes

The most notable difference between NF and RO membranes is NF membranes' ability to selectively reject divalent ions while allowing monovalent ions to pass through. It is commonly believed that NF and RO membranes do not have distinct pores in the way ultrafiltration and microfiltration membranes do. Although recent studies using atomic force microscopy (AFM) suggest that pores in NF membranes can be visualised, most membrane scientists prefer to describe these "pores" as the distances between the polymer chains of the membrane's material.

The transport mechanism and rejection properties of NF membranes are complex and remain active areas of research [86]. NF membrane rejection is typically attributed to a combination of steric, Donnan, dielectric, and transport effects. Various models have been developed to study the effect of different parameters on transport mechanisms and to predict NF membrane performance. The two major models are Sourirajan's "*sorption surface–capillary flow*" approach and the "*solution–diffusion*" theory [86].

The sorption surface–capillary flow model describes the preferential sorption of water molecules into the membrane and the desorption of multivalent ions (via dielectric forces), which excludes charged solutes—even those smaller than the membrane pores—from moving through the membrane (Donnan exclusion). Effective charge density, pore radius, and ionic strength determine the rejection of monovalent ions, which generally ranges between 0% and 50% for NF membranes.

The solution–diffusion theory, on the other hand, describes the membrane as a porous film into which both water and solute (ion) dissolve. Solute transport within the membrane occurs mainly under concentration gradient forces, while water transport depends on the hydraulic pressure gradient. Solute transport is governed by hindered diffusion and convection. For non-charged solutes, transport through NF membranes is primarily determined by steric exclusion. This steric exclusion mechanism applies to NF membranes as well as to ultrafiltration and microfiltration membranes. The separation between two different non-charged solutes is predominantly determined by differences in their size and shape.

The dissociation of ionisable groups at the membrane surface and within its pore structure is responsible for the membrane's charge in aqueous solution [87–89]. These groups may be acidic (e.g., sulfonic) or basic (e.g., carboxylic) in nature—or both—depending on the specific materials used in fabrication. The feed solution pH strongly influences the dissociation of these groups. The membrane may also exhibit an isoelectric point at a particular pH if its surface chemistry is amphoteric [90]. Moreover, NF membranes have a limited capacity for ion exchange, meaning some ions from the feed solution may adsorb onto the membrane surface, in some cases slightly modifying its charge [91,92]. Electrostatic repulsion or attraction occurs depending on ion valency, the membrane's fixed charge, and the local ionic environment resulting from these phenomena.

Because the dimensions of the NF active layer are on near-atomic length scales, detailed knowledge of its physical structure and electrical properties remains limited, leading to uncertainty and ongoing debate about the true nature of the separation mechanisms [93]. The role of dielectric exclusion, in particular, is especially contested [94]. Most commercially available NF membranes are inherently hydrophilic due to the presence of polar functional groups in their polyamide or cellulose acetate layers. This hydrophilicity supports water permeability and reduces fouling. However, additional surface modifications, such as plasma treatment, can further enhance wettability and improve anti-fouling performance.

2.3. Theory of Nanofiltration Membranes

Since nanofiltration membranes are charged, their separation mechanism is not solely based on filtration like ultrafiltration membranes, but also involves osmosis to some extent. This makes them a true hybrid, combining the features of ultrafiltration (UF) and reverse osmosis (RO) membranes in membrane treatment technology.

Generally, the primary factors affecting the performance of a nanofiltration membrane include membrane material properties, particularly the surface charge, along with operational phenomena such as concentration polarization and membrane fouling. The membrane charge influences electrostatic interactions with charged solutes, while concentration polarization leads to an accumulation of solutes at the membrane surface, reducing driving force and separation efficiency. Fouling, caused by organic matter, biofilms, or scaling, can significantly degrade performance over time. Therefore, while pore size provides some indication of molecular separation capabilities, it does not solely determine rejection efficiency. To ensure

optimal design and pollutant-specific removal, pilot testing of nanofiltration membranes under actual conditions is crucial.

Most nanofiltration membranes reject compounds/ions with a molecular weight greater than 300–400 g/mol. This is often referred to as the molecular weight cut-off. It is important to note that this value represents the size required for complete or near-complete removal. For partial removal, the range extends down to less than 100g/mol. Information published by Koch Membranes indicates that their nanofiltration membranes cover a molecular weight range from approximately 100g/mol to 20,000 g/mol. This is evidence that certain membranes could have a molecular weight cut of as low as 100g/mol. In addition, Long Beach Water Department (Long Beach, California), through their testing, confirmed that the smallest molecular weight they have shown significant removal (up to 90 percent) of aqueous salts, ranging in molecular weight from 60g/mol to 500 g/mol. With this range of removal, nanofiltration membranes provide engineers and scientists with a unique opportunity to produce customized water products.

Currently, there is a wide range of nanofiltration membranes available on the market, providing numerous options for targeting mass removals of specific or groups of constituents. Although current reverse osmosis technology can remove a larger mass of the same constituents as compared to nanofiltration membranes, this may not be an ideal solution. Reverse osmosis membranes remove not only the constituents of concern but also dissolved minerals and hardness to such an extent that the product water is aggressive toward metal and concrete conduits. Treatment systems must then add some of these minerals back in to get the hardness back. The result is “wasted” effort to overshoot the water quality objective and then bring it back to a level that can be used.

2.3.1. Transport of Uncharged Solutes in Aqueous Solution

Most nanofiltration membranes are hydrophobic; thus, they are used to remove charged molecules/ions (mostly inorganic) or uncharged (mostly organic) compounds from aqueous solution. For uncharged molecules, separation mostly occurs by a sieving effect where the solute's molecule size should be larger than that of the pore size in the nanofiltration membrane. It is assumed that there is no essential interaction between the solute molecules and the membrane molecules. As a pressure-driven process, the known Hagen–Poiseuille equation [95] is recommended for solvent transport, though strictly considered, this equation is valid for porous membranes

$$\bar{N}_A = \rho_A \bar{v} - D_{AB} \bar{\nabla} \rho_A \quad (1)$$

where $\bar{N}_A$ is the mass flow of component A through the membrane (mass per unit time per area), ρ_A is the mass density of component A, $\bar{v}$ is the mass average velocity of the fluid through the membrane, D_{AB} is the effective diffusion coefficient of component A in the membrane, and ∇ρA is the mass density gradient. In membranes where pore flow contributes significantly to flux, Darcy's Law is often used to characterize the mass average velocity

$$\bar{v} = -\frac{k}{\mu}(\bar{\nabla} p - \rho \bar{g}) \quad (2)$$

where κ is the Darcy Law permeability of the medium, μ is the fluid viscosity, $\overline{\nabla p}$ is the pressure gradient (i.e., the rate of pressure change with respect to position), ρ is the solution density, and g is the gravity vector. Introducing Eq. 2 into Eq. 1; restricting transport to only the x direction, which would typically be the direction perpendicular to the membrane surface, and neglecting gravity, yields:

$$N_{A\times} = \frac{\rho_{AK}}{\mu} \frac{dp}{dx} - D_{AB} \frac{dP_A}{dx} \quad (3)$$

The first term in Eq. 3 represents mass flux due to pressure-driven convection through pores, and the second term represents flux due to diffusion [95]. Diffusion through porous membranes is typically negligible relative to convection. In this case, the flux is directly proportional to the pressure gradient across the membrane. The applied pressure difference across the membrane, often called the transmembrane pressure difference, is the driving force governing transport of liquid through a porous membrane.

While Darcy's Law (Eq. 2) provides a foundational model for pressure-driven flow through porous media, it is subject to important limitations in the context of membrane processes. Specifically, it assumes laminar, single-phase, viscous flow through a homogeneous porous structure, which often does not reflect the heterogeneous and nanostructured nature of modern filtration membranes [95]. In systems such as nanofiltration or reverse osmosis, where pore sizes are on the nanometer scale, molecular-level effects—including steric hindrance, surface charge interactions, and electrostatic repulsion—play a dominant role in solute transport. Moreover, Darcy's Law does not account for key operational phenomena such as concentration polarization and membrane fouling, which affect transmembrane pressure and reduce long-term performance. Consequently, although Darcy's Law (when incorporated into Eq. 1 to yield Eq. 3) provides a useful approximation of convective flux, more comprehensive models (such

as the extended Nernst–Planck equation or the Spiegler–Kedem model) are often required to accurately predict solute transport in charged and asymmetric membrane systems [96].

While Darcy's Law provides a useful approximation for pressure-driven flow in porous membranes, it is insufficient for describing solute transport in nanofiltration (NF), where molecular-level interactions dominate. NF membranes often operate under the solution-diffusion model, which treats the membrane as a dense polymer through which solutes and solvents diffuse based on their solubility and diffusivity. In charged membranes or electrolyte solutions, the extended Nernst–Planck equation more accurately captures ionic transport by incorporating diffusion, convection, and electromigration. The Spiegler–Kedem–Katchalsky model also offers a thermodynamic framework for predicting coupled solvent and solute fluxes, making it suitable for modeling osmotic effects and solute rejection. Each model has unique strengths depending on membrane type, solute characteristics, and operational conditions.[97].

2.4. NF Membranes Characterisation

NF membrane characterization can be achieved using several methods, namely;

- Gas adsorption–desorption technique, also known as the Brunauer– Emmett–Teller (BET) method, allows the direct measurement of the surface area and pore size distribution [98–100].
- Atomic force microscopy (AFM), which allows the direct measurement of pore size and pore distribution, surface roughness, topography, and force interactions between membrane and colloids [100–103].
- Use of neutral solute rejection studies and models allows the indirect measurement of pore size and distribution [103–105].
- Reverse surface impregnation coupled with Transmission Electron Microscopy (TEM), allows the direct measurement of pore size and distribution [106].

Each of these methodologies can provide useful information if employed correctly. However, due to the length scales involved and the various imperfections associated with each method, a combination of methodologies is always recommended, as well as the application of logical rationale. Measurement of the charge properties of NF membranes is the other key variable required for process understanding, and these vary depending on the nature of the contact solution, particularly the concentration and pH.

2.5. NF Membranes Fabrication and Modification

NF technological advancement has resulted in the creation of better filtration technologies for the separation of inorganic and organic substances from solution in a liquid. Advanced methods such as interfacial polymerization (IP), nanoparticles (NPs) incorporation, and UV treatment have been employed in fabricating better-performing membranes [43]. Through these methods, membranes with higher selectivity, rejection tendency, and also overcoming fouling issues have been developed. However, drawbacks exist, such as membrane fouling. studies have gone into reducing fouling, increasing separation and rejection efficiency, as well as improving membrane lifetime and chemical resistance [43]. Some typical foulants can be organic solutes, colloids, inorganic solutes, as well as biological solids. Vast research works have used innovative membrane fabrication and modification techniques to produce membranes that have a significant improvement in terms of fouling propensity. These techniques can be categorized into IP and grafting polymerization [43]

The IP method usually involves phase inversion followed by interfacial polymerization to produce thin-film composite (TFC) membranes. Incorporation of additives such as nanoparticles in the thin film layer has been used, which leads to a thin-film nanocomposite (TFN). Furthermore, research works on grafting polymerization focused more on UV/photo-grafting, electron beam (EB) irradiation, plasma treatment, and layer-by-layer methods.

The interfacial polymerization technique is valuable for creating a thin active film layer for NF and RO membranes. It involves copolymerization of two reactive monomers to form the thin layers on the membrane surface. The development of thin-film composite (TFC) membranes through interfacial polymerization has gained attention in the past decade due to notable improvements in membrane characteristics such as selectivity and fouling resistance [107]. The reaction in this method is self-inhibiting as reactants are supplied, allowing an extremely thin film layer, within the 50 nm range, to be formed easily. This thin active layer determines the overall permeability, solute retention, and efficiency of the membrane.

Several types of monomers have been used in the IP process to improve membranes. Monomers such as bisphenol A (BPA), tannic acid, m-phenylenediamine (MPD), and polyvinylamine, which react with trimesoyl chloride (TMC) or isophthaloyl chloride to form the thin active film layer. Some studies [108] involve the application of a 2-step IP with TMC and MPD to increase the water permeability of the membranes. Another study [108] improved the antifouling properties and performance of membranes modified by IP, where BPA and TMBPA had been

used for the membrane development. The effect of varied concentration of monomer BPA in aqueous solution and also an effect of IP time were investigated towards the NF polyester TFC membranes [109,110].

Other types of monomers that present various improved membrane characteristics have been studied. For instance, polyhexamethylene guanidine hydrochloride (PHGH), which showed good bacteria inhibition properties, was successfully used to prepare an NF membrane using the IP method [111]. The addition of inorganic salts such as $CaCl_2$ during the IP process was used to improve pure water fluxes of composite NF membranes. The calcium ions were believed to possess the ability to combine with carbonyl groups, which would lead to the formation of a loose polyamide layer [112]. Furthermore, organic acids having different structures, such as ascorbic acid, citric acid, and malic acid, and with varying acidic strengths, have been studied during the fabrication of polysulfone (PSf) nanofiltration membranes. Addition of organic acids was found to improve the retention performance in the separation of xenobiotics such as 4-dinitrophenol (DNP) and p-nitrophenol (PNP) [113]. Synthesis of inorganic-polyamide nanocomposite membranes through metal-assisted interfacial polymerisation was also carried out. Titanium tetraisopropoxide, bis (triethoxysilyl)ethane, and phenyltriethoxysilane were the metal alkaloids used. Resultant membranes showed great improvement in terms of membrane structure and water permeability performance. The addition of larger amounts of metal alkoxide to the hexane solution increased both pore size and subsequently, water flux [114].

2.5.1. Plasma Treatment

Plasma treatment is another effective method that has been employed for surface modification of membranes. It is a process whereby gases such as oxygen or nitrogen can be applied to a polymer membrane as a plasma, to generate functional groups such as OH, N-H groups (related to the gases) with decreased membrane fouling [115]. This treatment increases the surface hydrophilicity and wettability of the membranes as a result of the introduction of polar groups onto the surface of the membrane, depending on the gases used. One advantage of the process is that only the physical and chemical properties of the polymeric surface are altered while the bulk properties of the membrane remain the same. Further research studies included the plasma treatment of NF membranes used for the separation of aqueous solutions of organic compounds [116].

Kim et al [109] performed the surface modification of polysulfone ultrafiltration membrane from hydrophobic to hydrophilic by oxygen plasma treatment, to control fouling. The hydrophobic surface of polysulfone membranes has been known to be susceptible to severe fouling during ultrafiltration of water solutions that contain protein [117]. This fouling mainly comes from protein deposited onto the membrane surface during filtration. The permeate flux was found to decrease by up to less than 5% of the initial flux when the membrane is fouled. This consequently increases permeation time [118]. Factors such as surface properties (chemistry, morphology, etc.), hydrodynamic conditions, ionic strength, and solute concentration contribute to fouling of the membrane [119]. The extent of fouling is dependent on the types of solute macromolecule–membrane interactions, such as hydrogen bonding, dipole interaction, van der Waals interaction, as well as electrostatic effects [120]. For protein fouling, the hydrophobic interactions between the protein molecules and the surface of the membrane are responsible for the fouling of the membrane. Therefore, to reduce the amount of protein molecules adsorbed onto the membrane surface, the hydrophobic surface is modified to a hydrophilic surface, using plasma. Also, adsorbed proteins are more easily removed from the surface of a hydrophilic membrane.

More so, the interaction of charges between membrane surfaces and protein molecules is another factor that affects protein adsorption onto the membrane surface [120–123]. The pH of the feed solution determines the charge characteristics of both the membrane surface and the protein molecules. When both the membrane and the protein molecules possess like charges, electrostatic repulsion occurs, preventing protein adsorption. Oxygen plasma treatment is an effective method for modifying membrane surfaces from hydrophobic to hydrophilic [124]. In the study, oxygen-containing polar groups were introduced onto the membrane surface, thereby altering its surface charge [125]. This modification reduced the extent of fouling and increased membrane flux.

In one experiment, a polysulfone membrane with a molecular weight cut-off of 30,000 Da was treated with oxygen plasma. The treatment was conducted at a flow rate of 20 standard cubic centimeters per minute with pressure ranging from 0.3 to 0.9 Torr, and at an applied power of 60W. Treatment durations ranged from 5 seconds to 120 seconds. Results showed that the contact angle of water decreased as treatment time increased, due to the introduction of hydrophilic functional groups onto the surface of the hydrophobic polysulfone membrane. The optimal plasma treatment time was found to be 20 seconds. Functional groups such as hydroxyl, carbonyl, and carboxyl were introduced and confirmed by XPS and contact angle

measurements. Fouling tests using gelatin demonstrated that the hydrophilic polysulfone membrane repelled hydrophobic gelatin molecules, resulting in reduced fouling. Furthermore, the isoelectric point of the polysulfone membrane shifted from pH 3 to 4.5. Consequently, the oxygen plasma-treated membrane exhibited a positive charge at pH 3 and a negative charge at pH 12. Since gelatin molecules have a positive charge at pH 3 and a negative charge at pH 12, charge repulsion occurs, further minimizing fouling and enhancing membrane flux during wastewater treatment.

Mohammad et al. [126] reported the treatment of nanofiltration membranes with NH_3 plasma to reduce fouling and increase hydrophilicity. Nitrogen-containing plasma was applied to polymer membranes to generate N–H functional groups, which enhanced surface hydrophilicity and reduced fouling. In their study, commercial membranes were subjected to low-pressure plasma treatment in a bell-jar reactor. Treatment times ranged from 1 to 10 minutes.

The results showed a progressive decrease in water contact angle with increasing treatment time. A 10-minute treatment at 90W improved both water flux and membrane performance. Treated membranes exhibited superior pure water flux, salt rejection, and antifouling properties compared to untreated membranes. These improvements were attributed to the increased hydrophilicity resulting from the introduction of polar surface functional groups. Enhanced salt rejection was likely due to plasma-induced surface cross-linking, while the reduced adsorption of BSA and humic acid was associated with the more negatively charged and hydrophilic surface. However, there are currently no widely reported applications of plasma-treated membranes for seawater desalination, which underscores the relevance of this study.

2.6. Electrodialysis

Electrodialysis (ED) is an electrochemical separation process in which ions are removed from a solution through charged membranes under the influence of an electric potential difference [127]. An electric field is applied to the feed water, causing ions to migrate through ion-exchange membranes. Increasing the conductivity of the feed solution lowers internal resistance, thereby reducing energy consumption.

The process is based on the principle that salts dissolved in water dissociate into ions—positively charged cations (e.g., Na^+, Ca^{2+}, Mg^{2+}) and negatively charged anions (e.g., Cl^-, CO_3^{2-})—which are attracted to oppositely charged electrodes. Anions move toward the anode (positive electrode), while cations migrate toward the cathode (negative electrode).

ED has seen increasing application in wastewater recovery and desalination of process streams in the pharmaceutical and food industries, largely due to its ability to maintain the nutritional integrity of products by avoiding chemical additives such as coagulants or regenerants. Notable applications include the demineralisation of milk whey and the adjustment of sweetness in fruit juices.

The process is conducted in a system composed of multiple electrodialysis cells, each with a feed (dilute) compartment and a concentrate (brine) compartment. Alternating anion and cation exchange membranes are placed between two electrodes. These cells are arranged into a stack known as an electrodialysis stack, which facilitates ion separation in a controlled, repeating configuration.

Within the stack, the dilute (D), concentrate (C), and electrode (E) streams flow through compartments formed by the membranes. Upon application of a direct current (DC) potential, anions in the dilute stream migrate toward the anode and pass through anion exchange membranes into the concentrate stream. They are prevented from further migration by the adjacent cation exchange membranes. Similarly, cations move toward the cathode, passing through cation exchange membranes but are blocked by anion exchange membranes, thus accumulating in the concentrate stream.

This movement of ions results in electrical current flow between the electrodes and ensures charge balance in both the dilute and concentrate streams. As the cycle continues, ion concentrations increase in the concentrate stream and are depleted in the feed stream, thereby achieving desalination. The electrode stream, which flows past the anode and cathode, can be composed of either the same solution as the feed or a separate supporting electrolyte.

containing a different species. Depending on the configuration of the stack, anions and cations from the electrode stream may be transported into the C stream, or anions and cations from the D stream may be transported into the E stream. In each case, this transport is necessary to carry current across the stack and maintain electrically neutral stack solutions.

2.6.1. Reactions at the Electrodes

Exchange of ions occurs at the electrodes. The chemistry of the exchange is represented below

At the cathode, water molecules gain electrons, and the atoms are dissociated. This results in the generation of hydrogen gas as represented in the equation

$2e^- + 2\ H_2O \rightarrow H_2\ (g) + 2\ OH^-$

while at the anode

$H_2O \rightarrow 2\ H^+ + ½\ O_2\ (g) + 2e^-$

or $2\ Cl^- \rightarrow Cl_2\ (g) + 2e^-$

Depending on the composition of the E stream and the ion exchange membrane arrangement, oxygen or chlorine gas is generated at the anode. The generated gases are subsequently released as effluent from each electrode.

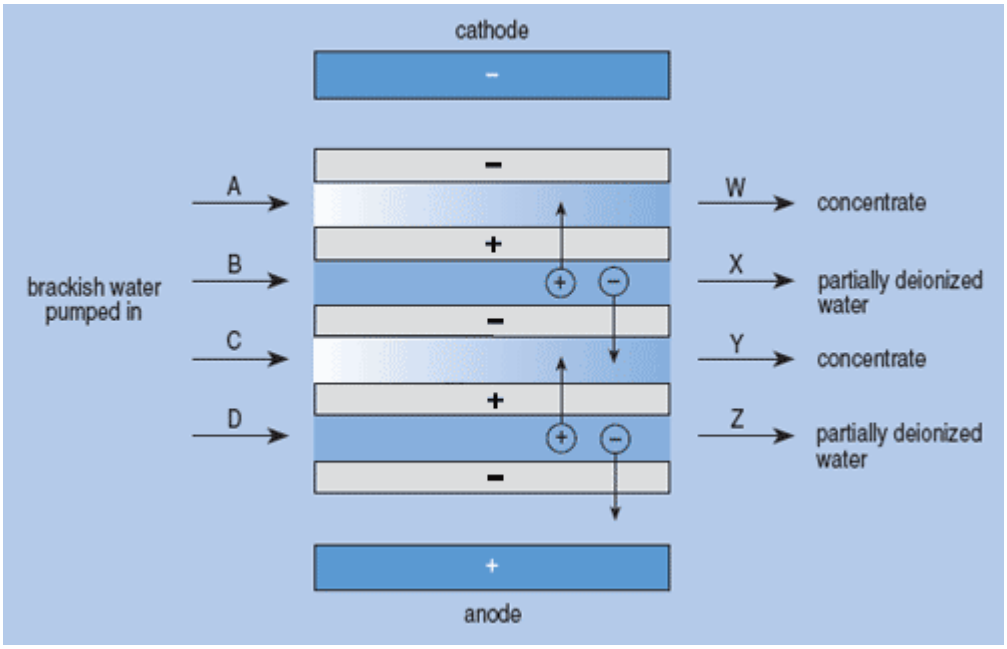

Figure 9: Schematic diagram of the Electrodialysis process for desalination [127].

The ion-permeable membranes used in the ED process are sheets of ion-exchange resins. These resins usually also contain other polymers, which help to improve the mechanical strength and flexibility of the resins. The resin component of a cation-exchange membrane consists of negatively charged ions/groups (e.g., $-SO_3^-$) that are chemically attached to the polymer chains (e.g., styrene/divinylbenzene copolymers). Ions with opposite charges to the fixed charge (commonly called counterions) are freely exchanged at these sites. The concentration of counter ions (e.g., Na^+) is relatively high; therefore, counter ions carry most of the electric current through the membrane. The fixed charges attached to the polymer chains repel ions of the same charge (commonly called co-ions) or anions. Since their concentration in the membrane is relatively low, anions carry only a small fraction of the electric current through a cation-permeable membrane. Attachment of positive fixed charges (e.g., $-NR_3^+$or $C_5H_5N^+R$,

where R = CH_3) to the polymer chains forms anion-permeable membranes, which are selective to the transport of negative ions, because the fixed -NR_3^+groups repel positive ions. This exclusion, as a result of electrostatic repulsion, is called Donnan exclusion.

The ED process is capable of removing between 25% to 60% of Total Dissolved Solids in water, resulting in 15% to 30% water recovery. ED process is also capable of removing aluminium, barium, boron, cadmium, calcium chloride, cyanide, and some volatile organic compounds. Some high-efficiency ED processes are also capable of purifying water of less than 2mg/l TDS.

Pre-treatment is necessary to achieve high efficiency of the ED process. This also helps to prevent issues like scaling. Pre-treatment can be carried out by pH adjustment.

However, to achieve higher water recovery rates, the TDS concentration in the feed must be below 2000 mg/l due to energy requirements. Some literature reports that ED is not suitable for desalination of water with high TDS because of the larger number of ions to be exchanged, and the amount of desalination energy is proportional to the ions exchanged [128-130], which indicates that ED is less suitable for desalinating high-salinity feed water. This contrasts with reverse osmosis, where the amount of water molecules transported during desalination is independent of the feed water's TDS concentration. Since ions are exchanged in ED, water molecules are also transported. The amount of ions exchanged is proportional to the water molecules transported; therefore, an increase in ions exchanged results in a corresponding increase in water molecules transported. This impacts the efficiency of the separation process. An increase in water molecules transported decreases system efficiency. Consequently, efficiency losses due to water transport become significant at higher feed water salinity. Additionally, high feed water salinity leads to low separation efficiency, caused by low membrane selectivity at high external salt concentrations and the limited ion exchange capacity of membranes [131,132]. This induces enhanced concentration polarization phenomena. As a result, the ratio of electrical current to ionic current is low at high salinity. This highlights a critical limitation of electrodialysis at elevated salinity levels. As ion exchange increases, more water molecules are co-transported through membranes via electro-osmotic drag, reducing separation efficiency. At higher feed salinities, membrane selectivity decreases because of a diminished electrochemical potential gradient and saturation of ion exchange sites. Consequently, concentration polarization intensifies, and the system's efficiency declines. The ratio of electrical current to effective ionic transport decreases, meaning more energy is

required per unit of ion removed, thereby limiting ED performance under high salinity conditions.

2.7. Factors affecting the performance of NF membranes [133]

Several operating parameters are considered when designing an NF process. These parameters affect the operation of a nanofiltration process.

- **Pressure**: The driving force responsible for separation in an NF system is the pressure difference. This is the difference between the applied hydraulic pressure and the feed osmotic pressure on the membrane. An increase in hydraulic pressure most time results in an increase in flux of the membrane.
- **Temperature**: An Increase in the process temperature results in increased membrane flux. This is a result of the reduction of feed water viscosity. Observations show that an increase in process temperature could also lead to reduced membrane rejection.
- **Cross Flow Velocity**: This is the rate of feed flow through the feed channel and across the membrane. Increasing the crossflow velocity in an NF membrane process increases the average flux due to efficient removal of the fouling layer from the membrane surface. However, the mechanical strength of the membrane and construction of the element and system hardware will determine the maximum crossflow velocity that can be applied. Running an NF membrane at too high a crossflow velocity may cause premature failure of membranes and modules.

CHAPTER THREE

MATERIALS, METHODS, AND EXPERIMENTAL

In this chapter, the materials, methods, and experimental works in this study are detailed. Most experiments were performed with the laboratory-scale dead-end filtration rig. This will be described in detail. Sample analysis methods as well as the materials used for the experimental work will be described. Filtration experiments will be carried out to indicate the different membrane performances as regards seawater desalination.

3.1. Laboratory Rig

The HP4750 stirred cell supplied by Sterlitech was used for the experiments in this work. It is a high-pressure stirred cell that is both chemically resistant and has a low hold-up volume (1 ml). This particular brand of stirred cell is able to perform a wide variety of membrane separations. It has a capacity of 300ml and a base diameter of 50mm with an effective cell area of 14.6cm^2 to allow a membrane size of 49mm. The cell is designed for safe operation to 1000 psi (69 bar) and can allow a maximum temperature of 121°C (250°F) at 55 bars (800 psig). The cell diameter is 5.1 cm (2.0 inches) and the cell height is 22.4 cm (10.0 inches).

Figure 10: HP4750 stirred cell from Sterlitech [source: Sterlitech]

The connections allow for a permeate outlet of 1/8inch, diameter 316L stainless steel tubing, and a pressure inlet of ¼ inch FNPT. The kit consists of a Stainless steel cell body, a cell top, a cell bottom, a cell top coupling, a cell bottom coupling, a porous stainless steel membrane support disk, O-rings, a top gasket, a permeate tube, a stir bar assembly, and a stir bar retriever.

The kit is assembled by a step-by-step process, which includes wetting the O-rings with a small amount of water or the fluid to be processed. The O-rings are inserted into the bottom of the

cell body, ensuring that the O-rings fit properly in the grooves. The piece of pre-cut membrane is placed over the centre O-ring. The membrane is installed with the active side toward the cell reservoir. In general, membranes coated on a substrate have a shiny, active side and a dull, substrate side. The stainless steel porous membrane support disk is placed on top of the membrane to hold the membrane in place. The cell bottom is fitted onto the cell body, aligning the circular groove with the circular ridge on the bottom of the cell body. 6. A 3-inch high-pressure coupling to clamp the cell bottom to the cell body, and the high-pressure coupling is tightened with 16 foot pounds of torque for 1000 psig (69 bar).

The permeate tube is inserted into the side of the cell body and tightened using a wrench. The Stir bar is then inserted into the assembly by lowering it into the cell with the stir bar retriever. At this point, the feed solution is poured into the cell body. The gasket is inserted on top of the cell body, ensuring it fits properly in the grooves. Thereafter, the 2-inch high-pressure coupling is used to clamp the cell top to the cell body, and then the high-pressure coupling is tightened with 16-foot pounds of torque for 1000 psi (69 bar) operation. After both clamps are properly attached, the cell is centred on top of a magnetic stirrer.

3.2. Operating the Cell

A high-pressure hose is attached to the fitting on the cell top. Thereafter, the other end of the hose is connected to the pressure regulator assembly on the inert gas (Nitrogen) supply or the compressed air supply. The magnetic stirrer is turned on to start the motion of the Stir Bar Assembly. The filtration is started by gradually pressurising the stirred cell, checking for leaks. Foreign material on the surface of the seals and insufficient tightening of the clamps are the most common causes for leakage.

*Figure 11: M*embrane filtration experimental setup (source: TECH INC)

3.3. Nanofiltration Membrane

The GE osmonics, Dow Filmtec Flat Sheet Membrane, PA-TFC, flat sheet NF membrane purchased from Sterlitech (Kent, US) was used in this study. It is made of polyamide thin-film composite, with a molecular weight cut-off of 150-300 Da and operates at a pH range of 2-10.

All the reagents that were used in this study were of analytical grade. Salts were obtained in high purity from Sigma Aldrich (UK).

3.4. Membrane Modification

3.4.1. Oxygen plasma treatment

Oxygen Plasma treatment of the NF membrane was performed using Henniker plasma HPT-100 benchtop plasma treater supplied by Henniker plasma. The HPT-100 machine has a 100mm diameter plasma process chamber in stainless steel, which contains vacuum-compatible materials. It features a high stability plasma generator which can be varied over a 0- 100W power range.

Under a vacuum, plasma source gas (O_2,) was introduced at 1 bar. The membrane was treated with the oxygen plasma for 1 min, 3mins, 5 mins, and 20 minutes, respectively, at 100% power,

gas flow rate of 20sccm. Oxygen gas was evacuated from the reactor after treatment. The treated membranes were quickly taken out of the reactor and compressed with deionised water through the dead-end filtration rig.

3.4.2. Ammonia plasma treatment

Surface modification of the membranes was carried out using the was performed using the Oxford PlasmaLab 80plus CVD, supplied by Oxford Instruments. At a vacuum, plasma source gas (NH_3) was introduced to 50 mTorr. power in a range of 8W and a predetermined treatment time of 50 secs was applied for treatment at a room temperature and pressure of 1000 mTorr. The treated membrane was removed and compressed with deionised water.

3.5. Analysis of filtrates

3.5.1. Conductivity measurements

Conductivities and pH measurements of filtrates from filtration experiments were takenusing the Jenway 3540 pH and Conductivity metre. The conductivity and pH probes were frequently calibrated to ensure accurate readings were obtained

3.5.2. Atomic Absorption Spectrometry (AAS)

This technique was used to determine the concentration of ions in samples. The PiAAcle 900F Atomic Absorption Spectrometer was used for sample analyses in this study. This technique uses the atomic absorption spectrum of a sample to assess the concentration of specific ions in it. It makes use of standards with known analytes and concentrations to establish the relation between the measured absorbance and the concentration of the analyte.

In the AAS, the electrons of the atoms in the atomiser are excited for some nanoseconds by absorbing a defined amount of energy. The energy is defined as the radiation of a given wavelength. This quantity of energy, i.e., wavelength, is specific to a particular electron transition in a particular element, because each element absorbs energy at a particular wavelength. In principle, each wavelength corresponds to only one element. The width of an absorption line is only in the region of a few picometers (pm). The technique derives its elemental selectivity from this phenomenon.

A detector is used to measure the flux of radiation without a sample as well as with a sample in the atomiser, and the ratio between the two values (known as the absorbance) is converted to analyte concentration or mass by the use of the Beer-Lambert Law.

The machine was calibrated with 5 samples of known concentrations of 0-10mg/l for each element that was analysed. A blank (pure water) calibration was also performed before elemental analyses.

3.6 Electrodialysis

The electrodialysis procedure is described in Chapter 5 of this work. The conventional electrodialysis apparatus is normally called a CED stack. The CED stack is made up of two electrodes (one anode and one cathode). There is an alternating anion exchange membrane (AEM) and a cation exchange membrane (CEM) between these electrodes. The membranes are separated by spacers to create diluate and concentrate chambers. The liquids flow through these chambers. When connected to an external power supply, an electrical potential is established by the power supply across the stack and which is housed within an anode chamber and a cathode chamber. All of the components are housed in a casing.

The ED 64002, containing 20 pairs, with an effective membrane area of 0.128m^2 CED stack, was used in this study, and it was manufactured by PCCell GmbH in Heusweiler, Germany.

All experiments were carried out at 20^{0}C, unless otherwise stated. Nanofiltration experiments were conducted under constant transmembrane pressure (TMP) conditions for each pressure setting. TMP was varied across six levels: 5, 10, 15, 20, 25, and 30 bar. For each experimental run, the selected TMP was maintained constant throughout the filtration process using a pressure-regulated feed system. This approach allowed assessment of membrane performance as a function of applied pressure under stable operating conditions.

3.7. Data Analysis and Error Representation

Error bars are graphical representations of the variability or uncertainty in experimental data. They provide a visual cue about the reliability and reproducibility of each data point. In this study, the error bars represent the standard deviation of replicate measurements for ion rejection at each pressure level during nanofiltration experiments.

The inclusion of error bars is important for several reasons:

- They help identify how consistent the experimental results are across repeated trials.
- They allow comparison of statistical significance between different pressure conditions or treatment methods.

- Small error bars indicate precise, repeatable measurements, while large error bars suggest greater variability in the system, potentially due to factors such as membrane instability, fluctuating feed conditions, or measurement errors.

All error bars presented in the experimental plots represent the **standard deviation** of three independent measurements ($n = 3$) performed under identical conditions. For each test condition—such as ion rejection, flux, or conductivity—the experiment was repeated three times, and the mean and standard deviation were calculated. The resulting error bars reflect the variability observed across these trials. In cases where the error bars appear constant across multiple data points, this is because the standard deviations were similar for each measurement set (typically within ±3–5% of the mean), due to the controlled laboratory environment and consistent experimental procedure.

CHAPTER FOUR

Introduction

In this chapter, membrane nanofiltration of salt solutions is investigated. Calcium and magnesium salt solutions have been filtered separately using an NF DK membrane. This is followed by the filtration of a mixture of calcium and magnesium salts. Filtration of synthetic seawater as well as natural seawater is also investigated and discussed. Also studied is the effect of pressure on their respective ion rejections by the nanofiltration membrane NF DK.

4.1 Desalination with Nanofiltration Membranes

4.1.1. Introduction to nanofiltration of salt Solutions

Although nanofiltration (NF) is a process that has seen increased usage over the last decade, for water treatment. It is increasingly common in industry, water purification, wastewater treatment, pharmaceuticals, biotechnology, and brackish water desalination. Continuous research is ongoing, aimed at understanding the various parameters involved in NF, such as particle sizes, charge effects, and electrostatic interactions based on Donnan Exclusion [134-136]. The Nanofiltration rejection behaviour for single components such as salts, pesticides, microorganisms, etc, is largely understood; however, the behaviour in multi-component systems becomes complex and less predictable [137]. That is, if there is a specific application involving an NF membrane, for instance, say for the removal of sulphates from mine waste streams (acid mine drainage), many membranes have to be screened in order to find a suitable membrane. Membrane behaviour in single components might be quite different from its behaviour in a multiple-component system.

General NF membrane behaviour shows that the rejection of uncharged solutes or ions appears to be a function of both the size and charge of the solute. This is in conjunction with the membrane properties such as pore size, membrane material, and membrane charge [138]. Recent studies show that for uncharged solutes, rejection is usually constant and/or could drop slightly with increasing feed concentration [139,140]. More so, the rejection of charged solutes is, on the other hand, determined by both the solute and the membrane properties. In addition to this, there is the effect of the charged solute and its interaction with the charged membrane surface, given that the surface charge of NF membranes is also influenced by the pH of the solution in contact with the membrane.

Furthermore, the negative charge on the membranes explains that for anion repulsion, rejection decreases as the valency of the anion increases. For instance, the retention of sulphate ions is

considerably higher than the retention of chloride ions. This trend applies to cations due to the requirement of the system for electroneutrality, which is the state of balancing out electrical charges within the system. However, for cations, the rejection increases with increasing valency of the cations. This is due to membrane charge shielding caused by higher valency cations. This would, for example, result in a higher rejection of $CaCI_2$ than of NaCl.

In mixed salt solutions, the mechanism of retention is more complex. For instance, in a mixed solution with NaCl and Na_2SO_4, it was reported that the concentration of the divalent anion influences the monovalent anion retention [141]. The addition of Na_2SO_4 to a solution of constant NaCl concentration results in a decrease in the retention of Cl as the concentration of Na_2SO_4 increases. To maintain electroneutrality in the system, the Na^+ ions, which readily pass through the membrane, are accompanied by a negatively charged ion. However, the negatively charged ions are repelled by the negatively charged membrane. The Cl^- ions with the lower potential are forced to permeate preferentially compared with the SO_4^{2-} ions, and even a negative retention of Cl^- has been observed. This is known as the Donnan effect.

Furthermore, the physical–chemical interactions of multivalent ions with the membrane are stronger than those typically existing with monovalent electrolytes; hence, higher rejection with NF membranes.

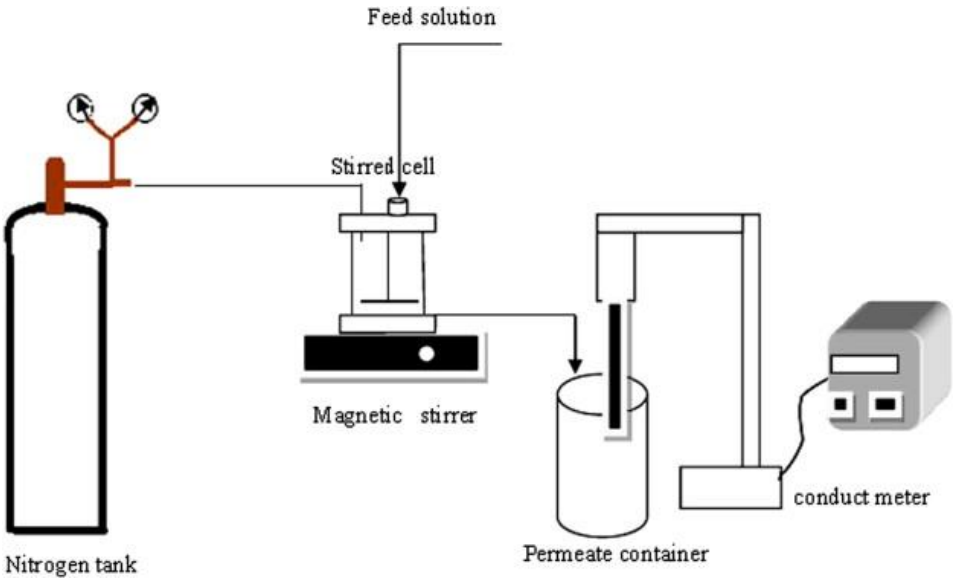

Figure 12: Schematic diagram of a nanofiltration process [123]

4.2 Filtration of NaCl solution

19, 345 mg/l of Na^+ solution was prepared from NaCl using deionised water. This concentration is representative of the sodium concentration in seawater. The mixture was stirred thoroughly

with a magnetic stirrer to ensure complete dissolution of the salt in the water. The conductivity of the salt was measured using the conductivity metre, and the readings were noted.

The salt solution was fed into a filtration cell and covered. Filtration was carried out under pressures of 5-30bar at room temperature (20^0C). The same process was repeated across temperatures 25^0C, 30^0C, 35^0C, 40^0C and 45^0C. Permeates of 30 mL were collected, with the first 5ml disposed of as waste for each experiment. The experiments were repeated three times to ensure the accuracy of the results.

Conductivities of the permeates were measured using the conductivity probe, and readings were taken and used to determine rejection

4.2.1 Water permeability and charged solute rejection

The membranes were characterised in terms of pure water permeability, as well as rejection (R) of Na^+. The permeability studies were performed at transmembrane pressure differences ranging from 5 to 30 bar. The permeate flow was determined.

4.3 Results and Discussion

4.3.1 Water Permeability

The membranes were characterised in terms of pure water permeability, porosity, as well as rejection (R) of uncharged solutes. The membranes used for the experiments were soaked in deionised water for 24 hours. They were also pressurised for 2 hours at pressures of 5 to 30 bars for 2 hours to avoid compression effects and establish leak tightness. The permeability studies were performed at transmembrane pressure differences ranging from 5 to 30 bar. The permeate flow (g.s -1) was measured using a balance.

The membrane permeability of a porous membrane can be determined by measuring the pure water permeate flux through the membrane at a given pressure. Water flux through a membrane can be described by Darcy's law. Darcy's law equation is used to define the ability of a fluid to flow through a porous medium such as a membrane. It is explained by the phenomenon that the amount of fluid flowing between two points is directly proportional to the driving pressure of the process. The driving pressure is the difference between the applied pressure and the osmotic pressure of the feed. The measurement of interconnectivity is known as permeability. Mathematically, Darcy's law is usually written as:

$$j\omega\ \alpha\ (\Delta P - \Delta\pi) \qquad (1)$$

where

α = direct proportionality sign

$j\omega$ = water flux (L.m^2.hr^{-1})

ΔP = pressure difference (k.pa or bar)

$\Delta\pi$ = osmotic pressure difference (k.pa or bar)

Introducing a proportionality constant,

$$j\omega = lp(\Delta P - \Delta\pi) \quad (2)$$

Where lp is the proportionality constant known as the permeability of the membrane.

Permeability is determined by obtaining the slope when a graph of $j\omega$ vs ΔP is plotted. The permeability of the membrane describes the porosity of the membrane. High permeability means a very porous membrane, while low permeability means a less porous membrane. Nanofiltration membranes generally tend to have significantly lower permeability than ultrafiltration membranes, because of smaller pore sizes and hydrophobicity.

$$\frac{j\omega}{(\Delta P - \Delta\pi)} \quad (3)$$

For pure water, osmotic pressure, $\Delta\pi = 0$, therefore

$$\frac{j\omega}{(\Delta P)} \quad (4)$$

Permeability can also be described as a function of membrane resistance and the viscosity of the feed solution. In this case, the permeability is inversely proportional to the product of the viscosity of the feed and the resistance of the membrane. Hence,

$$lp = \frac{1}{\mu Rm} \quad (5)$$

where μ is the feed viscosity

Rm is the resistance to flow of the membrane.

However, during nanofiltration experiments, total membrane resistance, R_{tot} comprises three separate resistances in series.

$R_{tot} = R_m + R_i + R_f$

Where R_i is the initial fouling resistance caused by concentration polarisation and fouling of the membrane during the start-up process

R_f is fouling resistance.

This is useful when dealing with membrane fouling.

Generally, membrane flux is defined as a function of the pressure gradient (the difference between applied pressure and osmotic pressure) and the resistances to flow determined by the membrane resistances and feed viscosity. Flux is directly proportional to the pressure gradient and inversely proportional to feed viscosity.

For the membrane used in this study, flux was determined in $L.m^2.hr^{-1}.S$

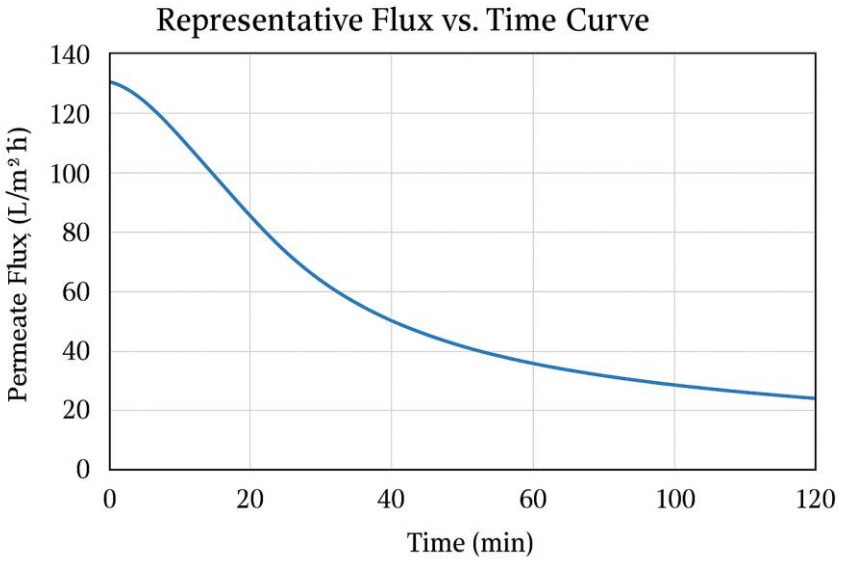

Figure 13: Representative Flux vs. Time Curve.

Although exact time-resolved data were not recorded during the nanofiltration experiments, a representative flux vs. time profile was developed to illustrate the observed fouling behaviour. As shown in Figure 13, the permeate flux exhibited a sharp decline within the first 30 minutes, likely due to membrane pore blocking and concentration polarisation. This was followed by a slower decline, suggesting the formation of a compressible cake layer on the membrane surface. After some time, the flow becomes steady but lower than at the beginning. This is

likely due to irreversible fouling, where the particles either get stuck deep inside the membrane or form a thick layer that is hard to remove.

The fouling was worse when using real seawater compared to synthetic salt water, which shows that natural seawater has more complex contaminants like organics and microbes that make fouling worse.

The error bars on the graphs show the variation in results from repeated tests. They were calculated from three similar experiments, which makes the results reliable.

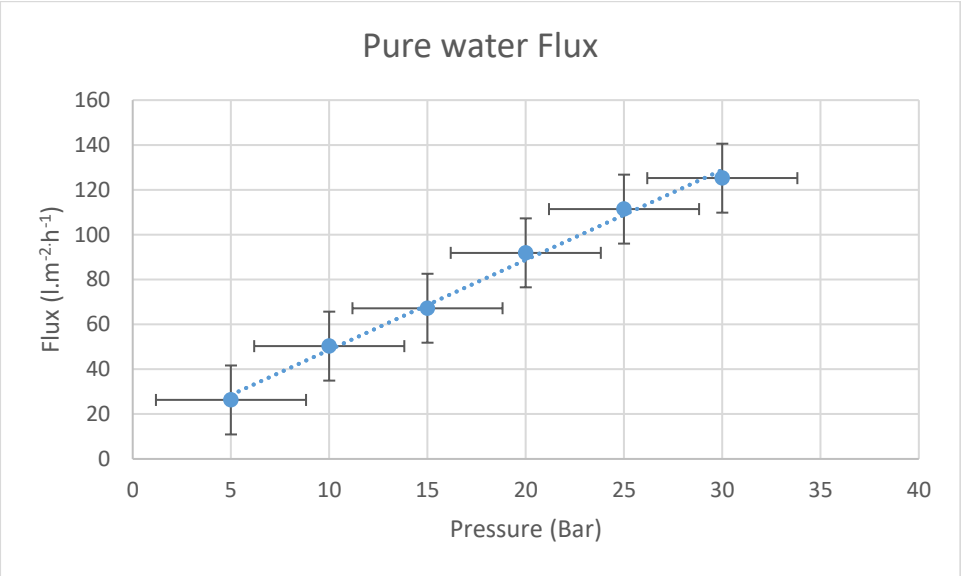

Figure 14: Pure water flux of the NF DK membrane with respect to pressure

From the figure above, it can be seen that an increase in pressure resulted in a corresponding increase in the flux of the membrane. Thus, at the pressure of 5 bar, the water flux was 26.3 l.m2.hr$^{-1,}$ and at the highest pressure of 30 bar, the flux was 125.2 l.m^2.hr$^-$1. This implies that the membrane behaviour obeys Darcy's law as the applied pressure is directly proportional to the amount of water passing through the membrane. Also, the calculated average flux of the membrane is 4.68 l.m^2.hr^{-1}. This again corresponds closely to the value provided by the manufacturer, which is an estimated 5 l.m2.hr^{-1}.

Filtration of NaCl solution with the same membrane showed a decline in flux as shown in the figure below

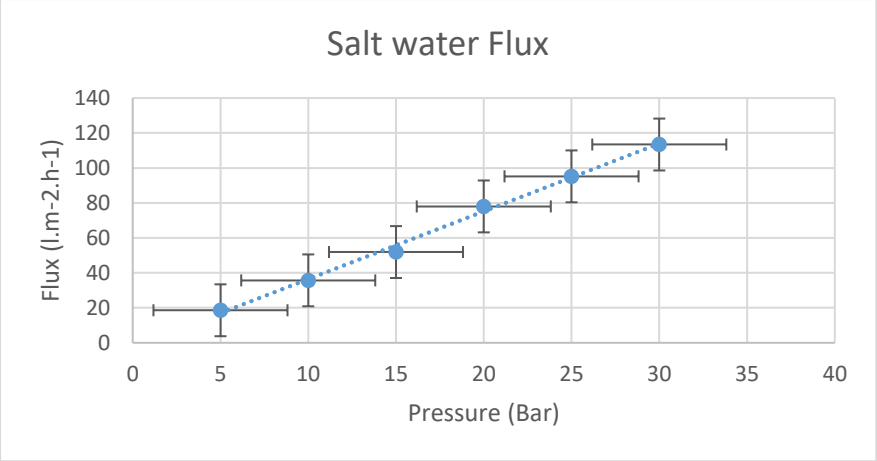

Figure 15: NaCl flux of NF DK membrane with respect to pressure

From the figure, pressure of 5b produced a flux of 18.6 $l.m^2.hr^{-1,}$ whereas at the highest pressure of 30b, the flux was 113.4 $l.m^2.hr^{-}1$. Again, it could be deduced that the membrane obeys Darcy's law due to the linearity of the flux curve. The calculated average flux is 3.7 $l.m^2.hr^{-}1$, signalling a slight decrease in flux when compared to clean water flux. It is therefore clear that the salt concentration influences the membrane flux.

When the salt and pure water fluxes are compared, the effect of concentration on the membrane flux can be further observed as in Figure 15 below.

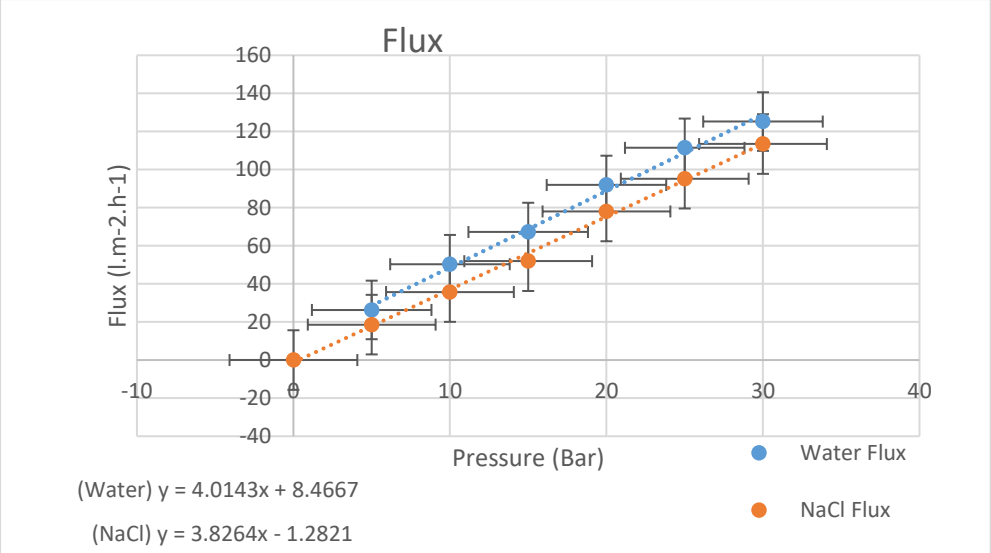

Fig 16: Pure water flux vs salt flux with respect to pressure.

From the figure, a slight decrease in permeability of the membrane is observed. The permeability for pure water was calculated as 4.01 $L.h^{-1}.m^{-2}.bar^{-1}$. This shows that the NF DK membrane has a low pore size and corresponding low porosity.

However, the calculated permeability for NaCl solution was 3.82 $L.h^{-1}.m^{-2}.bar^{-}1$. This signifies a reduction in permeability with an increase in the feed concentration. Furthermore, the theory of viscosity equally involves intermolecular activity. An increase in solute concentration leads to a corresponding increase in viscosity. This is due to the increase in hydrogen bonding with hydroxyl groups as well as the distortion in the velocity pattern of the liquid by hydrated molecules of the solute in the solution [138]. An increase in viscosity, therefore, resulted in a corresponding decrease in salt solution flux. Initial fouling of the membrane at the start of the process is also responsible for the resistance to flow of the feed across the membrane, resulting in lower permeability.

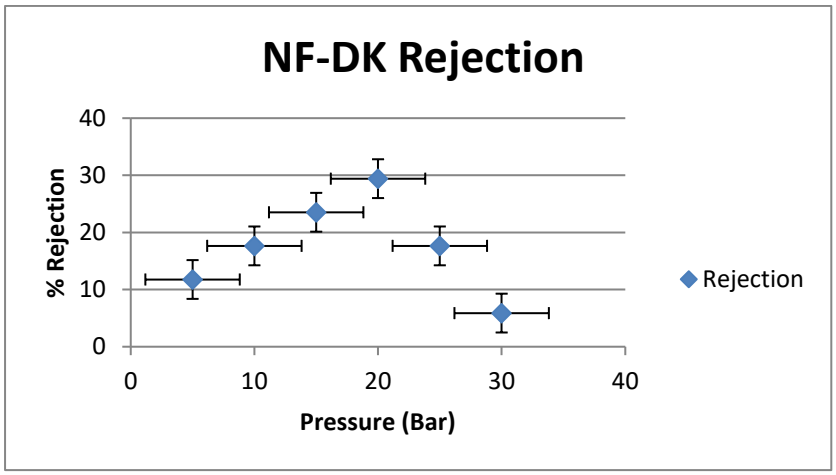

Figure 17: Na^{+} rejection with respect to pressure.

Filtration results show an increase in rejection with increasing pressure, peaking at 20 bar. Flux increases with pressure and rejection, sloping towards a maximum. At higher pressures, the water flux increases; however, the ion transport does not increase after 20 bars, since the driving force is not pressure but concentration dependent. This means that the actual salt concentration in the permeate is lower, and therefore, the rejection is higher at that pressure. At 20 bar, rejection is 29%. The decline in percentage rejection after 20bar indicated the optimum operating pressure to be 20bar. At higher pressure, there is higher flux and a decline in rejection.

Electrostatic repulsion and attraction play a vital role in the rejection of cations in a nanofiltration membrane [141]. In a neutral solution or environment, the NF membrane is negatively charged. Therefore, it can repel or attract ions in the solution, as the case may be. The physical–chemical interactions of monovalent ions with the surface of the membrane are

weaker than those of the divalent ions. Ions are easily transported through the membrane as a result of this. This explains the low rejection of Na^+ (below 50%) in an NF membrane.

Additionally, the high diffusion coefficient of Na (1.33×10^{-5} cm^2/s) is also responsible for its permeability, hence the low rejection.

4.3.2. Temperature effect on flux and rejection of Na^+

Filtration results at 25^0C showed a slight increase in flux with respect to applied pressure. A pressure of 1 bar produced a flux of 0.8-0.9l/m^2/hr. Percentage rejection follows the same trend as the 20^0C, with an optimum rejection of 19.8%. It is interesting to note that rejection has decreased with an increase in feed temperature.

At a temperature, 30^0C, 1 bar of pressure produced a flux of about 0.9l/m^2/hr. This also represents an increase in flux with increasing temperature. However, at this temperature, rejection increased with applied pressure, peaking at 30 bar at about 21.2%. Furthermore, there was a decrease in rejection as the feed temperature increased.

At 35^0C filtration results showed that the salt flux was 1.04-1.08l/m^2/hr, for 1 bar of pressure applied. Interestingly, this result is greater than the pure water flux produced at 1 bar. A further decline in rejection at the higher feed temperature was observed. The maximum rejection occurred at 15 bar, and that was about 16%. There was a decline in rejection with pressure above 15 bar.

A further increase in flux was observed as the temperature of the feed rose to 40^0C as observed flux ranged between 1.05 – 1.1l/m^2/hr, for 1 bar of pressure applied. Again, the percentage rejection continued to decrease at this temperature. The highest rejection was observed at 20 bar, which was 14.37%. There was also a decline in rejection to 13.23% at 30bar. The increase observed in flux is a result of reduced viscosity of the feed. Higher temperatures result in reduced viscosity. This consequently results in lower resistance to the flow of the solution across the membrane. Hence, higher feed mobility across the membrane. High viscosity also results in increased mobility of ions through the membranes. This explains the lower rejection.

4.4. Filtration of Double-Valent Salts

350 ml of salt solutions was fed into the filtration cell and filtration was carried out at pressures 5, 10, 15, 20, 25, 30 bars at 20°C. 25 ml permeates were collected and analysed to determine the percentage rejection of the membrane.

Concentrations of Ca and Mg ions similar to those observed in sea water were used in these filtration experiments. That is 1295mg/l of Mg from $MgCl_2$ and 416 mg/l of Ca from $CaCl_2$. Experiments involving the two salts, as well as a mixture of the salts, were carried out.

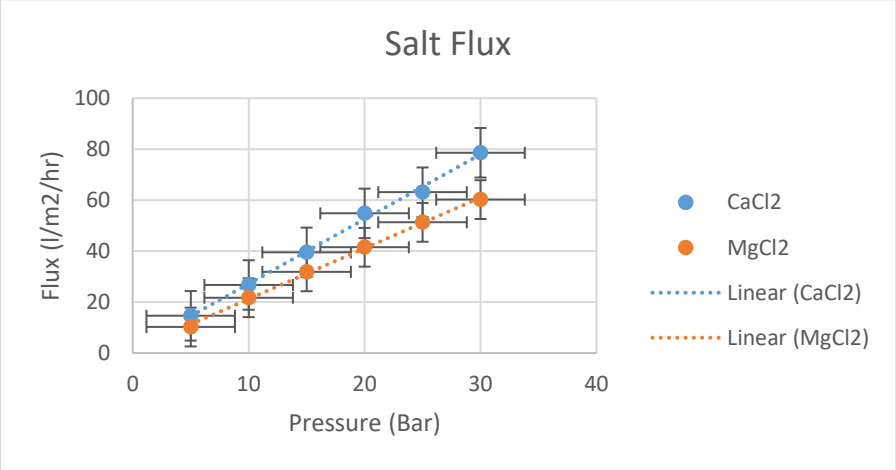

Figure 18: showing the effect of pressure on flux of 416mg/l of Ca^{2+} and 1295 mg/l of Mg^{2+} through NF membrane at $20^{O}C$.

Salt solution flux experiments performed on the membranes showed that the feed passage through the membrane increased linearly with transmembrane pressure. There was, however, no flux at zero pressure. Figure 18 shows that the highest flux was recorded when a transmembrane pressure of 30 bar was applied. The lowest flux was observed at a corresponding low transmembrane pressure of 5 bar. This, in comparison with the monovalent NaCl, shows that solvent permeability, at $20^{0}C$ is higher with the monovalent ions.

Generally, solvent flux decreases as the feed concentration increases. This explains the lower flux of magnesium ions in comparison to calcium ions, as shown in the figure.

Rejection results show that the degree of retention increased with increasing pressure of the cations, as shown in the figure below.

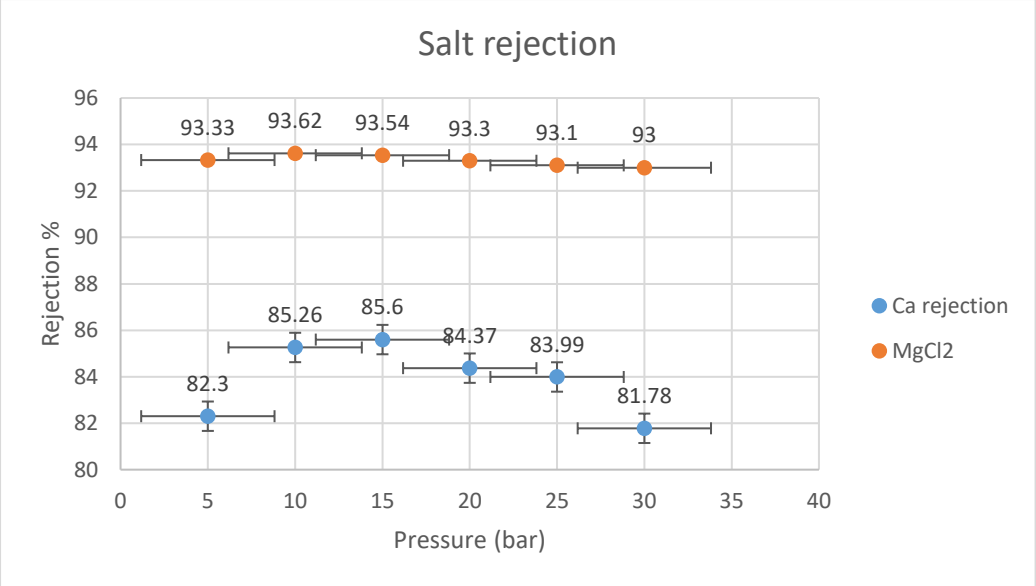

Figure 19: Divalent ions rejection with respect to pressure.

This is due to the increased electrostatic repulsion by the membrane.

Transport through a nanofiltration membrane involves both diffusion and convection [133]. At higher pressures, water flux increases, leading to a greater contribution from convective transport, while diffusion becomes less dominant. In some cases, this increased convective flow can enhance ion rejection, particularly for divalent ions, due to steric hindrance and charge effects. However, at very high pressures, concentration polarization effects may reduce rejection for some solutes

For both salts, rejection increased with increasing pressure and peaked at the same pressure of 15 bar. From 20bar, a decrease in rejection was observed for both ions. This could be explained by an increase in cross-flow velocity, which results from an increase in membrane flux. An increase in pressure results in a corresponding increase in membrane flux. So, as the pressure is increased, membrane flux is increased. This results in an increase in crossflow velocity, which occurs as a result of the efficient removal of the fouling layer from the membrane surface. This results in decreased rejection as more ions pass through the membrane.

Higher rejection of Mg is because Mg has a smaller hydration radius (8.6Å) as opposed to Ca (9.6Å), making it more strongly hydrated and less likely to pass through the membrane. Additionally, Mg^{2+} has a higher charge density (charge-to-size ratio), which leads to stronger Donnan exclusion (electrostatic repulsion by the membrane surface) [138].

Ca^{2+} rejection was 85.6%, while Mg^{2+} rejection was slightly higher at 93.54%. The higher rejection of Mg^{2+} is due to its higher charge density and stronger hydration energy, which result in greater electrostatic repulsion (Donnan exclusion) and lower permeability through the membrane. Additionally, Mg^{2+} has a slightly smaller hydrated radius than Ca^{2+}, which contributes to its higher rejection.

Studies [136] involving 5 Desal DK membranes showed that rejection of Ca ions increased with increasing concentration until it reached a maximum value for the membranes used for the study. Another investigation [137] involving the rejection of NaCl, Na_2SO_4, and $CaCl_2$ at different concentrations and pressures using Desal 5DK and PVD1 NF membranes showed that with the Desal 5DK, the rejection of NaCl and Na_2SO_4 decreased slightly as the concentration increased, while the rejection of $CaCl_2$ increased with increasing salt concentration. Typically, rejection increases as concentration increases it reaching a maximum for the NF membrane. This was also shown in studies involving the 5 NF membranes [136].

The selection of NF DK membranes for this study is justified by their well-documented performance in handling moderately saline solutions and their favourable selectivity characteristics. NF DK membranes, produced by GE (now SUEZ), are known for their high divalent ion rejection (e.g., Mg^{2+}, Ca^{2+}, SO_4^{2-}) while allowing partial passage of monovalent ions (e.g., Na^+, Cl^-). This makes them particularly suitable for applications such as wastewater treatment, brackish water desalination, and selective separation of specific ionic species. Moreover, DK membranes offer a good balance between flux and rejection rates, maintaining high water permeability without compromising salt removal efficiency. Studies have demonstrated that rejection by NF membranes, including DK types, increases with solute concentration until reaching a plateau—an ideal characteristic for targeting specific separation thresholds in this research [136]. Their robustness, chemical tolerance, and operational stability under varying feed compositions further reinforce their suitability for the objectives of this study.

4.4.1. Binary Mixtures of Charged Solute Rejection

In Figure 20, the effect of pressure on the flux of the $CaCl_2/MgCl_2$ mixture is shown.

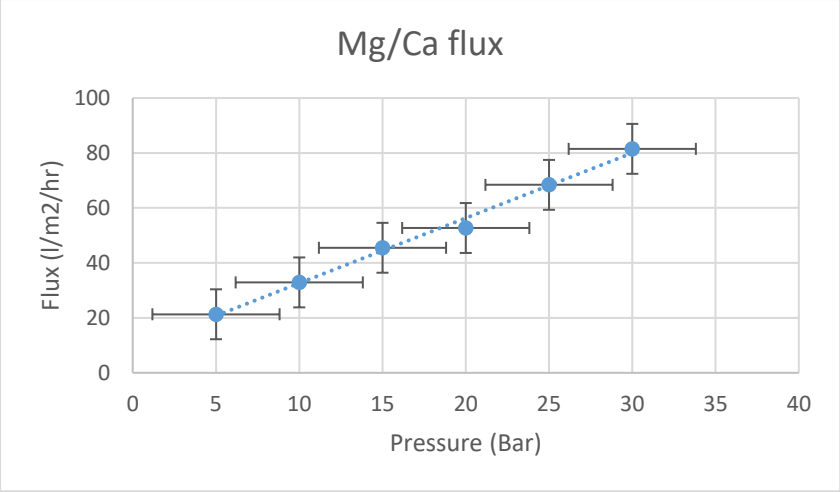

Figure 20: Effect of pressure on flux for binary Mg/Ca mixture filtration at 20^0C.

It can be said that the binary mixture obeyed Darcy's law, as a result of the linearity of the curve. The values show a slight decrease in flux with respect to pressure in comparison with $CaCl_2$, while slightly higher than that of $MgCl_2$.

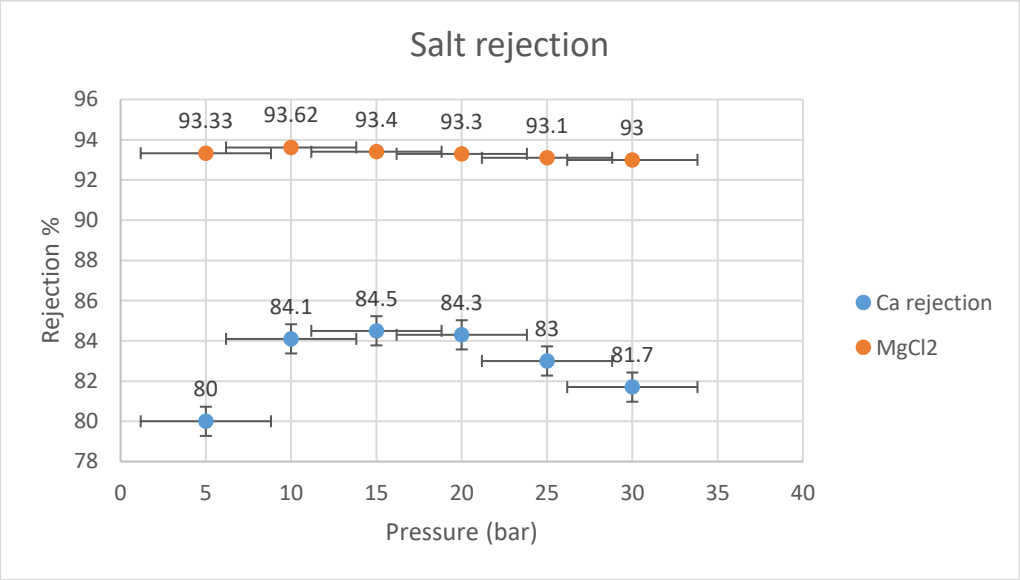

Figure 21: Rejection of binary mixture of $CaCl_2/MgCl_2$ as a function of pressure.

The figure shows that the rejection of the mixture is similar to that of the individual ions. The membrane behaviour is therefore the same. The rejection of magnesium ions is still higher than that of calcium ions. This is also related to their hydrated energies. Studies [137] showed a correlation between hydration energy and rejection. Hydration energy (also known as hydration free energy) can be defined as a measure of the stability of the hydrated ion with respect to the stability of its unhydrated form. Hydration free energy involves weak bonding between ions

and water molecules, forming a hydration shell. Therefore, it is exothermic in nature. Energy is released at the formation of the bond. Hence, removing the water molecules in the hydration shell requires energy. Lower hydration free energy allows ions to reduce the number of water molecules in their hydration shells, hence a higher likelihood to permeate. Hydration energy is also a function of the hydrated radius of the ions. Cations with small hydrated radii also have low hydration free energies and are likely to be rejected by the membrane.

Mg^{2+} has a smaller hydrated radius of 0.300nm and hydration free energy -1828 kJ/mol than Ca^{2+} with a 0.412nm hydrated radius and hydration free energy of -1306 kJ/mol. Therefore, $Ca^{2+,}$ having the larger hydrated radius and hydration energy, is expected to permeate more through the membrane. This explains the higher rejection observed with Mg ions over Ca ions.

4.5. Nanofiltration of seawater

Many researchers have studied the filtration of salts at different concentrations, but studies on nanofiltration of seawater remain inadequate. Figure 8 shows the effect of transmembrane pressure on synthetic seawater.

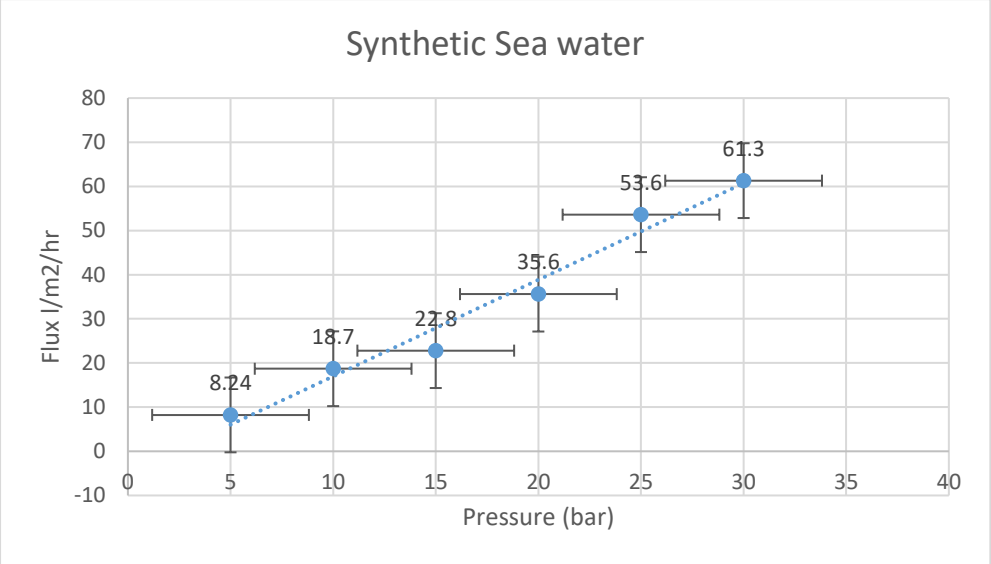

Figure 22: Effect of pressure on seawater flux through the NF membrane.

As the membrane continued to obey Darcy's law, it can be seen that the flux due to pressure has significantly reduced, in comparison to that of the calcium and magnesium salt solutions discussed earlier. Pressure of 5 bar produced a flux of 8.2 $l/m^2/hr$, whereas the highest pressure of 30 bar produced a flux of 61.3 $l/m^2/hr$. This is evidence that flux is affected by feed concentration. The concentration of the feed seawater is 35,000 ppm, using the Lymann and Fleming model for preparation of synthetic seawater [142].

The rejection of Ca^{2+} and Mg^{2+} in synthetic seawater was similar to their rejection in isolated ion solutions. This suggests that the presence of additional ions in the mixture did not significantly influence their rejection under the tested conditions. The similarity in rejection values across distinct ion solutions, mixtures, and synthetic seawater implies that membrane rejection of these ions is primarily governed by their charge density and hydration energy, with minimal interference from other solutes. The rejection of Ca^{2+} and Mg^{2+} in synthetic seawater was similar to their rejection in isolated ion solutions. This suggests that the presence of additional ions in the mixture did not significantly influence their rejection under the tested conditions. The similarity in rejection values across distinct ion solutions, mixtures, and synthetic seawater implies that membrane rejection of these ions is primarily governed by their charge density and hydration energy, with minimal interference from other solutes

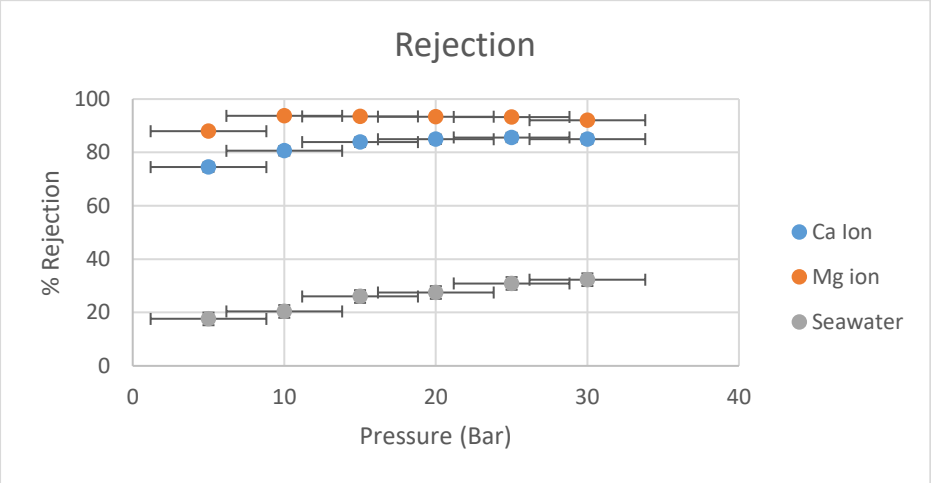

Figure 23: Effect of Operating Pressure on the Rejection of Ca^{2+}, Mg^{2+}, and Total Seawater Ions using Nanofiltration.

The graph shows the percentage rejection of calcium and magnesium ions, along with overall ion rejection in synthetic seawater, as pressure increases from 5 to 35 bar at 25°C using an NF DK membrane. Error bars represent ± standard deviation from three replicate measurements. Calcium and magnesium ions show high rejection rates above 10 bar, while total seawater ion rejection remains significantly lower due to limited exclusion of monovalent ions.

Overall rejection of the feed seawater is below 50%. The highest pressure of 30 bar produced 34.39% rejection of total dissolved solids (TDS) in seawater when compared with 85% for Ca^{2+} and 92% for Mg^{2+}. This represents about 40% drop in rejection. This can be explained by the fact that monovalent ions make up over 65% of the TDS of seawater, and from earlier

results, retention of monovalent ions (Na^+) is low (about 30%). It could therefore be deduced that over 60% of the TDS (mostly monovalent ions) in seawater permeates through the membrane. Hence, the NF membrane is only able to achieve just over 30% seawater TDS rejection.

4.6. Effect of Temperature on Filtration

Transport through NF membranes increases with an increase in temperature. The same was observed in the experiment, as shown in the figure below.

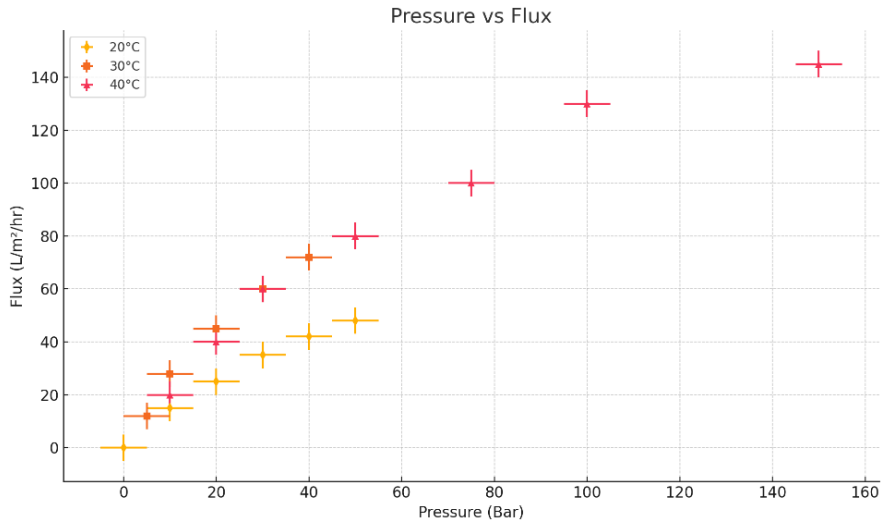

Figure 24: Temperature effect on NF of seawater with respect to pressure.

The figure above compares the permeate fluxes of synthetic seawater at 20^0C to 40^0C. Seawater at room temperature 20^0C produced the highest flux of 61.3l/m^2/hr, whereas at 40^0C, the flux was 137l/m^2/hr. This represents a 7.6% increase in flux from 20^0C to 30^0C and a further 31.8% increase from 30^0C to 40^0C. This is as a result of lower fluid viscosity at increased temperature, thus forcing more liquid through the membrane.

Previous studies demonstrated that the temperature has a significant impact on NF membrane performance. Goosen et al. [139] reported that polymeric membrane performance is sensitive to changes in the temperature of the feed. They reported an increase of up to 60% in the permeate flux when the feed temperature was increased from 20 to 40 °C. Other studies showed the existence of a linear relationship between feed temperature and water flux by NF membrane performances within the temperature range from 10 to 30 °C [140] and 20 to 70 °C [141]. It was found that the increase in flux as a result of flux increased temperature is as a result of the thermal expansion of the membrane material [141].

According to Sharma et al. [143], who studied the effect of temperature on the permeation characteristics of NF membranes, an increase in temperature resulted in increased average pore size and decreased pore density owing to the thermal expansion of the polymer constituting the active layer of thin-film composite membranes.

Dang et al [144] studied the effect of feed temperature on the rejection of trace organic contaminants using NF270. The report showed that an increase in the feed temperature from 20^0C to 40^0C resulted in an increase in the effective pore radius of the membrane from 0.39 to 0.44 nm.

However, in this research with seawater, an increase in flux can be attributed to increased viscosity.

Consequently, increased flux is expected to affect the rejection properties of the membrane. Filtration of seawater results as shown in the figure below, demonstrated a decrease in rejection as a result of an increase in temperature and flux.

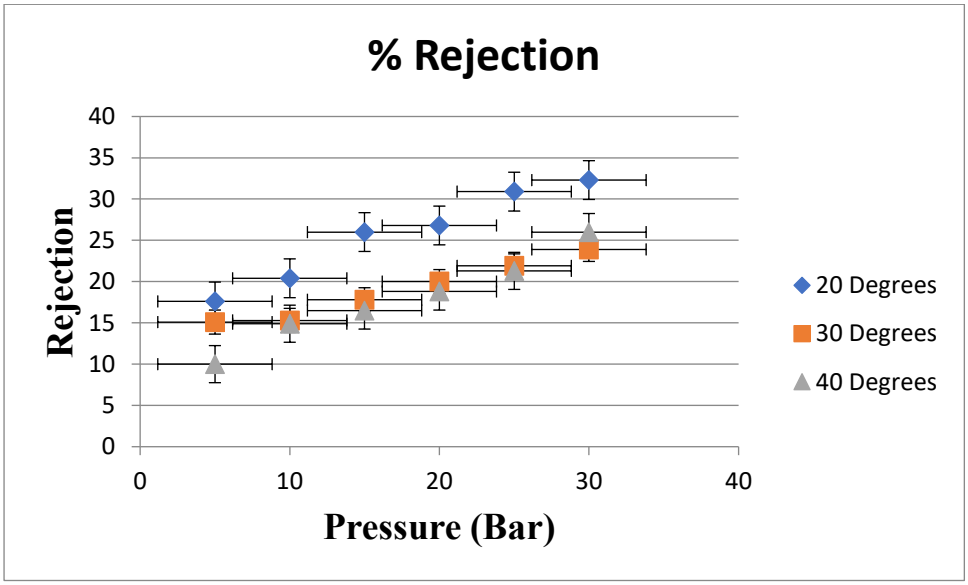

Figure 25: Effect of Feed Temperature on the rejection of ions in seawater using NF membrane

From the results (Fig. 25), filtration at 30°C recorded a 32.6% decrease in rejection compared to than at 20^0C, while at 40^0C produced a 5.7% decrease in rejection of ions in seawater. Dang et al [144] also reported that an increase in feed solution temperature adversely influenced the rejection of trace organic contaminants.

4.7. Conclusion

Nanofiltration of 19345mg/l, 1295mg/l, and 416mg/l of Na^{+}, $Mg^{2+,}$ and Ca^{2+}, respectively, was carried out using the NF DK membrane. These ions were prepared from their respective chloride salts. Synthetic and real seawater filtration experiments were also carried out using the same membrane. Water flux observations showed that the membrane observes Darcy's law, which explains that the membrane flux is directly proportional to the driving pressure of the system. Membrane flux increases with pressure. The highest operational pressure of 30 bar produced the highest pure water flux of 125 $l.m^2/hr$.

Feed flux and rejection are affected by the concentration of the feed. Monovalent ions have lower rejection than divalent ions under the same conditions. Sodium ions showed lower rejection (30%) than calcium (85%) and magnesium (93%) ions. This is explained by the phenomenon that the physical-chemical interactions of monovalent ions are weaker than those with divalent ions, thus allowing monovalent ions to readily pass through the membrane.

Smaller hydrated radius and hydration energy of Mg ions over Ca ions meant that the former has a better rejection than the latter, although they are of similar ionic strengths. An increase in temperature increased the membrane flux and reduced rejection. This is because an increase in temperature causes a corresponding reduction in viscosity, which results in a reduction of resistance to flow, thus allowing more liquid and ions to pass through the membrane.

About 70% (monovalent) of the ions in seawater passed through the membrane. This left rejection at about 30%. Hence, while the NF membrane is suitable for high levels of removal of cations from seawater, it is not suitable for achieving high rejection of ions in seawater.

The nanofiltration (NF) system tested in this study demonstrated rejection efficiencies of 85–93% for divalent ions (Ca^{2+}, Mg^{2+}), consistent with literature-reported ranges of 80–95% for calcium and 85–98% for magnesium [137]. Sodium rejection remained low, at under 20%, aligning with typical reported values of 10–40%.

CHAPTER FIVE

5.1 Introduction

In the previous chapter, nanofiltration was used as a means of seawater desalination. NF membrane can remove over 85% of divalent ions. However, with monovalent ions, the rejection is less than 40%. Seawater is made up of over 60% monovalent ions. Therefore, the NF technique is not suitable for seawater desalination if high water purity is desired, according to experimental results from the previous chapter.

In this chapter, another means of desalination, Electrodialysis, is explored. As with the previous chapter, the desalination properties of electrodialysis with divalent and monovalent ions have been studied. Experiments were carried out with 416mg/l of Ca^{2+} and 1295mg/l of Mg^{2+}. These concentrations represent the concentrations of these ions in real seawater. Separation of a mixture of Ca and Mg ions was also investigated. Finally, ED was used to treat synthetic and real seawater.

5.2. Electrodialysis Desalination

Electrodialysis (ED) is a desalination technique used to transport ions from one solution to another solution under the influence of an applied electric potential difference, using ion exchange membranes. This is carried out in a configuration known as an electrodialysis cell. The ED cell consists of a feed (dilute) compartment and a concentrate (brine) compartment formed by an anion exchange membrane and a cation exchange membrane placed between two electrodes, as earlier explained. In almost all practical electrodialysis processes, multiple electrodialysis cells are arranged into a configuration called an electrodialysis stack, with alternating anion and cation exchange membranes forming the multiple electrodialysis cells.

As a modern progressive electromembrane separation technique, ED has recently gained increasing attention in various branches of industry, such as water treatment. The production of drinking water from brackish water and seawater remains one of the most important industrial applications of ED [145,146]. This is in addition to the demineralization of solutions of widely varying industrial fluids, which are encountered in the food, pharmaceutical, and chemical industries. Brackish water desalination represents the largest application of this technology in desalination operations. ED is nowadays competitive with the conventional reverse osmosis process for brackish water treatment. Increasing ED applications within the wastewater recovery and desalination and process streams in the pharmaceutical and food

industry have also been observed in recent times. The reason for that is that the electromembrane separation process does not endanger the health and nutritional properties of the final product, e.g., by adding coagulants or regenerating agents. A demineralization of milk whey or a sweetness adjustment of fruit juices is an example of using ED in food processing.

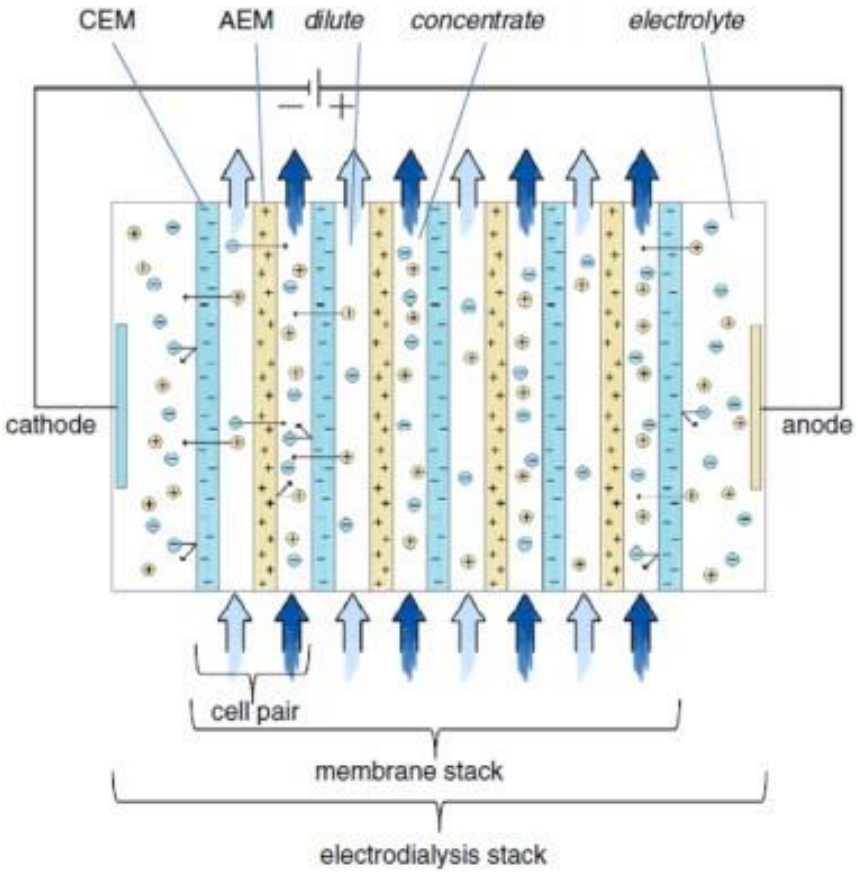

Figure 26: Schematic illustration of an electrodialysis cell [145].

5.3. Ion-exchange membranes

Ion-exchange membranes can be simply referred to as ion-exchange resins in film form. There are two different types of ion-exchange membranes: the cation-exchange membranes, which contain negatively charged groups fixed to a polymer matrix, and anion anion-exchange membranes, which contain positively charged groups fixed to a polymer matrix [147]. In a cation-exchange membrane, the fixed anions are in electrical equilibrium with mobile cations in the interstices of the polymer. The mobile cations are referred to as counter-ions. Mobile anions in the solution are called co-ions and are more or less completely excluded from the membrane matrix because of their electrical charge, which is identical to that of the fixed ions; hence, electrical repulsion. Due to the exclusion of the co-ions, a cation-exchange membrane is preferentially permeable to cations.

Anion-exchange membranes carry positive charges fixed on the polymer matrix. They therefore exclude cations and are preferentially permeable to anions. To extent, the co-ions are excluded from an ion-exchange membrane, depending on the membrane as well as on solution properties. Furthermore, cation- and anion-exchange membranes are classified as strong acid and strong base or weak acid and weak base membranes, respectively, depending on the degree of dissociation of the charged groups, i.e., SO_3^{2-} AND COO^- [147]. Strong acid membranes contain sulfonic acid as the charged groups. In weak acid membranes, carboxylic acid is the charge-carrying group. Quaternary and tertiary amines are the fixed charges in strong and weak base ion-exchange membranes, respectively.

Furthermore, ion-exchange membranes can also be distinguished according to their structure as homogeneous and heterogeneous. Homogeneous membranes are prepared by introducing an ion exchange moiety directly into the structure of the polymer the membrane is made of. This leads to a relatively even distribution of the charged groups over the entire membrane matrix. Heterogeneous membranes are prepared by mixing a fine ion-exchange resin powder with a binder polymer and pressing and sintering the mixture at an elevated temperature. This results in a structure where the ion exchange groups are clustered and very unevenly distributed in the membrane.

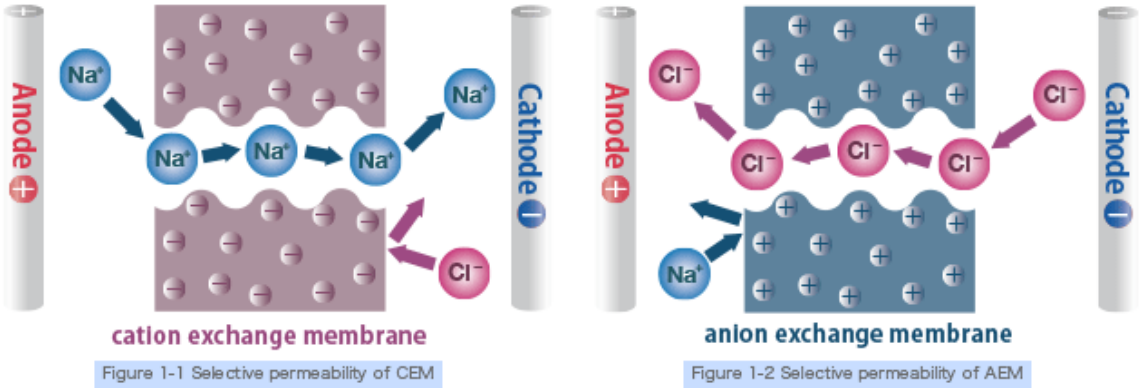

Figure 27: Illustration of the operational mechanism of ion exchange membranes used for electrodialysis [147].

The properties of ion-exchange membranes are determined by different parameters, such as the density of the polymer network, the hydrophobic or hydrophilic character of the matrix polymer and the type and concentration of the fixed charges in the polymer, and the morphology of the membrane itself. Properties such as high permselectivity, low electrical resistance, good mechanical and form stability, high chemical and thermal stability, and low production costs are the most desirable in ion-exchange membranes.

Recent advancements in electrodialysis have focused not only on traditional ion exchange improvements but also on hybrid system integration for enhanced energy efficiency. For instance, Ryu et al. [148] demonstrated a coupled electrodialysis–capacitive deionization (ED-CDI) system, where capacitive electrodes selectively removed monovalent ions before ED processing. This approach reduced the load on the ED stack, thereby lowering the total energy consumption of the system by up to 30% in brackish water desalination trials. Their results suggest that combining ED with complementary technologies may offer a pathway to low-energy desalination systems for specific feedwater compositions. Similarly, Gomez-Montano et al. [149] investigated the use of custom-designed 3D-printed spacers within ED membrane stacks to optimize fluid dynamics and ion transport. These spacers were shown to reduce pressure drop and enhance ion mobility across the membranes, resulting in higher desalination efficiency and lower energy consumption compared to conventional spacer geometries. Their findings highlight the scalability and adaptability of modular ED designs, which could be tailored for specific industrial or decentralized water treatment applications. These recent developments underscore a trend toward the modularisation and hybridisation of electrodialysis systems, aiming to improve ion selectivity and operational efficiency while reducing energy demands in real-world desalination applications.

In this chapter, the effects of operating conditions such as time, concentration, flow rate, pH, and power, in water treatment by an experimental ED cell are reported.

As in the previous chapter, 2l of solutions of NaCl, $MgCl_2$, and $CaCl_2$ were analysed to determine the percentage rejection of the membrane. Synthetic and natural seawater were also used as feeds to study the rejection of calcium and magnesium ions in a multi-ionic system such as seawater.

Concentrations of Ca and Mg ions, like those observed in sea water, were used in these filtration experiments. That is 1295mg/l of Mg from $MgCl_2$ and 416 mg/l of Ca from $CaCl_2$. Experiments involving the two salts, as well as a mixture of the salts, were carried out.

During the experiments, conductivity measurements from dilute and concentrate streams at various intervals were taken to determine the salinity and rejection of the ions at such times.

Calculations

R is the rejection in percentage and is defined as the following

equation:

$$R\% = \frac{(Ci - Cf)}{Ci} \text{ x } 100$$

where C_i and C_f are the initial and final ionic concentrations of the solution.

5.4. Effect of Feed Concentration on Rejection

Rejections of ions were observed to be dependent on feed concentration. Feeds with higher concentration required longer rejection times than the lower concentration feeds. 416 mg/l Ca^{2+} required less time to actualise 95% rejection than 1295 mg/l Mg^2. Feed conductivity was measured to be 2.08 mS and 8.49 mS for Ca^{2+} and $Mg^{2+,}$ respectively. Again, as with the previous chapter, these concentrations are representative of their concentrations in seawater.

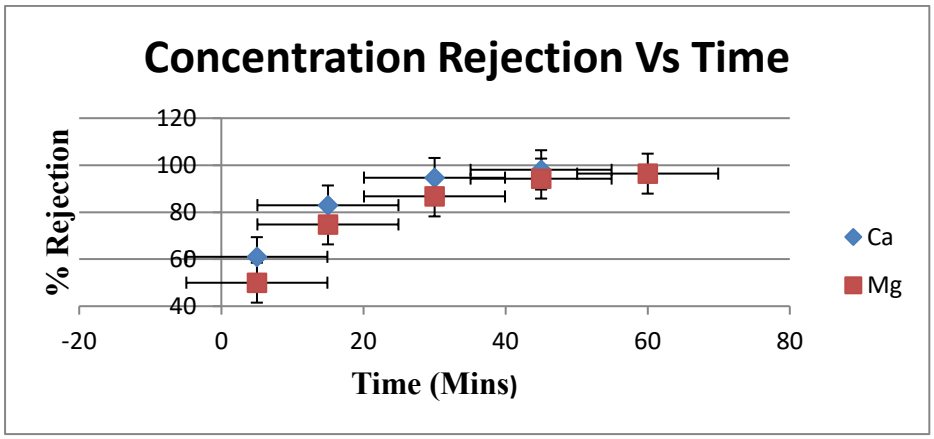

Figure 28: ED rejection of Ca and Mg ions with respect to time at 20^0C.

98% rejection of calcium ions was achieved in 45 minutes, while it took an hour to achieve a rejection of 91% for Mg ions. This suggests that rejection is dependent on concentration. High concentrations would require more time to achieve high rejection. This leads to a corresponding increase in the current requirement, which might affect operating costs.

Previous studies [147] involving ED desalination of various concentrations of NaCl showed the same trend. In the research, it took 17 mins to reduce 1g/l NaCl concentration by 50%. 90% rejection of 5 g/L NaCl took 60 mins, and for 10 g/L NaCl, it took 115 min to achieve 95% removal. However, in the experiments that involved feed salt concentrations of 20, 25, and 35 g/L NaCl, more time and voltage were required to desalt the solutions.

Again, the slight difference in rejection with respect to time could be explained by the higher concentration of magnesium than calcium. Ca^{2+} (Calcium) has a higher ionic mobility (6.2×10^{-8} $m^2/V \cdot s$) than Mg^{2+} (5.4×10^{-8} $m^2/V \cdot s$).

Higher mobility means Ca^{2+} migrates faster under an applied electric field, leading to quicker rejection in electrodialysis.

Mg^{2+}, being smaller but more hydrated, moves more slowly due to stronger water molecule interactions.

With 10,752mg/l of NaCl, observations in this experiment showed that higher concentrations of ions in the feed solution required a longer time of treatment. Again, this concentration of NaCl simulates that of sea water.

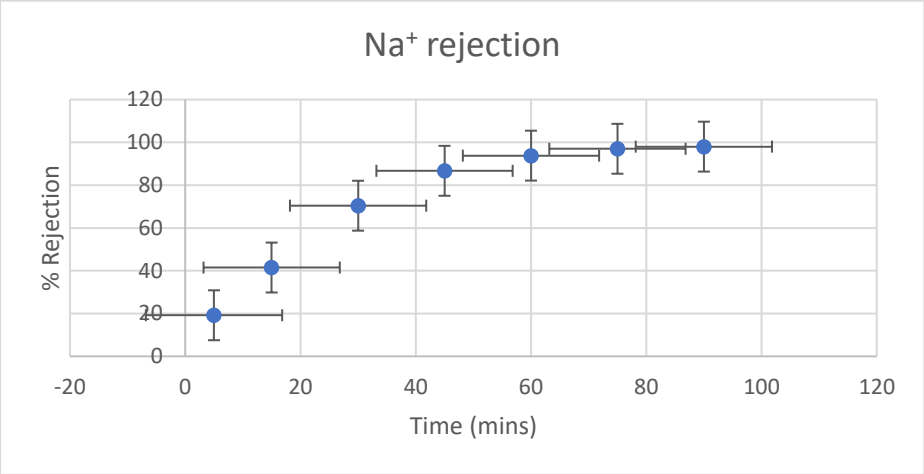

Figure 29: ED rejection of Na ions with respect to time at 20^0C.

From Figure 29, in a little over 15 minutes, the concentration of Na ions in the feed was reduced by 50%. This is like the results obtained by [147]. Ca^{2+} (Calcium) has a higher ionic mobility (6.2×10^{-8} $m^2/V \cdot s$) than Mg^{2+} (5.4×10^{-8} $m^2/V \cdot s$).

Higher mobility means Ca^{2+} migrates faster under an applied electric field, leading to quicker rejection in electrodialysis.

Mg^{2+}, being smaller but more hydrated, moves more slowly due to stronger water molecule interactions.

A similar trend was observed with the mixture of calcium and magnesium as shown in the figure below.

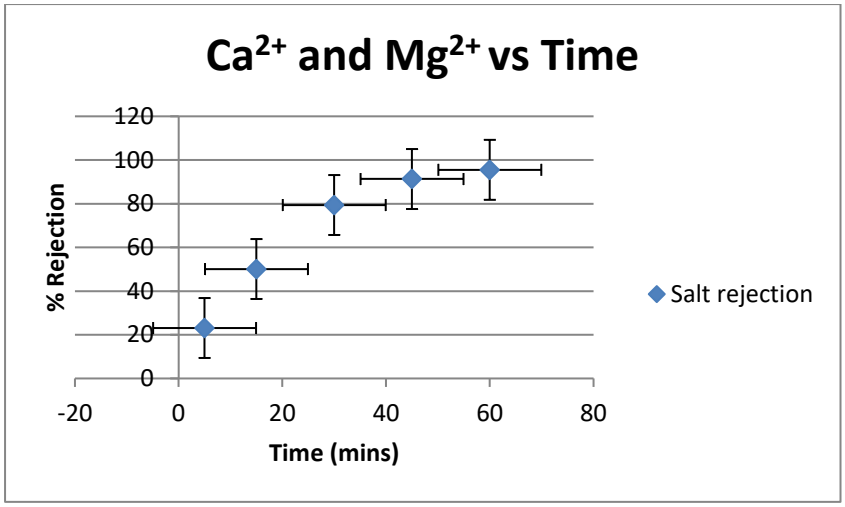

Figure 30: *Conductivity-measured* rejection of a binary mixture of Ca and Mg ions with respect to time using ED

Figure 30 above shows that it takes about an hour to achieve 98% rejection of both ions from the feed.

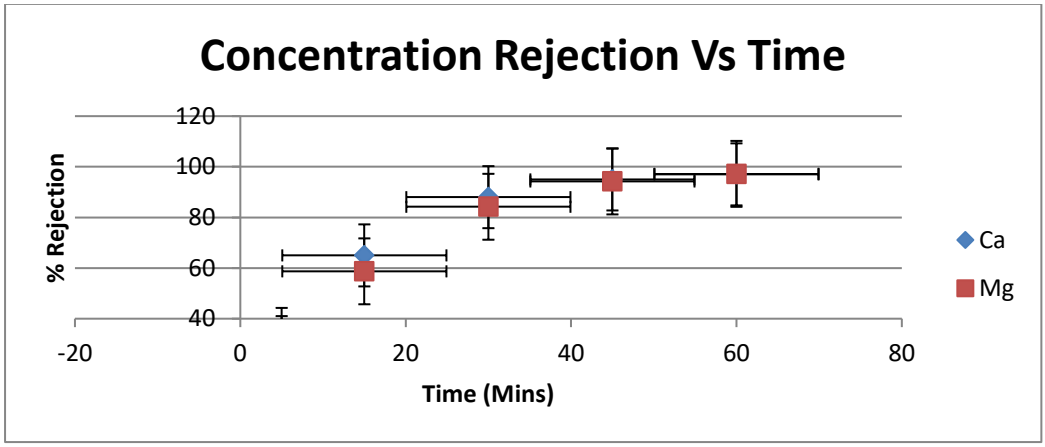

Figure 31: ED rejection of binary mixture of Ca^{2+} and Mg^{2+} ions with respect to time

Figure 31 above shows the rejection of the distinct ions in the solution.

Experimental results for the binary ion mixture showed a reduction in rejection efficiency for both ions compared to their solutions. Specifically, while 98% of calcium ions were rejected within 45 minutes and 95% of magnesium ions were rejected within 73 minutes in their respective single-ion solutions, it took 60 minutes to achieve 97% rejection for the mixed solution.

This reduction in rejection kinetics can be attributed to the presence of multiple competing ions, which may hinder the transport of individual species through the membrane. Additionally,

ion interactions, charge shielding effects, and potential membrane fouling due to deposit formation could contribute to the observed decrease in separation efficiency as the process progresses.

Experiments with synthetic sea water again showed the same trend.

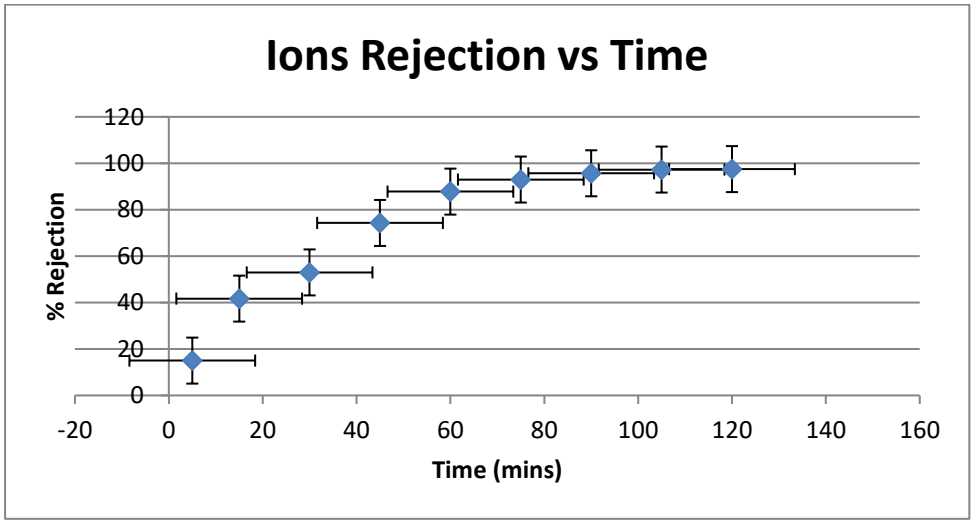

Figure 32: Conductivity measured rejection of ions in synthetic seawater with respect to time at 20^0C.

From Figure 32, it is seen that after an hour of operation, 87% rejection of all the cations was observed. However, it takes 2 hours to achieve 97% rejection of all the cations. An interesting trend that can be observed here is that the rates of exchange of cations are reduced with time. For instance, after 5 minutes, 15% of the ions were exchanged in the process. 10 minutes later, this number had more than doubled to 41%, representing an over 100% increase in rejection rate. After an hour, 87% rejection of the TDS has been achieved. At that point, the rejection rates began to drop as a further 15 minutes of operation produced just 93% rejection, and the next hour produced just about 97% rejection. In other words, the rate of ion exchange increases initially until about an hour of operation, after which a decline gradually sets in. Again, this can be explained because of membrane deposits as the operation progresses.

Rejection of Ca^{2+} and Mg^{2+} slightly decreased in the presence of other ions such as Na^{+}, K^{+} and Strontium in seawater, and the distinct rejections for the respective ions were the same. In 45 minutes, 95% of hardness has been removed from the feed seawater, as indicated in Figure 5.6.

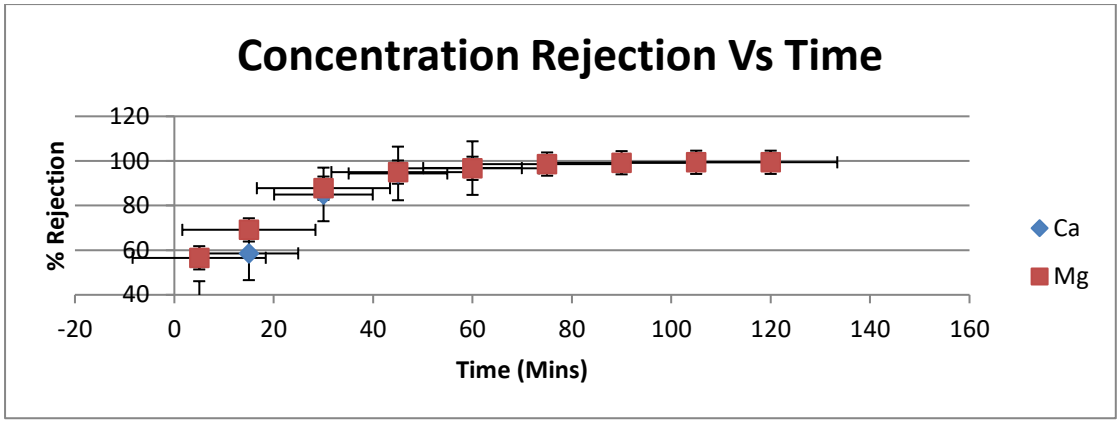

Figure 33: Concentration-measured rejection of hardness in synthetic seawater with time using ED

In comparison with the binary mixture, this figure is slightly less, given that 98% of hardness was removed after 45 minutes.

Experiments with real seawater indicated the same behaviour as with synthetic seawater.

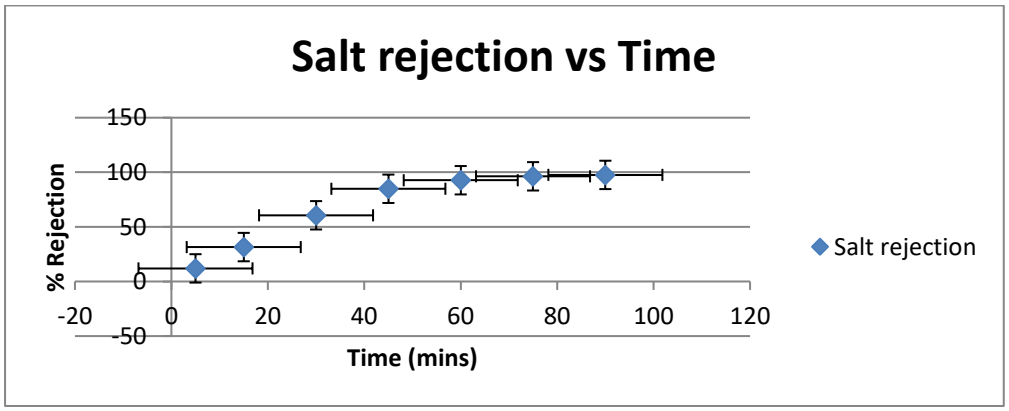

Figure 34: Conductivity-measured rejection of ions in real seawater with respect to time by electrodialysis

The rejection values in Figure 34 were obtained using conductivity values for the diluate at the various times of operation. It could again be inferred that synthetic seawater showed the same electrodialytic behaviour as real seawater. The rejection rates of the real seawater are slightly higher than those obtained for the synthetic seawater, despite having slightly more TDS, as detected through the conductivity measurements of the feed seawater. The conductivity measurements taken at 20^0C are 41.4mS and 47.3mS for synthetic and natural sea water, respectively. For instance, the concentration of Ca^{2+} and Mg^{2+} in the two feed sea water samples differed. The real sea water has less calcium (367mg/l) and magnesium (442mg/l)

than the synthetic seawater, which has 416mg/l calcium and 1295mg/l of magnesium. From figure 34, in 30 mins, 60% of the TDS was removed, while 97% TDS was removed in 90 mins.

5.5. Effect of pH on ion exchange

The pH of the synthetic seawater was slightly increased from 7.5 to 8.5, and the resultant effect is a slight reduction in rejection rates.

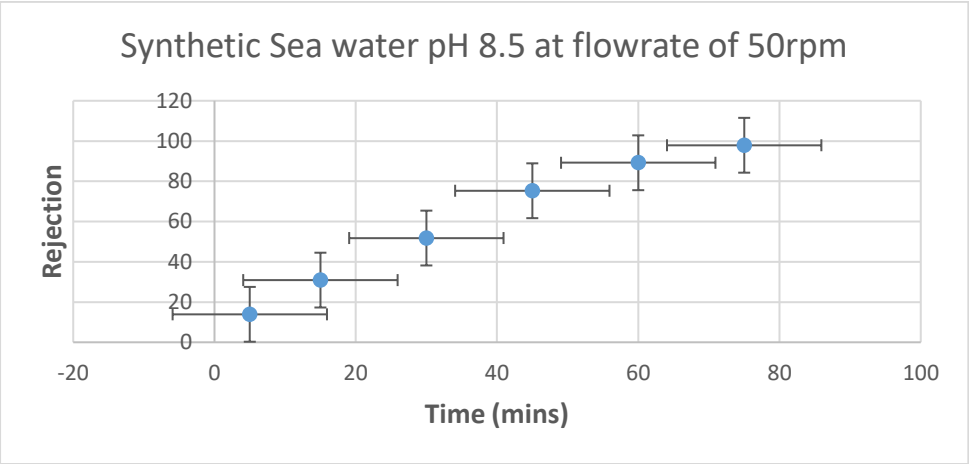

Figure 35: Conductivity-measured rejection of ions in seawater of pH 8.5 with respect to time.

In 30 minutes, only 36% of the total dissolved solids (TDS) were removed when the pH was increased to 8.5, as shown in Figure 5.8. This contrasts with a 53% rejection achieved at the same time for seawater at pH 7.5. Furthermore, after 75 minutes, approximately 86% rejection was achieved at pH 8.5.

This trend may be attributed to changes in the physical and electrochemical properties of the ion-exchange membrane. At higher pH levels, membrane swelling can occur due to increased hydration of functional groups, potentially expanding pore sizes and reducing the membrane's selectivity. This results in an increased flux but reduced rejection, as more ions can pass through.

Additionally, increasing pH leads to a higher concentration of hydroxide ions (OH^-) in the system, which affects ion interactions. In this experiment, NaOH was used to adjust the pH of seawater. The increased OH^- concentration enhances the negative charge on the membrane surface, altering electrostatic interactions. This can reduce the rejection of positively charged ions due to reduced electrostatic repulsion, allowing more cations to pass through.

Ion-exchange membranes used in electrodialysis (ED) typically consist of a polymer matrix with functional groups firmly attached to the pore walls. These functional groups play a crucial role in ion selectivity and transport within the system.

These functional groups are capable of dissociation when placed in aqueous surroundings. For instance, sulphonic or carboxylic acids, which are capable of being deprotonated and are characteristic of cation exchange membranes. The mobilities of these bound groups are often one, and they are assumed to be distributed uniformly throughout the membrane.

When an exchange membrane carrying an anionic group such as $-SO_3H$, or $–CH_2\ N^+R_3Cl$, is immersed in water, it swells sufficiently such that the ionisable group will release the small counter ion, e.g., H^+ or Cl^-, while the oppositely charged group, known as the fixed ion, remains covalently bonded to the skeleton. When the membrane is placed in an aqueous electrolyte, some salt will enter the membrane. The sorbed ions, which have a charge that is like the fixed ions, are called co-ions. The concentration of these co-ions increases with the concentration of the electrolyte.

When an electrical current is passed through the membrane, these counter ions can enter it from one side and leave it from the other side. These movements result in the formation of a concentration gradient. The swelling of membranes when placed in electrolyte solutions occurs throughout their structure because of the binding of the water of hydration. The insertion of the water among the ions enables some counter ions to diffuse away from the fixed ions, thereby creating an osmotic pressure which draws more water into the membrane and increases the swelling. An equilibrium is eventually reached when the polymer chain's internal elastic forces are balanced by osmotic pressure forces.

At low pH, it is assumed to have a high proton concentration in the solution, leading to the protonation of the functional groups on the active parts of the membrane, making the charge of the membrane positive. Conversely, at high pH, due to the low proton concentration in the solution, resulting in the de-protonation of these active parts, the membrane becomes more negative. Hence, allowing more positive ions to pass through it by electrostatic interactions and resulting in lower rejection values.

5.6. Effect of flow rate on separation

The flow rate of the synthetic seawater feed was slightly elevated to 60 rpm from 50 rpm to study the effect of flow rate separation. The initial flow rate was 50 rpm.

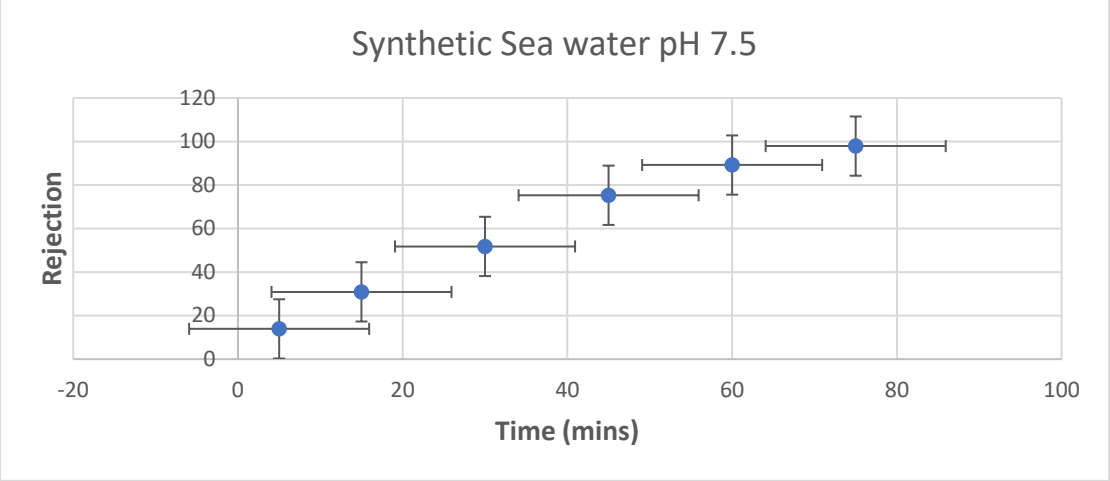

Figure 36: Effect of flow rate of 60 rpm on the separation of ions in seawater at 20^0C.

As can be seen from the figure, at constant concentration and temperature, an increase in flow rate increased the cell performance when compared with the values obtained with a flow rate of 50 rpm in Figure 36. At the increased flow rate of 60 rpm, 97% removal of the TDS was observed just after 75 minutes of operation. This shows an increase in the cell performance, given that it took 2 hours to achieve the same level of rejection at a lower flow rate of 50 rpm. This is because an increase in the feed velocity leads to increased separation. The same trend is observed with an increase in pH.

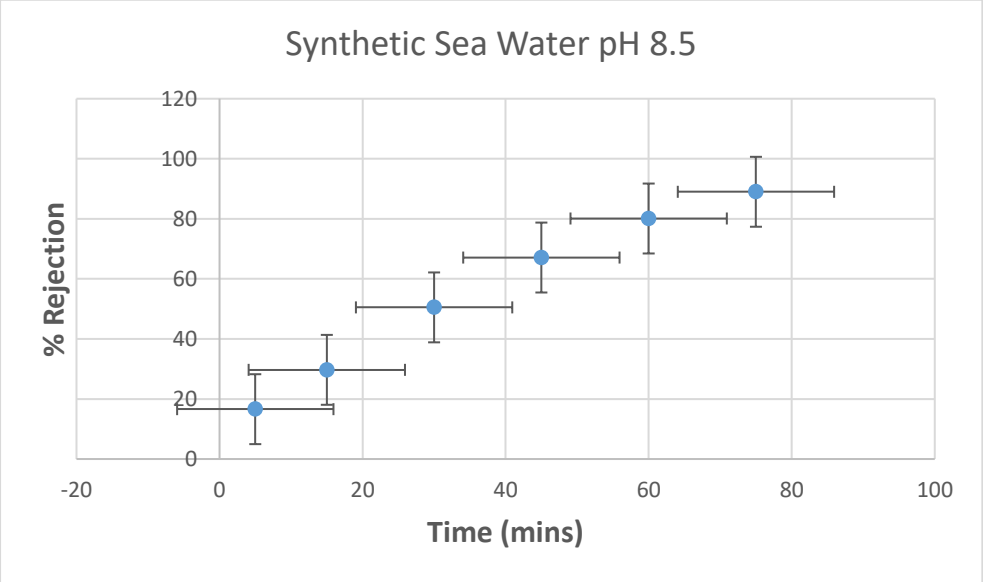

Figure 372: Combined effect of flow rate on ED separation at a flow rate of 60 rpm and pH 8.5

From figure 37, it can be inferred that increasing the flow rate resulted increase in rejection, but this was again hampered by an increase in pH to 8.5, where the flow rate was 50 rpm. 75 mins of operation produced 89% removal of TDS.

Operational flow rate is important because it plays a vital role in the efficiency as well as economic evaluation of the system. At 50 rpm, the flow rate is 0.1L/m. This means that 0.1 L of permeate is produced in one minute, or 6 L of pure water is produced in an hour. At 60 rpm, the output flow rate is 0.12L/m of pure water.

5.7. Effect of operational current on ED permeability

In ED, the applied current determines the potential gradient, which in turn influences the ion permeability. The relationship between the applied current and the rejection is studied in this experiment.

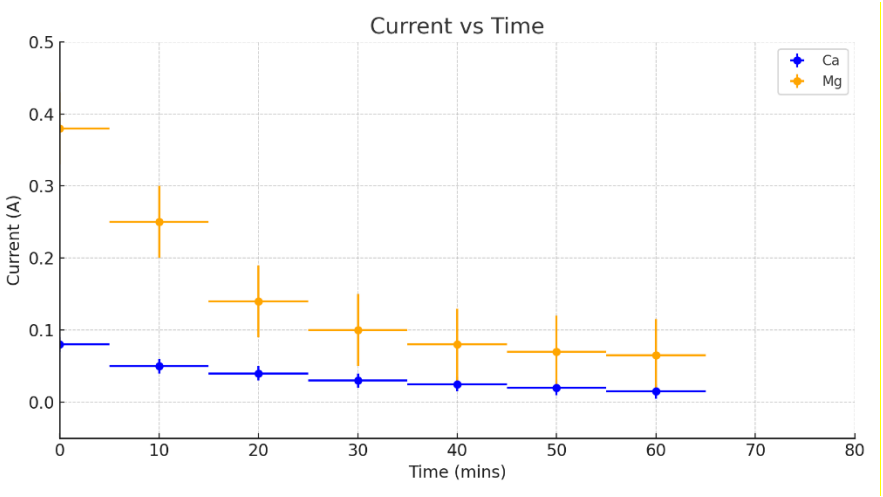

Figure 383: Effect of time on applied current on ED rejection of Ca^{2+} and Mg^{2+} at 20^0C and 50 rpm flow rate

It was observed that the applied current decreases over time. Figure 38 also shows that the effect of the applied current diminishes as the separation process progresses. This can be attributed to the relationship between feed concentration and current demand. As the concentration of ions in the diluate decreases, the applied current also decreases.

This trend can be explained by the fact that a higher ion concentration in the feed requires a greater electrical driving force to sustain ion migration. As the concentration of ions in the solution decreases, the electrical resistance increases, resulting in a lower applied current.

For the experiment with Ca^{2+} (416 mg/L), the initial applied current was 0.17 A, which dropped to 0.01 A after 45 minutes. In contrast, for Mg^{2+} (1295 mg/L), the initial applied current was 0.62 A, which is higher than that of calcium due to the greater ion concentration in the feed solution. After an hour of operation, the current decreased to 0.06 A.

.

The same trend is observed with the experiments involving binary mixture, synthetic, and real sea water.

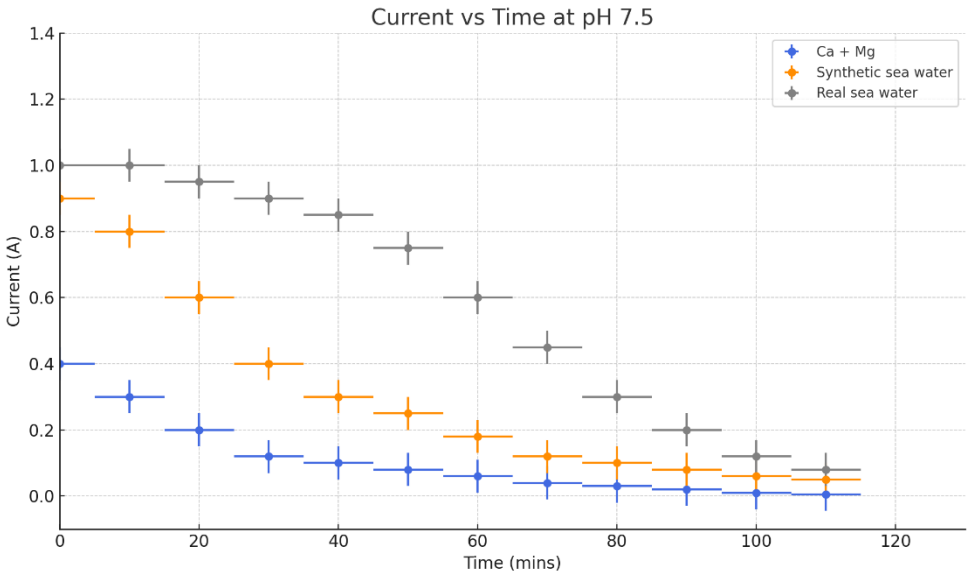

Figure 394: Effect of time on applied current on ED rejection of mixture of Ca^{2+} and Mg^{2+}, synthetic and real seawater at 20^0C and 50 rpm flow rate

From Figure 39, a current of 1 amp was applied at the start of each of the experiments involving seawater, while 0.3 amp was applied for the binary mixture. The concentration of ions in seawater is higher than that of the mixture of Ca^{2+} and Mg^{2+}. Hence higher operating current is required for the experiments involving seawater. However, current decreases with a decrease in time in each of the experiments. A further illustration of the relationship between current and rejection is shown in the figures below

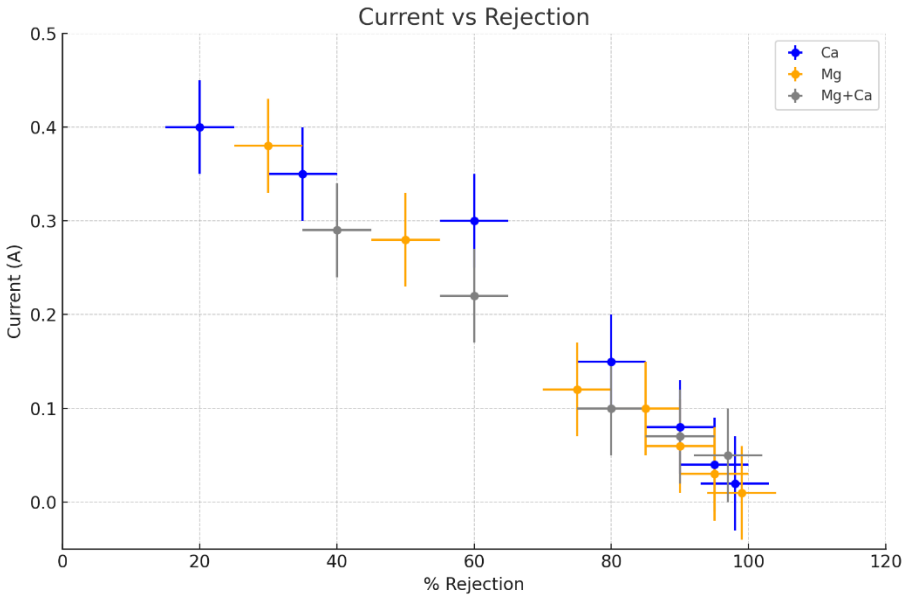

Figure 40: Relationship between current and Rejection of Ca^{2+}, Mg^{2+}, and mixture of Ca^{2+} and Mg^{2+} at 20^0C.

After 5 minutes, the decrease in salt concentrations slowed for each experiment, which was accompanied by a smaller incremental drop in the current between the two electrodes. This can be attributed to both concentration polarization in the membrane boundary layer and depletion of electron carriers in the diluate. Concentration polarization refers to the existence of concentration gradients at the membrane boundary layer, resulting from ion exchange through the membrane due to electric current. When this occurs, the electric potential in the membrane is reduced. Sufficient current is necessary between the electrodes for desalination to occur in an ED process. Therefore, as the current declines, the rejection continues to decrease until a minimum value is reached, beyond which no further rejection is observed. This behaviour is characteristic of concentration polarization, a major limiting factor in electrodialysis performance. As ions accumulate at the membrane surface, a concentration gradient forms between the membrane interface and the bulk solution. This gradient reduces the effective driving force (electric potential) across the membrane, thereby lowering ion transport efficiency. As a result, the applied current becomes insufficient to sustain ion exchange, leading to a gradual decline in ion rejection. Once the limiting current density is reached, further increases in voltage do not enhance ion removal, and rejection plateaus. This phenomenon underscores the importance of optimizing operating parameters to minimize concentration polarization and maintain effective separation.

From Figure 40, a slightly linear relationship between rejection and current can be observed. Calcium had an initial feed concentration of 416 mg/l and required an initial current of 0.17 amp at the start of the experiment. As the concentration of Ca ions decreased in the diluate, the current continued to drop until 95% of the ions were removed, reaching the lowest value of 0.01 amp. Similarly, magnesium, with an initial feed concentration of 1295 mg/l, required 0.37 amp, nearly double the amount needed for calcium. This value decreased until the maximum rejection of 91% was achieved, at which point the value was 0.06 amp. At this lowest value, further rejection could not be attained.

Experiments involving the binary mixture of Ca and Mg ions showed a similar trend. A higher combined concentration of ions in the feed solution meant the initial required current was 0.39 amp. Again, an increase in rejection resulted in a decrease in the required current between the electrodes. At 95% rejection, the current dropped to a minimum value of 0.4 amp. No further rejection was observed beyond this value.

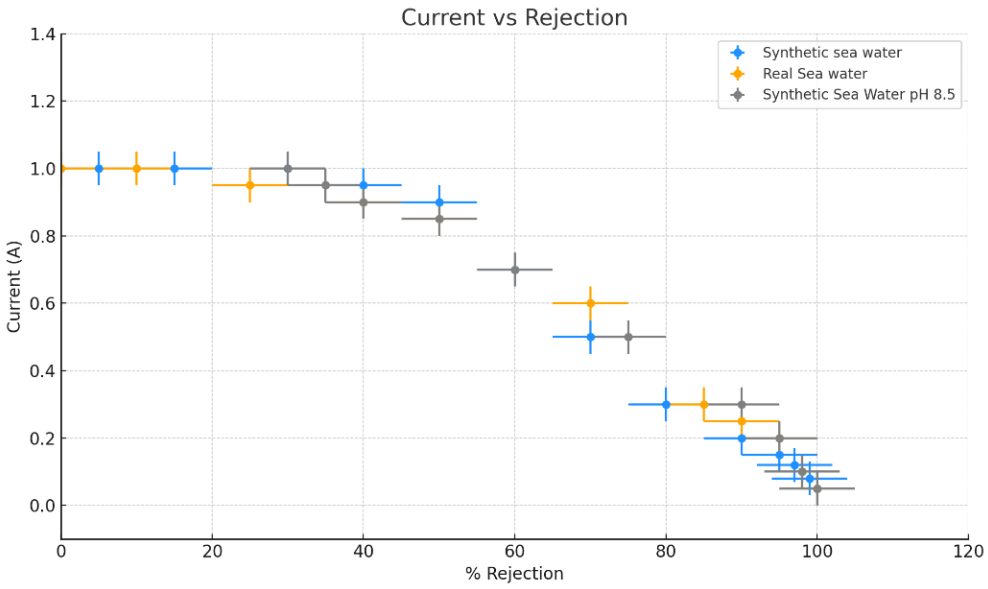

Figure 415: Relationship between current and Rejection of ions in synthetic sea water at pH 7.5 and 8.5 and real seawater at 20^0C.

Higher concentration of ions in the feed seawater meant the initial current was 1 amp for each of the experiments. The maximum rejection value for the synthetic and real seawater was 97%. At those points, the value of the final current was 0.07 amp and 0.09 amp, respectively, because of a decrease in concentration of the diluate. An increase in pH made a very slight difference in the current requirement and performance, as can be observed from the figure.

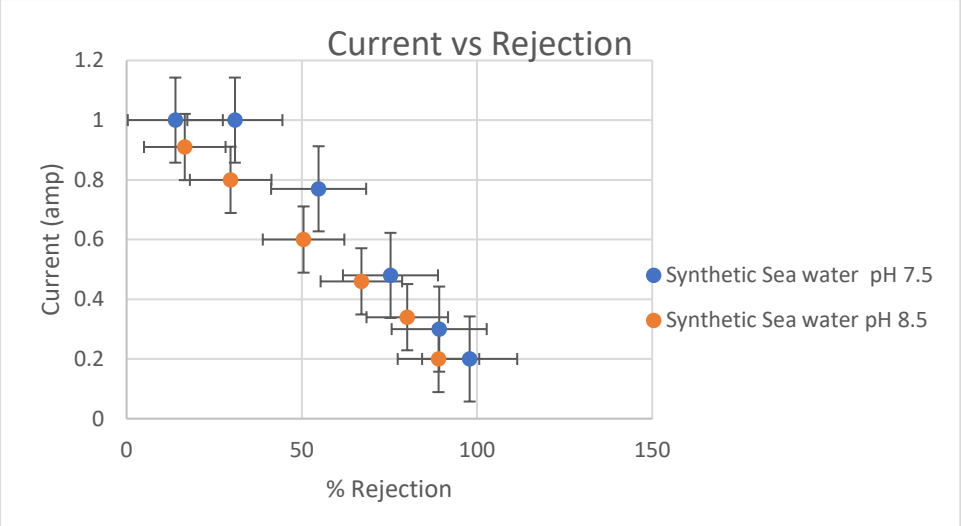

Figure 42: Relationship between current and Rejection of ions in seawater at a flow rate of 60 rpm at 20^0C

From Figure 42, when the flow rate was increased to 60 rpm, the same trend (which is a decrease in power with an increase in rejection) was observed. However, a slight increase in pH resulted in slightly lower current requirement.

5.8. Energy Consumption Comparison

Nanofiltration vs Electrodialysis: Energy efficiency is a critical factor in membrane-based desalination processes. Typical nanofiltration (NF) systems treating brackish water consume approximately 0.5 - 1.5 kWh/m³ [150], while electrodialysis (ED) systems operate at around 1.0 - 2.5 kWh/m³, depending on feedwater salinity and system configuration.

Although ED can achieve high ion selectivity, its energy requirements increase significantly with rising feedwater salinity, narrowing its advantage in seawater treatment. NF, on the other hand, benefits from high water permeability and lower pressure operation, resulting in relatively lower energy consumption at comparable salt rejections. This study's findings are consistent with these trends, highlighting that process selection should consider both energy cost and final water quality requirements.

5.9 Conclusion

Electrodialysis (ED) results showed up to 97% TDS removal within 75 minutes. This aligns with documented removal efficiencies for ED processes, which range from 60–98% for divalent and monovalent ions, depending on runtime, membrane type, and solution concentration [151].

An investigation into the desalination of water using electrodialysis was made. This included studying ion exchanges with Na^{+}, Mg^{2+}, Ca^{2+}. A mixture of Ca^{2+} and Mg^{2+} ions, as well as synthetic and real seawater, was also investigated. Effects of operating conditions such as concentration, current, flow rate, and temperature were also studied.

The concentration of the feed influences the rejection and the operational time of the procedure. Feeds with higher concentration require more time for near-complete exchange to take place. Ca^{2+}, which had the least concentration, required the least operational time. On the other hand, synthetic and natural seawater with higher concentrations required more time to achieve the same degree of ion exchange. This will influence the economics of operating a larger-scale desalination plant.

Monovalent ions, such as Na^{+} ions, tend to have a shorter operational time than divalent ions.

An increase in pH results in reduced rejection rates of the seawater. pH affects the physical properties of the membrane as well as increases the concentration of ions in the feed seawater. Therefore, feed samples with higher pH would require more time and energy to desalinate than neutral feeds.

Furthermore, feed concentration influences the applied current. Higher feed concentration results in higher operating current requirements. This will also affect the economics of operating the process. The current also decreases as the concentration of ions in the feed decreases. This continues to a point where there is no further incremental decrease observed for the current concentration of ions in the solution.

Increasing the flow rate increases rejection and consequently decreases operational time. The flow rate of the seawater was increased from 50 rpm to 60 rpm, which increased the output flow rate by 20ml/min.

However, the drawbacks of electrodialysis, as observed in this study, are that the procedure is not capable of removing inorganic materials as well as microorganisms from seawater.

Secondly, from an economic point of view, the production rate of pure water from seawater is low in comparison with NF membrane filtration.

CHAPTER SIX

NOVEL SURFACE MODIFICATION OF THIN FILM COMPOSITE NANOFILTRATION MEMBRANE BY PLASMA

Chapter 5 presented a study on the use of Electrodialysis for the desalination of seawater. However, as seen from Chapter 5, ED requires a lot of energy, which could affect the cost of operation. Furthermore, ED is not capable of removing microorganisms and organic materials because the membranes only work on the principles of ion exchange. Hence, the further search for an alternative novel, cost-effective method of seawater treatment.

In this chapter, surface modification of nanofiltration membrane using oxygen plasma is reported. The resultant membrane is applied in desalination experiments, and the results are reported.

6.1 Introduction

As discussed in Chapter 2, modification methods are being developed to improve membrane performance in terms of flux, rejection, and anti-fouling properties. Generally, membranes are categorized by pore size, structure, and separation mechanisms. For example, microfiltration (MF) and ultrafiltration (UF) membranes, with their large pores as well as high permeate flux, are used widely for primary treatment. Nanofiltration (NF) and reverse osmosis (RO) membranes, on their own, are used to achieve rejection of ions and organic materials under high-pressure-driven conditions as discussed earlier in Chapter 2. Industrial and academic interest in NF and RO membranes is rising because of the development of high-performance thin-film composite (TFC) membranes.

TFC membranes are composed of a polyamide (PA) thin-film layer (for selective separation of substances) and a polysulfone (PSU) substrate layer (for mechanical strength). Current studies are focused on either replacing each layer with other materials or modifying the layers for better stability and performance. However, because the PA thin-film layer in many TFC membranes largely controls the membrane performance, which includes permeate flux, solute rejection, and fouling, it is important to understand how the performance of the PA thin-film layer could be further improved.

In many applications, the choice of polymers is based on certain favourable bulk properties, such as thermal stability, mechanical strength, or solvent resistance. However, the surface characteristics of the selected polymer can be less than optimal, in terms of fouling control, for

instance, which establishes the importance of surface modifications of polymers [152]. To improve the surface characteristics of a membrane, surface modification via plasma treatment can be used.

Upon attainment of enough energy, a gas can be excited into the plasma state. This plasma is a partially ionized consisting of mixture consisting of ions, electrons, excited species, as well as free radicals [152], neutral atoms, light quanta, and molecules in the ground state and in any excited states. Plasmas can be divided into two categories, which are non-polymer-forming plasmas and polymer-forming plasmas. Non-polymer forming plasma consists of simple gases, such as N_2, H_2, O_2, and noble gases, while the polymer forming plasmas comprise almost all organic molecules that are capable of conversion into a vapour phase. These molecules, such as ammonia, methane, and ethanol, can then be polymerized under plasma conditions.

Plasma surface treatment refers to a plasma reaction that either alters the molecular structure of the material surface, or atomic substitution within the material, or atomic deposition on a substrate material. Plasma treatment is a useful tool in the modification of surface properties. Currently, more and more attention is being given to its applications in membrane separation science [152]. The accelerated electrons generated from the plasma possess sufficient energy to cleave the chemical bonds in the membrane structure to form macromolecule radicals. This operation subsequently initiates graft copolymerization [153]. Plasma treatment can be achieved by either regular plasma treatment [154,155] or plasma graft copolymerization (PGC) [156]. Highly surface-selective low-temperature plasma techniques have been used to modify various types of membranes, specifically to achieve the reduction of protein–surface attractive interaction, which is effective against fouling. For example, simple inert gas [157,158], nitrogen or oxygen plasmas have been used to increase the surface hydrophilicity of membranes [159], and ammonia plasmas have successfully yielded functionalized PSf membranes [160]. Improved hydrophilicity increases membrane flux. Furthermore, studies involving a water plasma treatment that renders asymmetric PSf membranes permanently hydrophilic have been reported [161]. This technique was also successfully applied to PES membranes as well as polyethylene membranes [162]. Ar-plasma treatment followed by graft copolymerization with acrylamide in the vapor phase was used to render PES membranes highly hydrophilic. Reports showed that the grafting yield for polyacrylamide on the membrane surfaces increased nearly linearly with the Ar-plasma pre-treatment time, with the grafting yields (GY) higher than 100μg/cm^2. The membranes obtained a permanent hydrophilicity. There was almost no change in contact angle after 1 year. BSA adsorption was reduced to less

than half that of the initial membrane (306 to 148µg/cm2), thus significantly reducing membrane biofouling.

Exposing a polymer to non-polymer-forming plasma results in a reaction with the plasma-activated gas, creation of free radicals in the polymer, and/or physical ablation. Plasma polymerization results in ultrathin coatings or surface-modified layers. In some cases, when the polymer is exposed to plasma for a longer time, deposition of vaporized polymer elements takes place. Plasma modification can be used to change the surface properties of membranes for application in several filtration processes, including gas separation, microfiltration, ultrafiltration, and pervaporation, and has been the subject of numerous publications [163].

Further studies [163] have reported the use of oxygen plasma treatment to increase the hydrophilicity of UF membranes and combat fouling during the separation of water solutions containing protein molecules. This membrane fouling originates mainly from protein deposited onto membrane surfaces, and this decreases the permeate flux of the fouled membrane to about less than 5% of the initial flux and consequently increases the permeation time [164] of the process. Hydrophobic interaction between the membrane surface and protein molecules is one of the major causes of fouling [165-168]. Therefore, by modifying the membrane surface from hydrophobic to hydrophilic, the adsorption of surface protein molecules on the surface of the membrane can be reduced. This modification also makes the membrane easier to clean, because adsorbed protein molecules are more easily removed from the hydrophilic surface of the membranes.

Plasma surface treatment also alters the charge distribution on the surface of the membrane. And this is a useful factor for membrane separation, because separation is dependent on the charge on the membrane surface as well as the charge of the ions in the feed solution.

Oxygen plasma treatment is, therefore, a useful method for the modification of membrane surfaces from hydrophobic to hydrophilic. During this procedure, oxygen-containing polar groups are introduced to the membrane surfaces, and this alters the surface chemistry on the membrane surface.[169-171].

This chapter reports the surface modification of NF membrane with oxygen and ammonia plasma and its effect on flux and separation.

6.2 Results and Discussions

6.2.1. Oxygen Plasma Treatment

NF DK membranes were washed with deionised water and dried with an air blow gun. Henniker plasma HPT-200 machine was used for the surface treatment. The machine is a microprocessor-controlled benchtop plasma treatment system that is ideally suited to surface activation, cleaning, and modification of a wide range of materials, including polymers, metals, glass, and ceramics.

Under a vacuum, plasma source gas (O_2,) was introduced into the machine at 1 bar. The membrane was treated with the oxygen plasma for 1 min, 3 mins, 5 mins, and 20 minutes, respectively, at 100W power, gas flow of 20sccm. Oxygen gas was evacuated from the reactor after treatment. The treated membranes were removed from the reactor and stored in deionised water, ready for use.

6.2.2. Membrane Characterisation

FT-IR characterisation was carried out using the PerkinElmer Spectrum Two FT-IR spectrometer to study the addition of functional groups on the membranes by the plasma treatment. Contact angle measurement was also used to determine the effect of the treatment on its water permeability.

6.2.3. Membrane Performance tests

Pure water flux was carried out on the treated membranes using the cross-flow method. 416mg/l of Ca^{2+} from $CaCl_2$, and 1295mg/l of Mg^{2+} from $MgCl_2$ solutions were also filtered with the membranes. A mixture of the ions was also filtered in the experiments. The percentage rejection was determined by the electrical conductivity of the feed and permeates.

6.2.4. Contact Angle Measurements

The water contact angle was determined by a sessile drop method. A video capturing system was used to capture the droplet image. At least 10 measurements on the membrane were performed to minimize experimental errors.

The contact angles of all the treated membranes are given in the tabulated form.

Untreated Membrane	1 Min Plasma Treated Membrane	3 minutes plasma-treated membrane	5 minutes plasma-treated membrane
32.75^0	21.15^0	20.45^0	18.60^0

Table 2: Contact angle measurements of membranes

The results above indicate a decrease in contact angle for oxygen plasma-treated membranes. The contact angle of the untreated membrane was 32.75^0. Upon treatment with oxygen plasma for 1 min, the contact angle decreased to 21.15^0. This is approximately 11^0 differences. Treatment for 3 mins resulted in a further decrease by approximately 12^0, while 5 mins of treatment produced a difference of 14^0. This indicates an increase in hydrophilicity with time.

The contact angle of the water droplet decreased as plasma treatment time increased since hydrophilic functional groups, such as carboxyl and hydroxyl groups, were introduced on the surface of the hydrophobic NF membrane by oxygen plasma treatment [172]. A decrease in contact angle signifies hydrophilicity. And hydrophilicity increases with treatment time.

6.2.5. FT-IR Measurements

FT-IR spectra of the oxygen plasma-treated membranes as well as the untreated membrane.

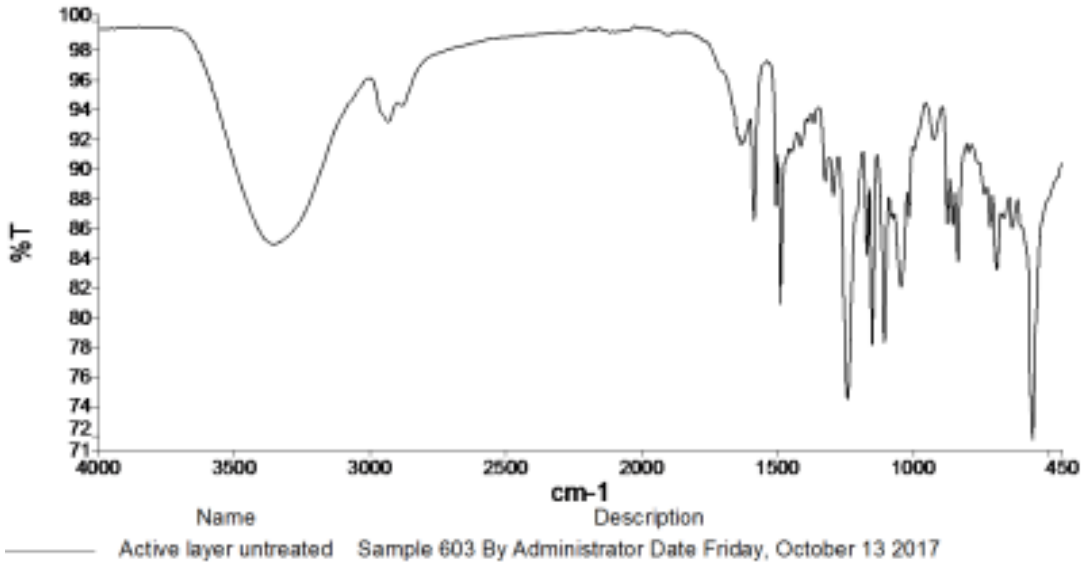

Figure 43: FT-IR spectra of untreated NF membrane

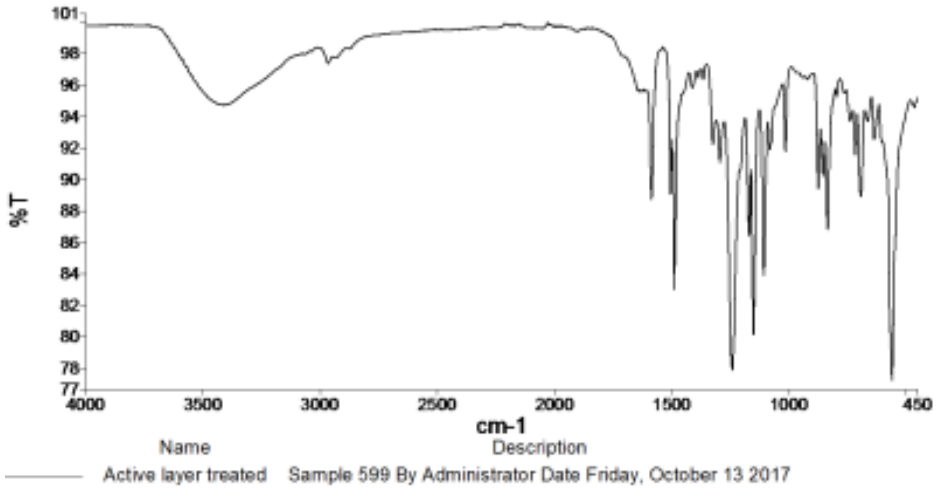

Figure 44: FT-IR spectra of 1 min oxygen plasma-treated NF membrane

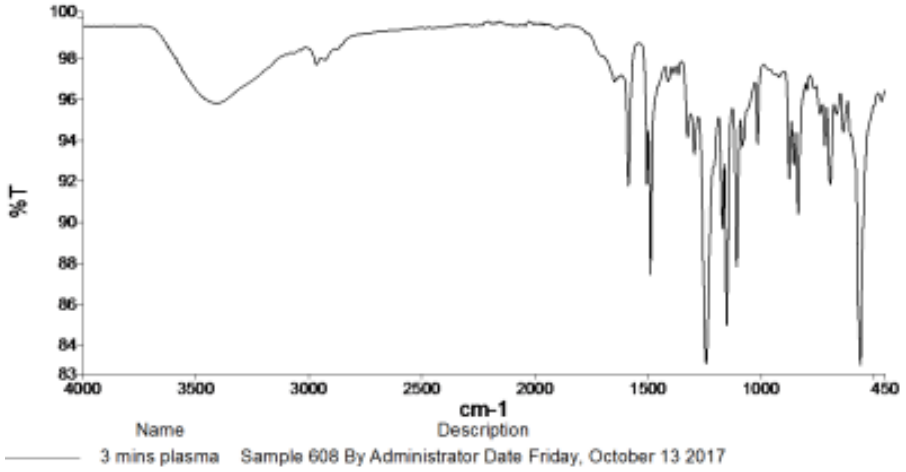

Figure 456: FT-IR spectra of 3 mins plasma-treated membrane

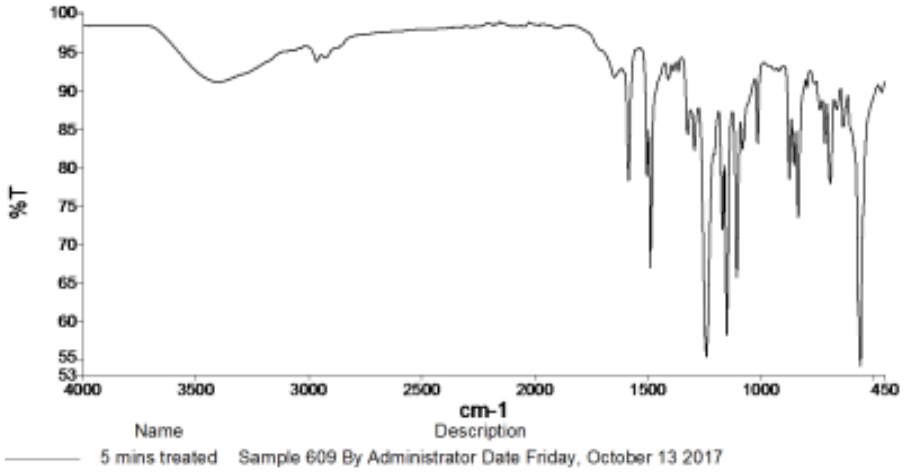

Figure 467: FT-IR spectra of 5 mins oxygen plasma-treated NF membrane.

Upon O_2 plasma treatment, the NF membrane is functionalized with oxygen-rich polar functional groups such as hydroxyl, carbonyl, or carboxyl. This treatment with oxygen forms peroxides on the membrane surface. The peroxides undergo further decomposition and form oxygen-containing radical groups, such as hydroxyls, carbonyls, or carboxyls. Gryta et al [173] treated laboratory-synthesized ultrafiltration polypropylene membranes with oxygen plasma to produce oxygen-enriched surfaces. X-ray photoelectron spectroscopy results from the research showed that the atomic ratio of oxygen to carbon increased from 2.8% to 23.3% after 9 min plasma treatment, compared to the untreated polypropylene membranes.

However, Figure 43 shows the infrared spectra of the untreated NF membrane. The peak in the region of 3400cm^{-1} is indicative of the amide functional group. A decrease in intensity of the N-H peak was observed upon treatment with oxygen plasma for 1 minute (Fig. 44). The transmittance increased from 84% (for the untreated membrane to 95%. A similar trend was observed for the 3 and 5-minute treated membranes, respectively. This indicates a reduction in the strong N-H bonds with oxygen plasma treatment as a result of the oxygen reacting with the polyamide to form a carboxyl functional group COO^-) on the surface of the membrane. The active layer of the membrane surface is made of polyamide. Reduction in Cross-Linking and Polyamide Density. Oxygen plasma can break down some amide (N–H) bonds in the polyamide layer, leading to partial degradation of the dense selective layer.

This decreases the membrane's selectivity, making it easier for certain ions to permeate, thereby lowering rejection.

Furthermore, XPS analysis concluded that the oxygen plasma-treated membrane surfaces contain carbon atoms that are doubly bonded (C—O) to oxygen and/or singly bonded (O–C—O) to oxygen [174]. This, therefore, is indicative of a correlation between the formation of oxygen-containing functional groups and the improvement of hydrophilic properties. The peak in the region of 3400 cm^{-1} is characteristic of N–H stretching vibrations from amide functional groups. Upon treatment with oxygen plasma for 1 minute (Figure 44), a decrease in the intensity of the N–H peak was observed, with transmittance increasing from 84% (for the untreated membrane) to 95%. A similar trend was observed for membranes treated for 3 and 5 minutes.

This indicates a reduction in strong N–H bonds upon oxygen plasma treatment, likely due to the oxidation of polyamide, leading to the formation of carboxyl ($–COO^-$) functional groups

on the membrane surface. Given that the active layer of the NF membrane is composed of polyamide, these chemical modifications suggest increased surface oxidation.

Furthermore, X-ray photoelectron spectroscopy (XPS) analysis by Tsai et al. [174] confirmed that oxygen plasma-treated membranes exhibit an increase in carbon atoms bonded to oxygen, either as doubly bonded carbonyl groups (C=O) or carboxyl-like structures (O–C=O). This correlation between oxygen functionalization and membrane surface chemistry suggests an enhancement in hydrophilic properties, which may improve membrane performance.

6.3. Pure Water permeation with time

The figures below show the pure water flux of the plasma-treated membranes.

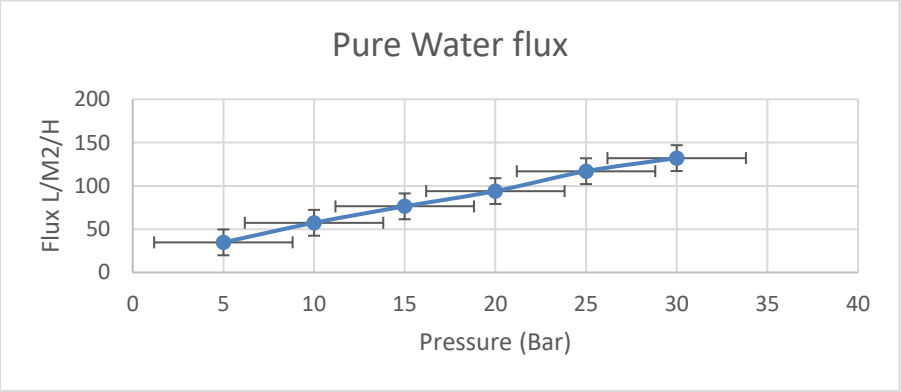

Figure 47: Pure water flux of 1-minute oxygen plasma-treated NF membrane with respect to pressure

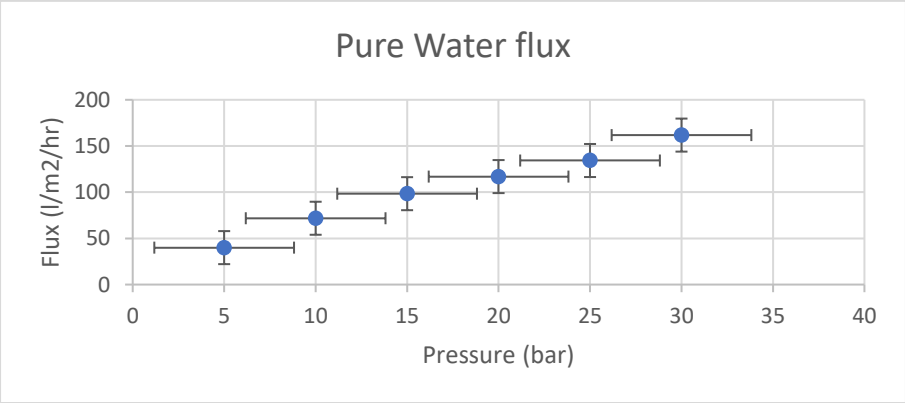

Figure 488: Pure water flux of 3-minute oxygen plasma-treated membrane with respect to pressure.

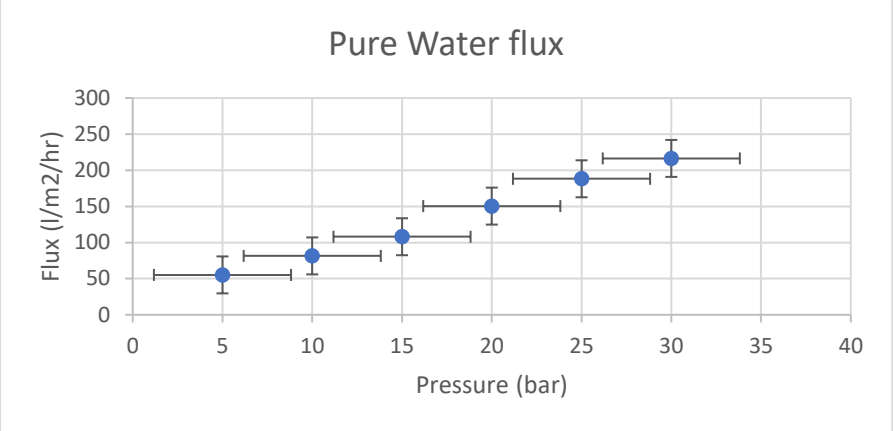

Figure 499: Pure water flux of 5-minute oxygen plasma-treated NF membrane with respect to pressure.

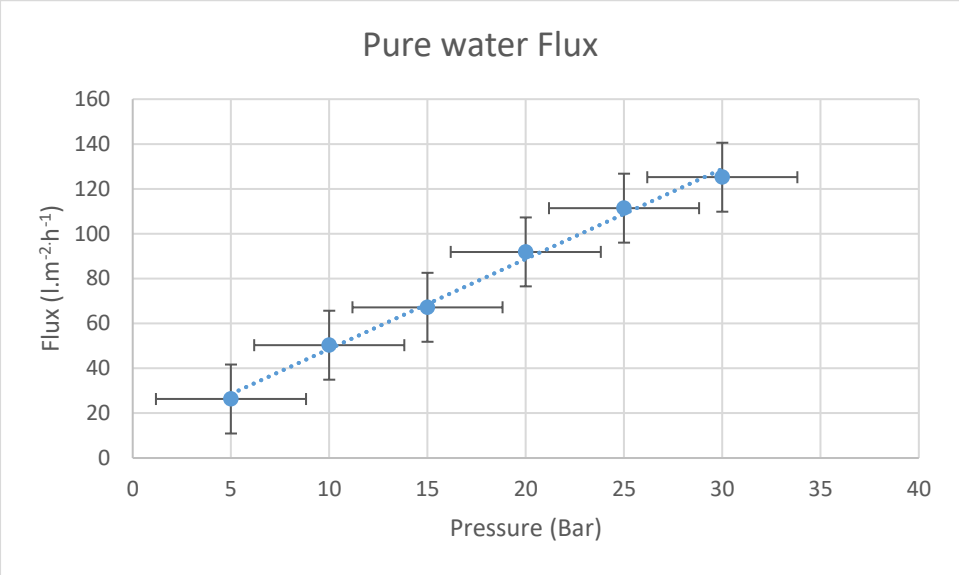

Figure 50: Pure water flux of the NF DK membrane with respect to pressure

From figures 47 - 49 above, the flow rate of pure water increased with plasma treatment time.

Pure water flux for the 1 min oxygen plasma-treated membrane was 7 $L.m^{-2}h^{-1}$ for 1 bar of pressure. A pressure of 5 bar produced a flux of about 35 $l\ m^{-2}h^{-1}$, while the highest flux of 132 $l\ m^{-2}h^{-1}$ was produced at 30 bar. This is against 26.3 $l\ m^{-2}h^{-1}$ for 5 bar and 125.2 $l.m^{2}.hr^{-1}$ for 30 bar observed for the untreated membrane in chapter 4. The average flux for the untreated membrane is 5 $l\ m^{-2}h^{-1}$.

There was a further increase observed with the 3-minute treated membrane. At 5 bars, the produced flux was 40 $l\ m^{-2}h^{-1}$, while the highest flux of 161 $l\ m^{-2}h^{-1}$ was produced at 30 bars. Similarly, a higher increase in flux was observed with the 5-minute treated membrane. 5 bars

of pressure produced 55 l $m^{-2}h^{-1}$ while 30 bars produced 216 l $m^{-2}h^{-1}$ of flux. This suggests that oxygen plasma treatment has rendered the NF membranes more hydrophilic and that the hydrophilicity of the membrane increases with treatment time.

6.4. Effect of Treatment on Salt Flux

Figure 50 below shows the relationship between salt flux and pressure for the three plasma-treated membranes

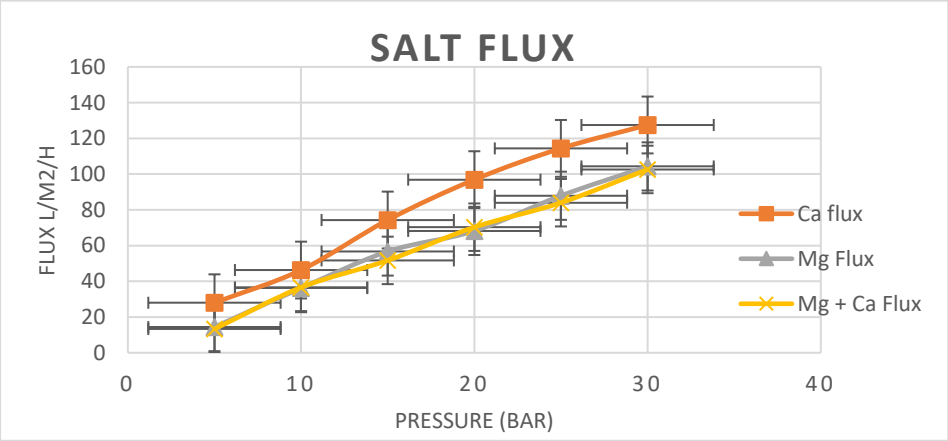

Figure 51: Permeation fluxes of 416 mg/l Ca^{2+}, 1295mg/l Mg^{2+}, and a mixture of Ca^{2+} and Mg^{2+} 1-minute plasma-treated NF membrane with respect to pressure.

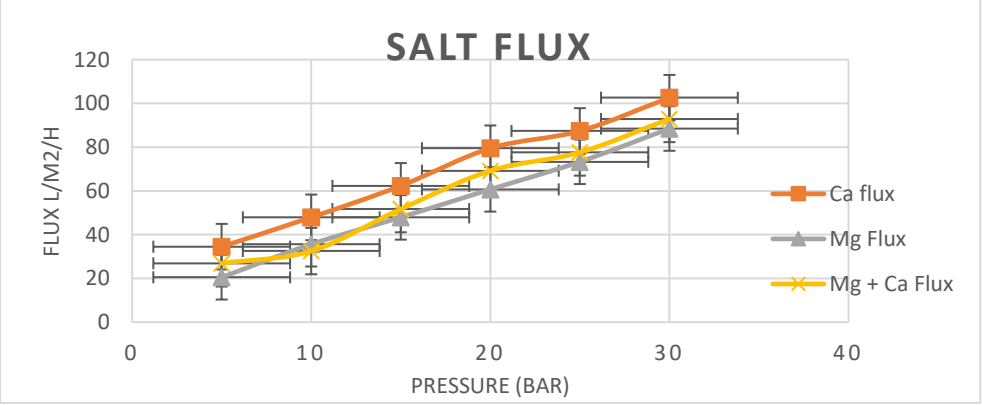

Figure 52: Permeation fluxes of 416 mg/l Ca^{2+}, 1295mg/l $Mg^{2+,}$ and a mixture of Ca^{2+} and Mg^{2+} for 3-minute oxygen plasma-treated NF membrane with respect to pressure.

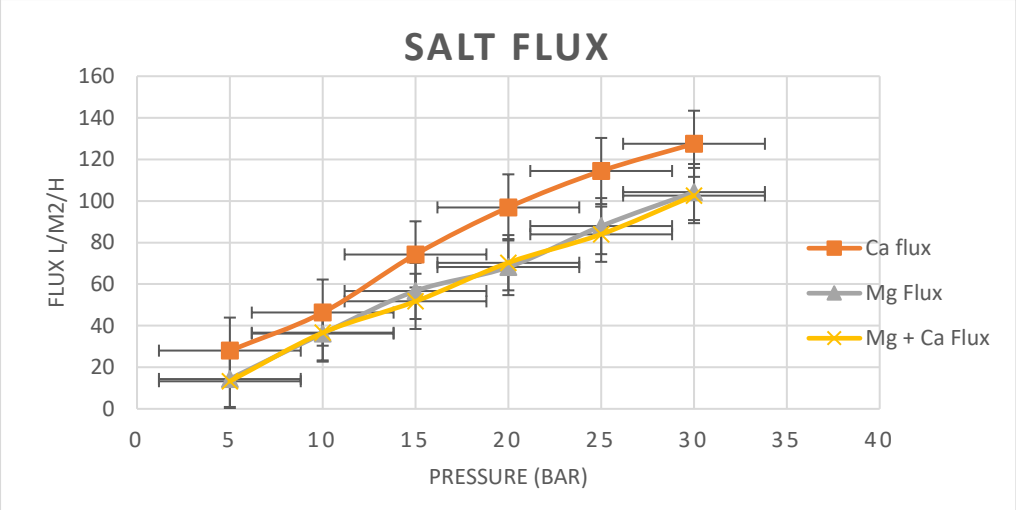

Figure 5310: Permeation fluxes of 416 mg/l Ca^{2+},1295mg/l $Mg^{2+,}$ and a mixture of Ca^{2+} and Mg^{2+} for a 5-minute oxygen plasma-treated NF membrane with respect to pressure.

The results from the figure indicate that flux increases with an increase in pressure, as with the untreated membrane. However, the measured flux with the treated membranes remains higher than the untreated membranes. Also, feed concentration affects the permeation flux of the membrane. An increase in feed concentration decreases permeate flux for all three membranes. Across the three membranes, the Ca feed had recorded the highest flux. This is because it is the least concentrated feed. The feed mixture of Ca and Mg, with the highest feed concentration, recorded the lowest flux of the three treated membranes. However, these still show an improved average flow rate in comparison with the untreated membrane.

For the 1-minute treated membrane (Fig. 50), 5 bars of pressure produced fluxes of 28, 14.4, and 13.3 l $m^{-2}h^{-1}$ for Ca, Mg, and the mixture of Ca and Mg, respectively, while 30 bars produced 102.6, 104, and 103 l $m^{-2}h^{-1}$ for the three respective feed solutions. In comparison with the untreated membrane, these figures are significantly higher. The highest flux values recorded (at 30b) for Ca and Mg are 30 l $m^{-2}h^{-1}$ and 60 l $m^{-2}h^{-1}$, respectively. This is also a testament to the higher permeability of the oxygen plasma-treated membranes.

Pressure (Bar)	**Ca flux (lm2/hr)**	**Mg flux (l.m2/hr)**	**Mg+Ca flux l.m2/hr)**
5	28	14.4	13.3
10	46.3	36.2	36.6
15	74.3	56.7	51.7
20	96.9	68.2	70.3

25	114.4	87.9	84
30	127.5	104.3	102.6

Table 3: Permeation fluxes of 416 mg/l Ca^{2+},1295mg/l $Mg^{2+,}$ and a mixture of Ca^{2+} and Mg^{2+} for 1-minute oxygen plasma-treated NF membrane with respect to pressure.

The 3-minute treated membrane (Table 3) had fluxes of 34, 20, and 26 l $m^{-2}h^{-1}$ of the respective feed solutions produced by 5 bars of pressure, while 30 bars of pressure produced 102, 88, and 92 l $m^{-2}h^{-1}$ for the respective feed solutions.

Pressure (Bar)	**Ca flux (lm2/hr)**	**Mg flux (l.m2/hr)**	**Mg+Ca flux L.m2/hr)**
5	32	15.6	15.6
10	53.8	38.9	34.1
15	78.2	55.3	59.3
20	94.56	81.2	74
25	124.9	115.6	110.5
30	144.5	131.4	124.4

Table 4: Permeation fluxes of 416 mg/l Ca^{2+},1295mg/l $Mg^{2+,}$ and a mixture of Ca^{2+} and Mg^{2+} for 1-minute oxygen plasma-treated NF membrane with respect to pressure.

These flux values can be seen to be higher than those of the 1-minute treated membrane. Whereas for the 5 minutes treated NF membrane (table 4), 5 bars of pressure produced 34, 30, and 24.1 l $m^{-2}h^{-1}$ for Ca, Mg, and Ca + Mg feed solutions, respectively, and 30 bars of pressure produced 102, 92, and 89 l $m^{-2}h^{-1,}$ respectively.

Therefore, treatment of the NF membrane for 5 minutes made it the most hydrophilic.

6.5 Effect of Membrane Treatment on Rejection

While it is important to observe the effect of treatment on the membrane flux, rejection is equally crucial. This section studies the effect of the oxygen plasma treatment on rejection.

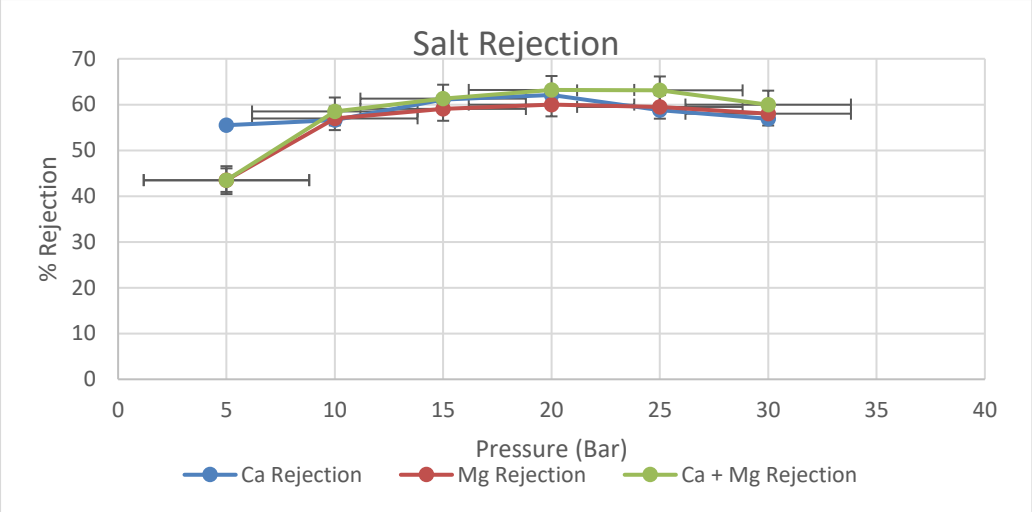

Figure 54: Rejection of 416 mg/l Ca^{2+},1295mg/l $Mg^{2+,}$ and a mixture of Ca^{2+} and Mg^{2+} for 1-minute oxygen plasma-treated NF membrane with respect to pressure

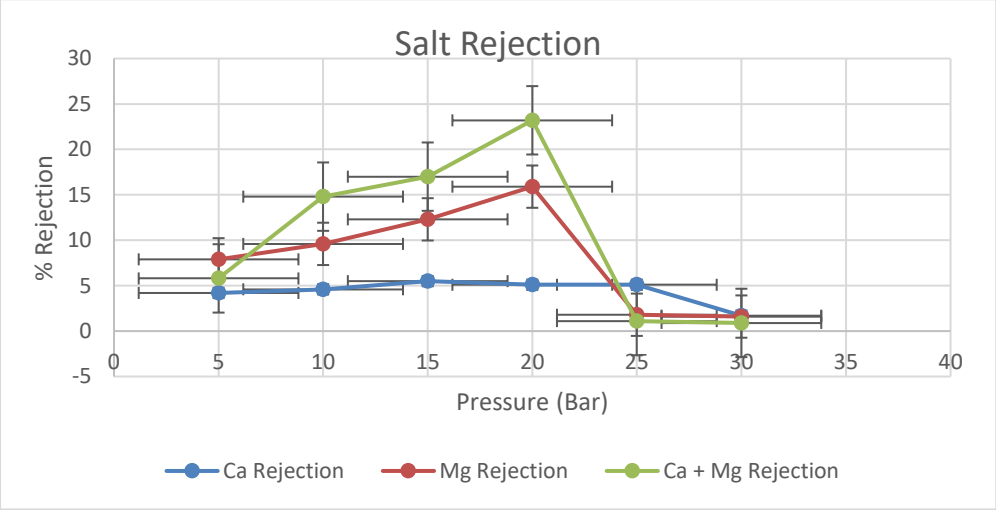

Figure 55: Rejection of 416 mg/l Ca^{2+},1295mg/l $Mg^{2+,}$ and a mixture of Ca^{2+} and Mg^{2+} for a 3-minute oxygen plasma-treated NF membrane with respect to pressure.

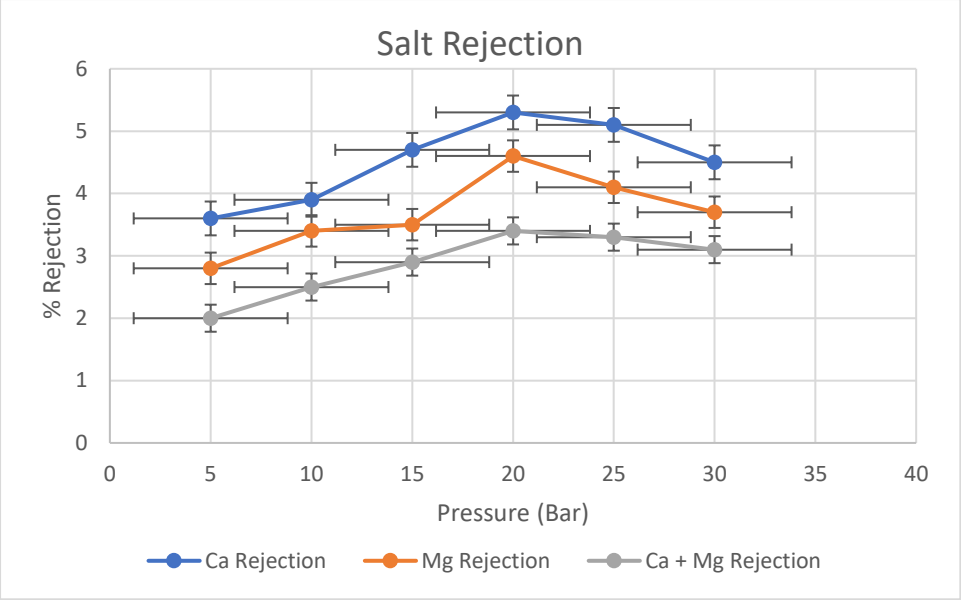

Figure 56: Rejection of 416 mg/l Ca^{2+},1295mg/l Mg^{2+} and a mixture of Ca^{2+} and Mg^{2+} for 5-minute oxygen plasma-treated NF membrane with respect to pressure

Results from the figure indicate that rejection increased with pressure until 20 bar, reaches a maximum, it then starts to decline. In this case, rejection peaked at 20 bars of applied pressure, after which it began to decline, for the three treated membranes and across the three feed solutions. This means that at the peak, pushing more feed through the membrane because of an increase in pressure results in increased ionic interaction between the feed and the membrane surface. This reduces the screening effect of the membrane at that point.

Again, generally, rejection is affected by feed concentration, despite the membrane treatment. Also, an increase in pressure affects rejection, as can be seen from the figure.

However, rejection decreases with plasma treatment time. The 1-minute plasma-treated membrane produced the highest rejection curve of the three, whereas the 3-minute-treated membrane produced the least rejection. For the 1-minute treated membrane, 5 bars of pressure produced 55%, 43%, and 42% Ca, Mg, and Ca + Mg ions rejection, respectively, while 30 bars of pressure produced 56%, 58%, and 23% rejection of the ions, respectively.

A similar trend was observed for the 3-minute treated membrane, where 5 bars produced 4.2%, 7.9%, and 5.8% rejections of Ca, Mg, Ca + Mg ions, respectively. While 30 bars produced 1.7%, 1.6%, and 0.9% of the three feed ions, respectively. These values are significantly lower than those of the 1-minute treated membrane. However, the lowest rejection occurred with the 5-minute treated membrane, where 5 bars of pressure produced, 3.6%, 2.8% and 2.0% rejection

of the 3 feed ions, respectively, whereas 30 bars of pressure produced 4.5%, 3.7% and 3.1% rejection of the respective ions in the feed solution.

5 bars of pressure reduced the Ca ions by 50% for the 1-minute treated membrane, and the highest rejection (62%) occurred at 20 bars.

The introduction of negatively charged functional groups (e.g., $–COO^–$) alters the membrane's zeta potential.

This can reduce electrostatic repulsion for certain ions, allowing them to pass through more easily and decreasing rejection, particularly for monovalent ions (e.g., Na^+). Those $-COO^-$ groups reduce the ability of the membrane to effectively shield ions from the surface, thereby increasing the ion permeability of the membrane. Increased treatment time further reduces the performance of the membrane, as seen in the figure above in terms of rejection. This is because increased treatment time allows for the formation of more functional groups on the surface of the membrane, which increases the ion permeability of the membrane.

6.6. NH_3 Plasma Treatment

Plasma treatment has been shown to enhance membrane permeability while reducing solute rejection as treatment time increases, primarily due to alterations in surface porosity and chemical functionality [172]. Subsequent studies have investigated plasma-treated membranes for fouling control, demonstrating that surface modifications can significantly improve hydrophilicity and reduce organic and biological fouling [175]. Common plasma gases used for such modifications include nitrogen, ammonia, argon, helium, and their mixtures, each contributing distinct functional groups that influence membrane surface properties [176,177]. Yu et al. [178] applied nitrogen plasma treatment to polypropylene microporous membranes and reported a 63% increase in permeability compared to untreated membranes, attributing the improvement to enhanced antifouling characteristics. In the present study, we evaluate the impact of ammonia plasma treatment on nanofiltration thin-film composite (NF TFC) membranes, focusing on changes in membrane performance and solute rejection. Previous work has shown that nitrogen-containing plasma introduces functional groups such as amines and imines, which increase surface hydrophilicity and reduce fouling tendencies [179].

This section investigates the effect of NH_3 plasma treatment of NF TFC on membrane performance, which includes permeate flux and salt rejection. Characterisation using contact

angle and zeta-potential measurements is performed to verify membrane properties before and after plasma treatment.

6.6.1. Experimental

The membrane was rinsed with deionised water and then left to dry. Low-pressure plasma treatment in a CVD plasma deposition reactor was used for the treatment. The plasma system was evacuated below 3 mTorr at every start to remove residual moisture. At a vacuum, plasma source gas (NH_3) was introduced to 50 mTorr. power in a range of 8W and a predetermined treatment time of 50 secs was applied for treatment at a room temperature and pressure of 1000 mTorr. The treated membrane was removed and compressed with deionised water.

6.7. Membrane Characterisation

6.7.1. Water contact angle

Water contact angles of the treated membranes were measured, and the results are represented in the table below

Untreated Membrane	50 Seconds Plasma Treated Membrane	1 min plasma treated membrane
40^0	29.6^0	28.6^0

Table 5: Water contact angle for NH_3 plasma-treated membrane*s*

Different treatment times were applied while the other parameters, such as temperature, power, flow rate, and pressure, remained constant. A reduction of about 26% in contact angle was observed at initial treatment for 50 seconds. A further 4.5% decrease was observed when the membrane was treated for 1 min. This indicates that much of the change, because of the treatment, took place before 50 seconds of treatment. Longer treatment time resulted in a lesser percentage decrease in contact angle.

A decrease in water contact angle indicates an increase in hydrophilicity. Hence, from Table 5, it is inferred that ammonia plasma treatment improves surface hydrophilicity of NF TFC membranes as indicated by a decrease in water contact angles. Similar results were obtained by Kim et al [180] who studied the effect of treatment time and applied power on contact angle.

According to the study, longer plasma treatment time produced maximum effect on the membranes regardless of membrane type.

6.8. Effect of treatment on Water permeation

Pure water flux experiment results carried out to determine the effect of the plasma treatment on the membrane are shown in Figure 53 below.

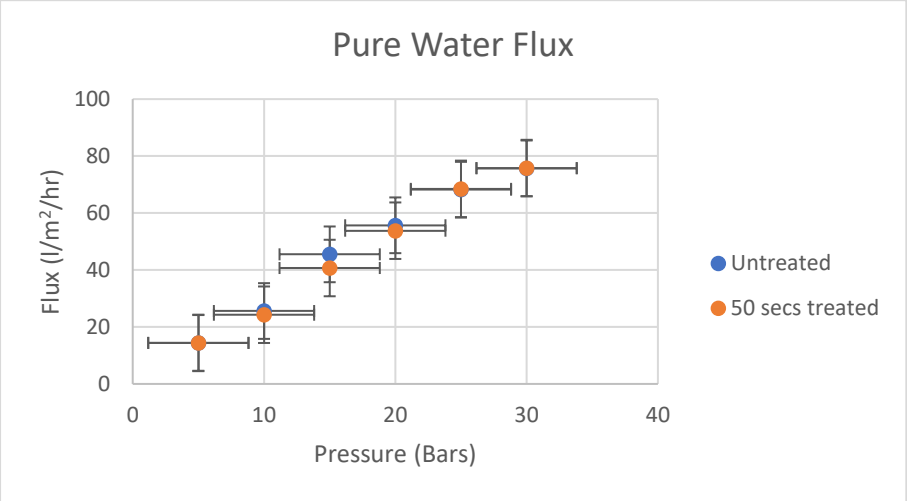

Figure 57: Pure water fluxes for 50 secs NH_3 plasma-treated NF membrane, and the untreated membrane with respect to pressure.

As indicated in the figure, the pure water permeation of the 50-second treated membrane is very similar to that of the untreated membrane. A pressure of 5 bars produced the same flux of 14.4 l/m^2/hr for both membranes, while 30 bars of pressure produced a flux of 75 l/m^2/hr for both membranes.

Given the decrease in contact angle of the treated membrane, which confirms its hydrophilicity, it is expected that pure water permeability would be higher than that of the untreated membrane. However, similar fluxes were observed, which may be attributed to a phenomenon known as hydrophobic recovery—the process by which a membrane gradually regains its original hydrophobic character over time [156]. This recovery is driven by the reorientation and mobility of polymer chains at different depths of the membrane, which can cause surface functional groups to migrate inward or reconfigure. Kim et al. [181] demonstrated that ammonia plasma-treated nanofiltration (NF) membranes exhibited significant reductions in contact angle, confirming increased hydrophilicity; however, the long-term stability of these changes was influenced by treatment time and applied power. [182] further showed that hydrophobic recovery is time-dependent and varies with plasma species and treatment conditions, with shorter treatment durations and lower power levels leading to faster recovery. In contrast, higher plasma power generates stronger surface interactions and more stable functional group bonding, resulting in slower hydrophobic recovery [183]. These effects are attributed to differences in bonding stability and energy input during plasma treatment, which govern the durability of surface modifications.

NH_3 plasma introduces hydrophilic amine ($-NH_2$) groups onto the membrane surface.

This improves water affinity, allowing easier water transport across the membrane, thereby increasing flux.

However, the effect on flux is generally **less pronounced** than with oxygen plasma because $–NH_2$ groups are less hydrophilic than –OH or $–COO^-$ groups from oxygen plasma.

6.9. Effect of treatment on salt flux

Hydrophobic recovery of the treated membrane meant that the membrane had lost its hydrophilicity, as shown in Figure 57 below.

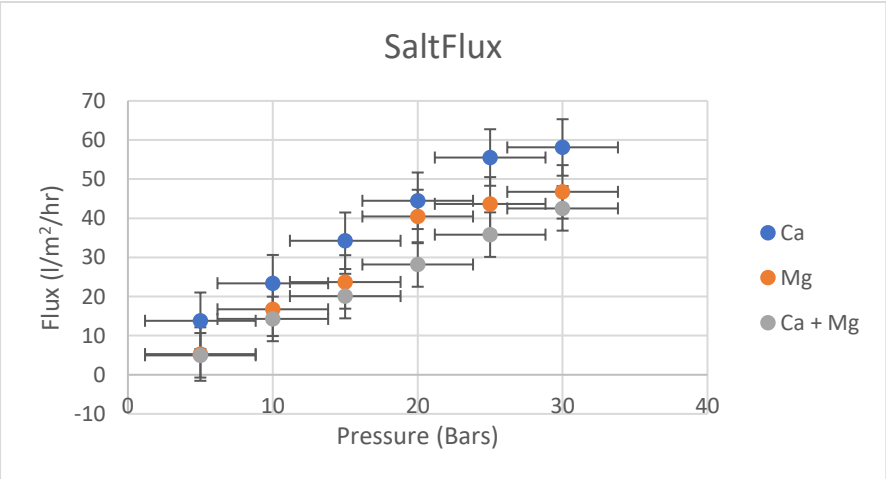

Figure 58: Salt flux of 416 mg/l Ca^{2+},1295mg/l Mg^{2+}, and a mixture of Ca^{2+} and Mg^{2+} for 50 secs NH_3 plasma-treated NF membrane with respect to pressure.

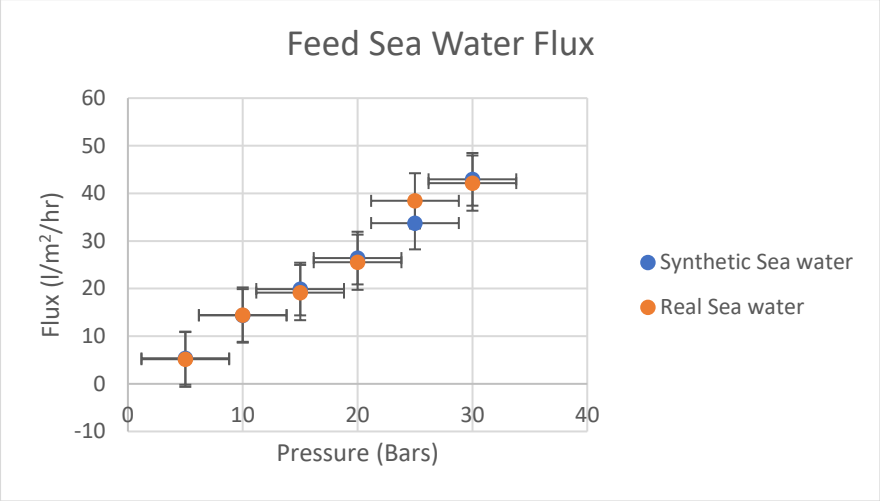

Figure 59: Feed flux of synthetic and real seawater for 50-sec NH_3 plasma-treated NF membrane with respect to pressure.

From the figures above, the membranes could be seen to be restored. Salt flux is affected by feed concentration. 5 bars of pressure produced 13.8 l/m^2/hr, 5.29 l/m^2/hr and 4.98 l/m^2/hr fluxes of Ca, Mg and Ca + Mg ions feed solutions respectively while 30 bars of pressure produced 58.10 l/m^2/hr, 46.75 l/m^2/hr and 42.53 l/m^2/hr fluxes of Ca, Mg and Ca + Mg ions feed solutions respectively. The same results are shown in Table 6 below.

Pressure (Bar)	**Ca flux (l/m^2/hr)**	**Mg flux (l/m^2/hr)**	**Ca + Mg flux (l/m^2/hr)**
5	13.8	5.29	4.98
10	23.4	16.73	14.27
15	34.25	23.73	20.11
20	44.47	40.46	28.19
25	55.53	43.69	35.82
30	58.1	46.75	42.53

Table 6: Salt flux of 416 mg/l Ca^{2+},1295mg/l Mg^{2+} and a mixture of Ca^{2+} and Mg^{2+} for 50-secs NH_3 plasma treated NF membrane with respect to pressure.

Experiments with synthetic seawater and real seawater showed similar fluxes to those of the mixture of Ca and Mg feed solutions. 5 bars produced about 5.34 l/m^2/hr and 5.17 l/m^2/hr fluxes of synthetic and real seawater, respectively, while 30 bars produced 42.95 l/m^2/hr and 42.16 l/m^2/hr fluxes of the respective feed (Table 7 below).

Pressure (Bar)	**Synthetic Seawater flux (l/m^2/hr)**	**Real SeaWater flux (l/m^2/hr)**
5	5.34	5.17
10	14.36	14.45
15	19.91	19.17
20	26.41	25.54
25	33.77	38.43
30	42.95	42.16

Table 7: Feed flux of synthetic and real seawater for 50-sec NH_3 plasma-treated NF membrane with respect to pressure.

6.10 Effect of Surface modification on rejection

Results of ionic rejection are shown in Figure 6.11 below

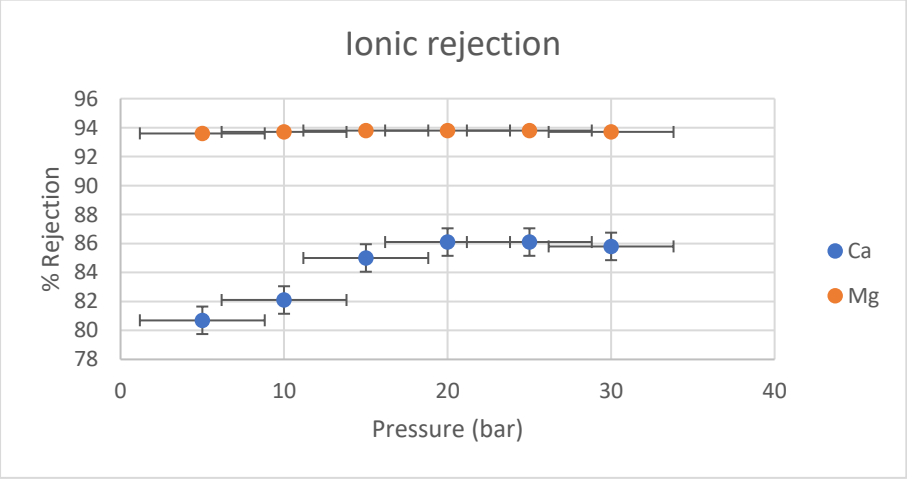

Figure 60: Rejection of 416 mg/l Ca^{2+},1295mg/l Mg^{2+} for 50 secs NH_3 plasma treated NF membrane with respect to pressure.

A slight increase in rejection was observed with Ca ions, peaking at the point of application of 25 bars of pressure. At this point, the rejection was 85 l/m^2/hr, beyond which a slight decrease

was observed. This is similar to the results obtained with the untreated membrane. With Mg ions, a pressure of 5 bars produced a rejection of 93% (Table 8). Rejection slightly increased, peaking at 15 bars of pressure, which produced a rejection of 93.8%. A further increase in pressure produced a slight decrease of 0.1% in rejection. Again, this is similar to the behaviour of the untreated membrane (chapter one).

Pressure (bars)	**% Rejection Ca^{2+}**	**% rejection Mg^{2+}**
5	79.3	93
10	79.4	93.7
15	81.7	93.7
20	81.8	93.7
25	82.4	93.7
30	81	93.7

Table 8: Rejection of 416 mg/l Ca^{2+},1295mg/l Mg^{2+} for 50 secs NH_3 plasma treated NF membrane with respect to pressure.

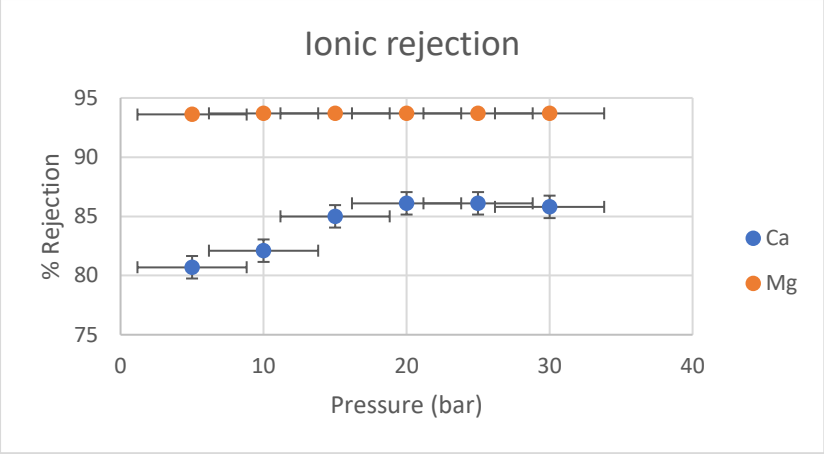

Figure 61: Rejection of mixture of 416 mg/l Ca^{2+} and 1295mg/l Mg^{2+} for 50 secs NH_3 plasma treated NF membrane with respect to pressure.

The rejection results of a mixture of Ca and Mg ions showed similar results. This indicates that the membrane behaviour remains unchanged from the untreated membrane (chapter one). Ca ion rejection peaked at 20 bars of pressure.

Pressure (bars)	**% Rejection Ca^{2+}**	**% rejection Mg^{2+}**

5	80.7	93.6
10	82.1	93.7
15	85	93.8
20	86.1	93.8
25	86.1	93.8
30	85.8	93.7

Table 9: Rejection of mixture of 416 mg/l Ca^{2+} and 1295mg/l Mg^{2+} for 50 secs NH_3 plasma-treated NF membrane with respect to pressure.

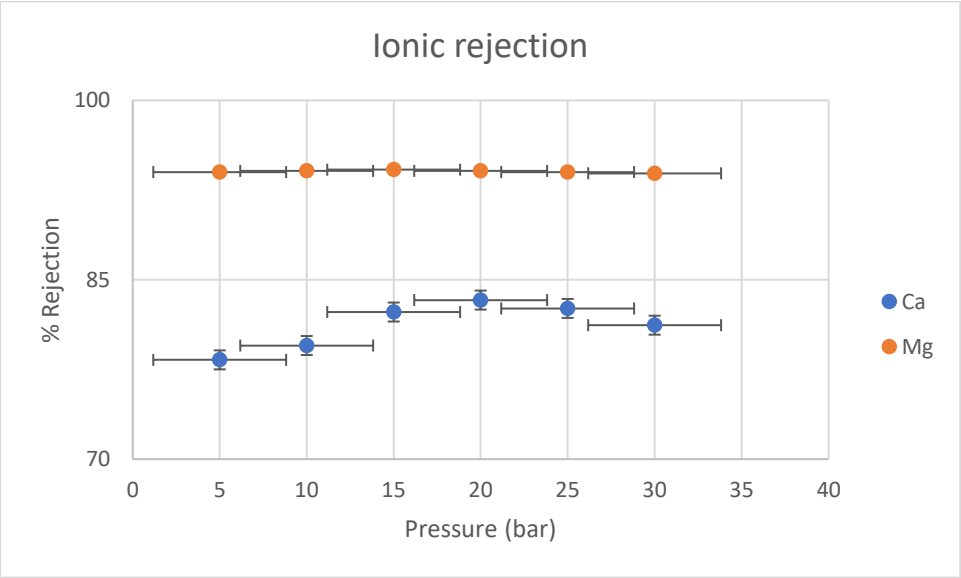

Figure 62: Rejection results of Ca and Mg ions in synthetic seawater as a function of pressure with a 50-second NH_3 plasma-treated NF membrane.

The membrane showed similar behaviour when used to filter synthetic seawater. All the results indicated that the membrane behaviour is not so different from the untreated membrane.

This confirms the hydrophobic recovery of the membrane, which appears to restore the properties of the membrane.

Plasma gas surface modifications are challenged by the long-term chemical instability of the functional groups introduced during treatment. Two key mechanisms—post-plasma oxidation and polymer chain reorientation—are known to contribute to the hydrophobic recovery of hydrophilized membranes when exposed to atmospheric conditions such as environmental air [184,185]. Post-plasma oxidation involves reactions between unreacted free radicals remaining on the membrane surface and ambient gas molecules, leading to the formation of hydroxyl, carbonyl, carboxyl, and amine groups [184,186]. Upon exposure to air, free carbon radicals on the modified surface undergo oxidation, altering the surface chemistry. In parallel, polymer chain reorientation occurs when plasma-generated polar functionalities migrate from the membrane surface toward the bulk polymer, reducing surface polarity over time [186]. These phenomena are often detected by an increase in water contact angle as the membrane ages, and their severity is influenced by treatment conditions such as plasma power, exposure time, and gas composition [187].

6.11 Conclusion

The surface of the TFC nanofiltration membrane was changed from hydrophobic to hydrophilic through oxygen plasma treatment. That was because of the introduction of polar functional groups such as carbonyl, hydroxyl, and carboxyl groups to the surface of the membrane. The membranes were treated for 1 min, 3 min, and 5 min. A decrease in water contact angle was used to confirm the hydrophobicity of the resultant membrane.

Hydrophilicity increased with increased treatment time. 5 mins treated membrane recorded the highest pure water and salt flux of the three. On the other hand, rejection of ions decreased with an increase in treatment time. This suggests that the performance of plasma-treated membranes is dependent on the treatment time.

Consequently, oxygen plasma treatment of TFC NF membranes increased flux and decreased rejection. From the study, the optimum treatment time was 1 minute. Plasma treatment of under 1 minute could yield better rejection results.

Further studies investigated the surface modification of NF membrane by NH_3, plasma. Likely introduction of NH_2 groups made the membrane hydrophilic. Hydrophilicity of the resultant membrane was confirmed by a decrease in water contact angle measurements: 29^0 and 28.6^0 for the 50-second and 1-minute treated membranes, respectively. Filtration experiments were performed with the 50-second treated membrane.

Pure water flux and filtration of salt solutions showed that the treated membrane exhibited the same behaviour as the untreated membrane. This is an indication that hydrophobic recovery of the 50-second NH_3-treated membrane occurred almost immediately as a result of immersion in water and exposure to atmospheric conditions. Post-plasma oxidation of the free radicals on the membrane is likely responsible for the hydrophobic recovery of the treated membrane.

The higher stability of the functional groups could be achieved by altering treatment conditions such as time, power, and flow rate of the NH_3 gas.

CHAPTER SEVEN

INVESTIGATING THE USE OF POROUS SILICON FOR WATER DESALINATION

7.1. Introduction

Previous chapters of this thesis explored membrane techniques for water desalination. In this chapter, we explore the possible use of porous silicon as a membrane for water treatment. Pores of nanometre-scale are etched into a silicon wafer to create porosity. The resultant silicon is fitted onto a filtration rig for cross-flow pressure-driven filtration experiments (as described in chapter one).

7.2. Background

Desalination methods can transform saltwater reserves into usable freshwater sources but require significant amounts of energy input to be successful [188-191]. However, despite advances in desalination technology, the cost and scale of currently available techniques for water desalination remain too expensive for use in developing countries, where water shortage is already a current problem [192]. Therefore, new techniques that can lead to low-cost materials and energy-efficient processes for water desalination are of critical importance to a sustainable future.

Currently, the most commonly used methods of desalination include multi-stage flash distillation and reverse osmosis. The flash distillation technique is the most energy-intensive because it requires approximately 25 kWh/m^3 of energy that is dissipated after condensation [193,194]. Reverse osmosis (RO), which requires approximately 5 kWh/m^3 is more energy-efficient than flash distillation. However, it makes use of membranes most often made from cellulose or polyamides and is operated under high pressure to remove salt or contaminants in water [195 -198]. Consequently, this drives up the cost of operating the process.

Here, we investigate the use of porous silicon for water desalination. Silicon is a material that is abundant on Earth. It is cheap and environmentally/biologically compatible. It is also readily adaptable to the already well-developed silicon manufacturing infrastructure. Previous studies involved the use of porous silicon for the removal of salt in water [199]. Porous silicon was used in capacitive deionization to reduce the salinity of saltwater. The authors demonstrated that, with surface passivation of the porous silicon material with carbon, (that is transforming the highly porous material into an electrochemically stable template for water desalination),

the porous silicon was able to achieve up to 0.52% salt removal from 500mM NaCl solution, which represents the concentration in brackish water, and 0.36% salt removal from 10mM NaCl concentration (as in freshwater). This was achieved with an estimated energy input of 1.45 kWh/m^3.

There are several ways of creating nanoscale pores on silicon, such as electrochemical etching and metal-assisted etching. Metal-assisted etching was used in this work. This technique is described in the next section.

7.3. Experiments

For this study, reclaimed polished monocrystalline silicon substrates were used.

For metal-assisted etching, metal nanoparticles required for the technique were sputtered onto the Silicon surface using the PVD75KJ laker machine. Due to the constraints on sample size with deposition and characterization equipment, emitter-doped silicon wafers were cut into 30 mm x 30 mm samples. To achieve the deposition, a DC power of 8W was used with 30sccm Ar corresponding to a deposition rate of 0.5Å/s, using a Kurt J Lesker PVD 75 with a Torus magnetron source.

Following the deposition of metal nanoparticles onto the surface of the silicon substrates, wet chemical etching was performed. The etch solution consisted of Hydrofluoric Acid (50% concentration), Hydrogen Peroxide (30% concentration), and De-ionised Water with the ratio of 5:2:15, respectively. The samples were etched in the solution for 60 seconds before being thoroughly rinsed with de-ionized water and blow-dried with compressed nitrogen gas.

After etching of substrates to create a porous surface, Scanning Electron Microscopy was used to assess the surface topography.

7.3.1. Metal Deposition

The process of pore creation on a substrate is dependent on the metallic particles deposited.

Due to the simplicity and reproducibility of the deposition method, physical vapor deposition (via sputtering) of gold nanoparticles was chosen. The choice of gold was informed by the fact that it is a noble metal and not readily oxidized by Hydrogen Fluoride. Oxidation of the metal inhibits etching. Sputtering is typically used to deposit a thin film of a material onto a substrate. Since the porous silicon would require nanoparticles to create the pore structures, experimentation was carried out to observe deposited gold particle dimensions. In this process, the Si beneath the Au particles is etched much faster than the Si without Au particle coverage.

As a result, the noble metal sinks into the Si substrate in the presence of the etchant, which is HF, generating pores in the Si substrate.

Reclaimed, polished silicon samples were sputtered with gold particles. A crystal monitor was used to give an estimation of the thickness of the layer deposited. Following the deposition, Scanning Electron Microscope imaging was used to visualize and measure the particle size. Three different deposition thicknesses were performed, estimated to be 10nm, 15nm, 20nm, and 25nm using the crystal monitor.

The first step was to observe the surface of the silicon after deposition. Scanning electron microscopy enabled a high-resolution image to be taken of each of the sample surfaces (Fig. 7.1). SEM also allowed for accurate measurements of the particle diameters. The particle diameters vary over the surface of the silicon. Due to the variance, the average particle size was determined by measuring numerous particles and taking an average (over an area of 200 nm x 200 nm). As the particle size differed across each of the three samples analysed, an average was found for each using the same method as above. The 10nm, 15nm, 20nm, and 25nm samples revealed average particle diameters of 8nm, 18nm, 19nm, and 23nm, respectively. The 20nm sample has the largest variation in particle size, but they average out at 20nm. The results from the deposition trials revealed that sputtering equipment can produce isolated nanoparticles without any additional annealing processes.

A Scanning Electron Microscope (SEM) was subsequently used to determine the pore size and depth of the etched silicon.

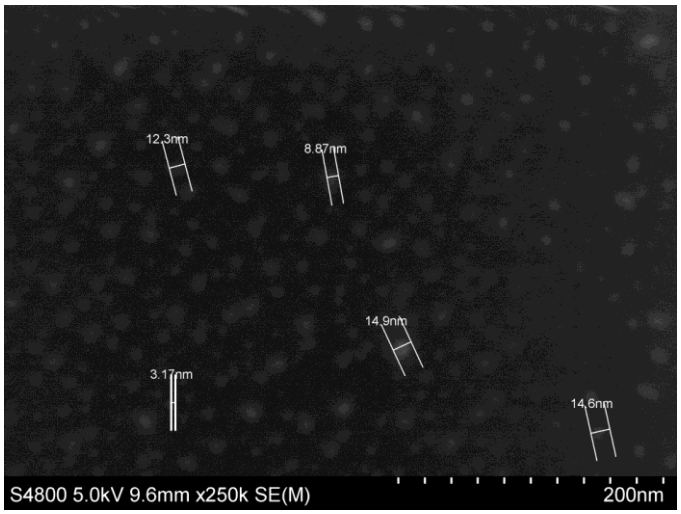

Figure 63: Surface of the Silicon Wafer showing deposits of Au nanoparticles

Figure 63 shows the initial deposition of gold particles on the silicon wafer. Observations show that the nanoparticles are of different sizes. However, clusters of the gold nanoparticles were observed as shown below.

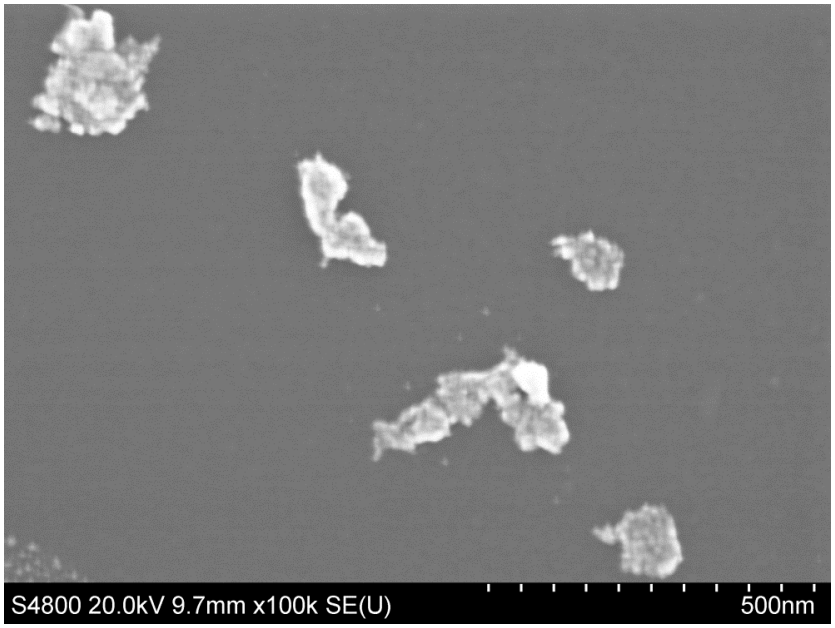

Figure 64: Clusters of gold nanoparticles on the silicon wafer substrate

7.3.2. Chemical Etching

Following the successful nanoparticle deposition process, the samples were chemically etched for 2 minutes, 5 minutes, and 10 minutes, respectively, in a solution of hydrofluoric acid, hydrogen peroxide, and de-ionized water. After etching, the samples were immediately introduced into a beaker of de-ionised water to stop the chemical reaction. The samples were dried using a blow dryer were reimaged using the SEM.

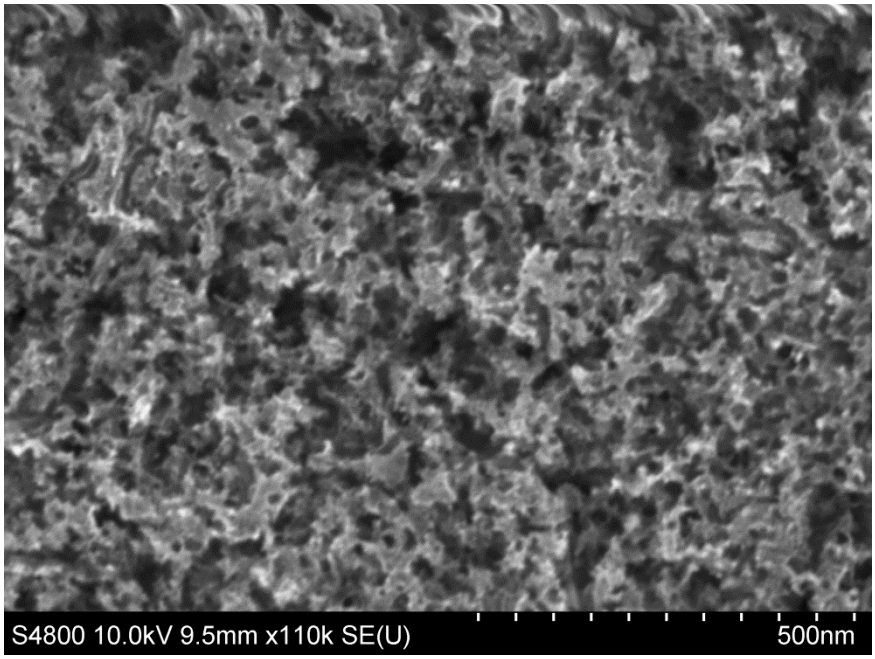

Figure 65: Pores created on the silicon after 2 mins etching of the silicon substrate

From the SEM images obtained of the newly formed PSi layer, it is evident that the surface of the polished silicon has changed significantly. From its original flat, polished surface, the gold particles that were once on the silicon surface have burrowed into the silicon and created pores. From inspection of the SEM images, the diameter of the pores relates to the diameter of the deposited metal nanoparticles. The pores have an average size of 10nm.

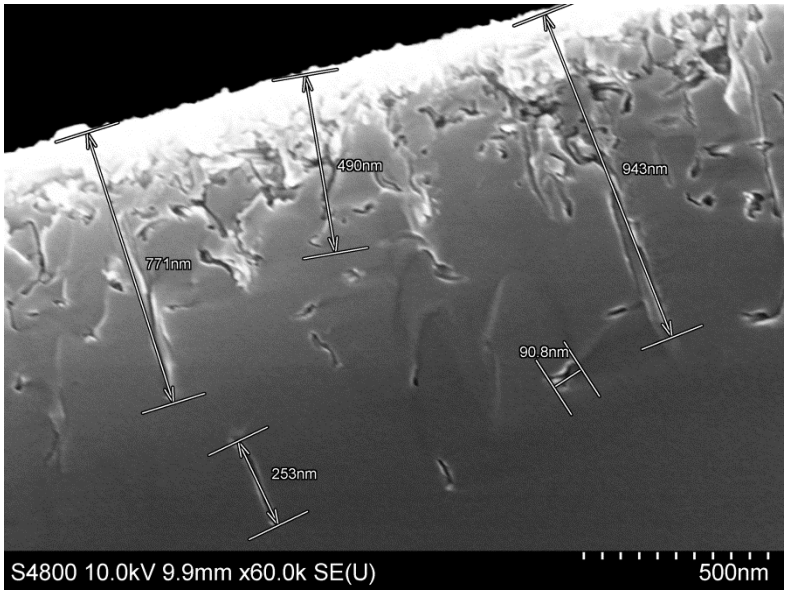

Figure 66: Cross-sectional image of 2 mins Metal-assisted etching of polished silicon substrate

A cross-sectional image of the 2-minute silicon showed a penetration depth of an average of 800nm, out of a silicon thickness of 572µm.

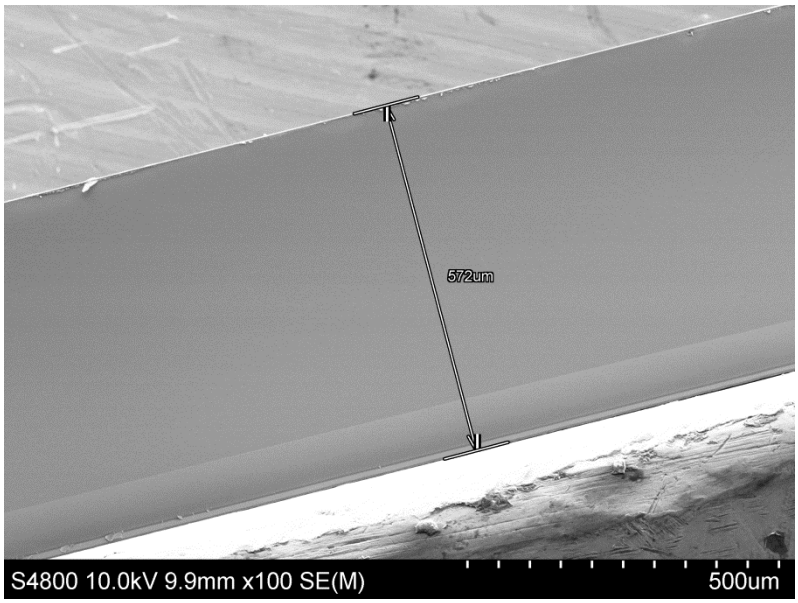

Figure 67: The thickness of the original polished surface silicon wafer before etching.

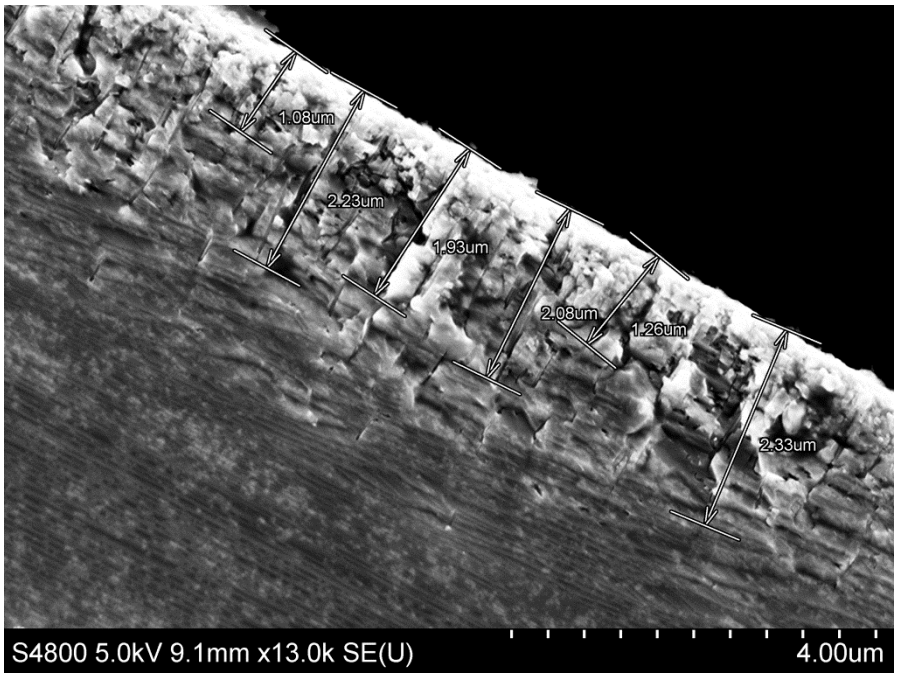

Figure 68: Cross-sectional image of 5-minute metal-assisted etched silicon

From 68 above, it is observed that 5 minutes of etching created a pore depth of an average of 1.9µm, out of a silicon thickness of 572µm.

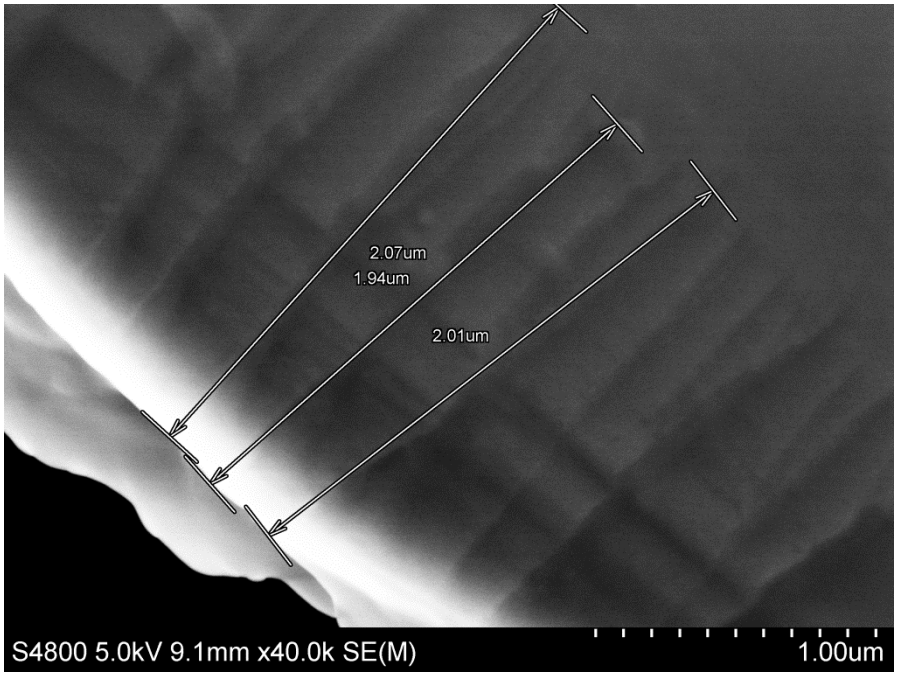

*Figure 69: C*ross-sectional image of 10-minute metal-assisted etched silicon.

The 10-minute etched silicon showed a pore depth of over 2µm.

Observations from the images show that longer etching times produce deeper pores on the silicon. Hence, etching all through the entire wafer would take a longer time. However, the etch rate becomes slower with time.

Since the aim is to bore through the silicon wafer, the etch time was increased to 3.5 hours. The product is a deeper etch but did not bore through the material. As shown in Figure 70.

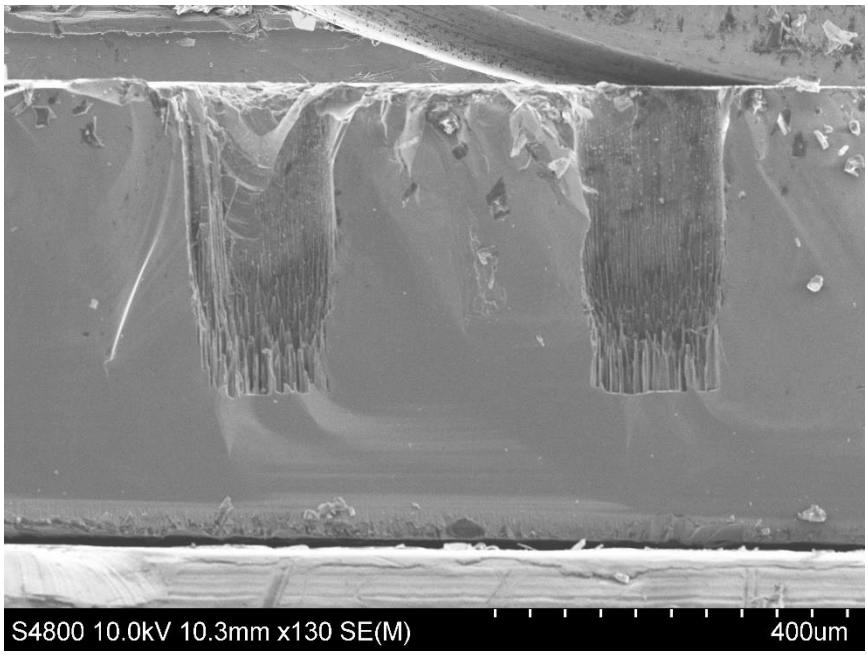

Figure 70: Cross-sectional image showing the etch depth of the silicon substrate after 3.5 hrs metal metal-assisted etching.

From the figure above, only about one-third of the silicon was etched in 3.5 hours.

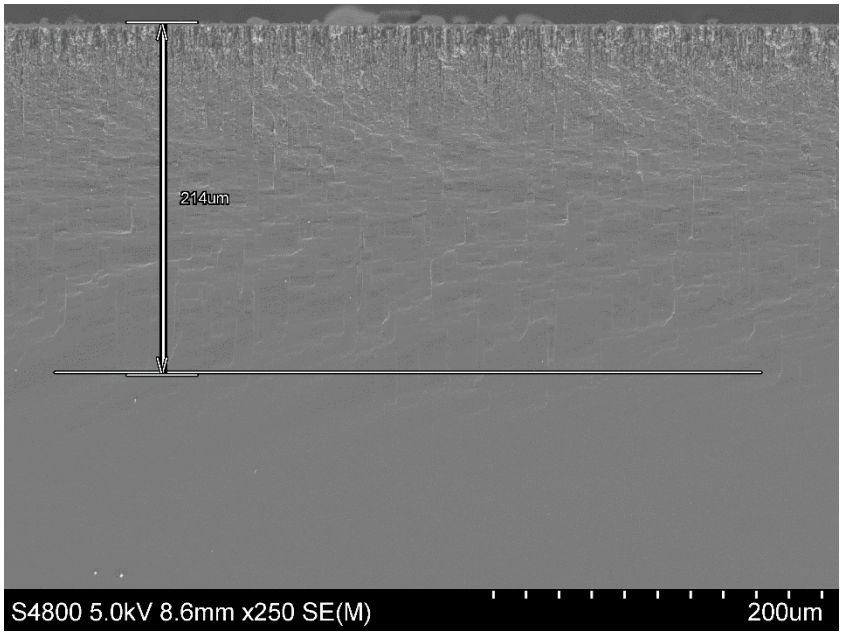

Figure 71: cross-sectional image showing the etch depth of the silicon substrate after 4 hrs metal metal-assisted etching.

From the figure above, 4 hours of etching produced 214µm of pore depth. This is just about half of the wafer thickness.

Observations showed that the etch rate seemed to decrease with time. After 3.5 hours, the etching progressed at a slower rate. This is time and energy-consuming. Therefore, a dry etch was carried out on the surface of the silicon wafer before proceeding with the wet etch.

7.3.3 Silicon Dry Etching

The silicon dry etching process is called the Bosch process. SF6 plasma is used to etch the silicon, and then a C4F8 passivation layer is applied to protect the sides of the pores that have been created. This alternate switching process is used to etch down the silicon.

The Bosch process is based on alternating multiple steps of etching and sidewall passivation of the silicon wafer (Fig. 72).

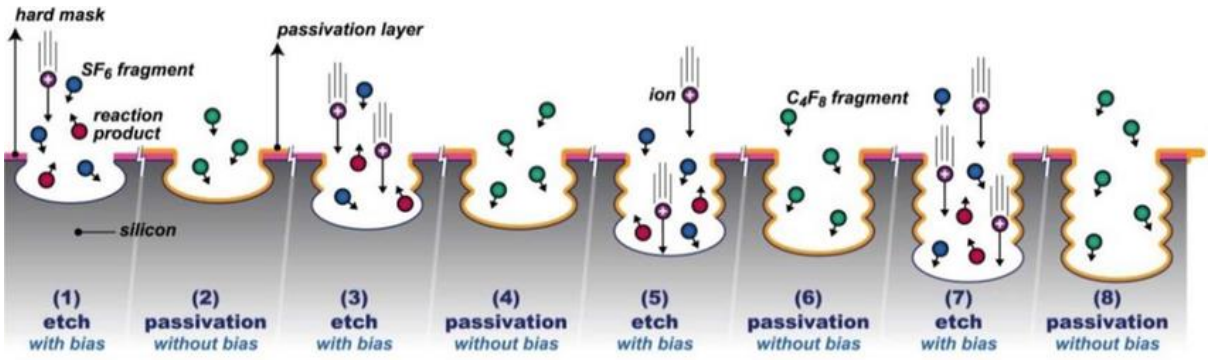

Figure 72: Schematic diagram of the Bosch process silicon etch with a pre-patterned hard mask on top, using alternating etch and passivation half-cycles [206].

During this process, Sulfur hexafluoride (SF6) plasma is used to attack the silicon wafer from a nearly vertical position to create holes in the silicon wafer. This is followed by the deposition of a chemically inert passivation layer with Octafluorocyclobutane (C_4F_6). The passivation layer protects the entire substrate from further chemical attacks and prevents further etching on it. However, during the etching phase, the directional plasma ions that bombard the substrate attack the passivation layer at the bottom of the trench (but not along the sides). They collide with it and sputter it off, exposing the substrate to the chemical etchant.

Each stage lasts for several seconds and is repeated many times over, resulting in a large number of very small etch steps that are uniform in all orientations, taking place only at the bottom of the etched pits.

The Bosch process was used to create several windows on the surface of the wafer, as seen in Figure 72.

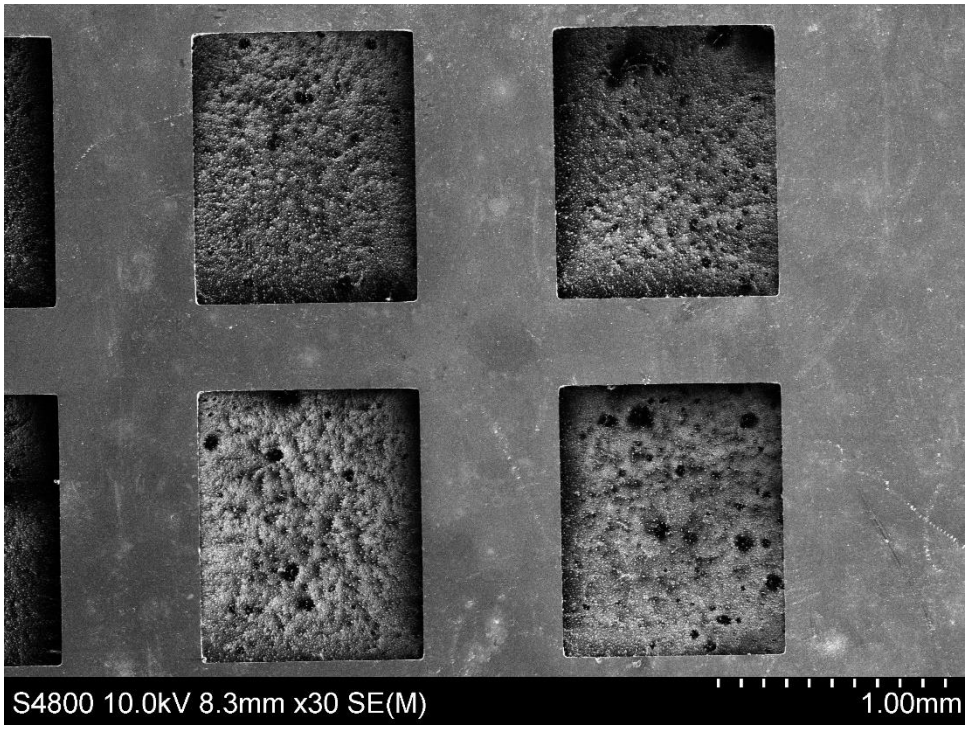

Figure 73: Windows created on the surface of the 500 µm-thick silicon wafer through the Bosch process.

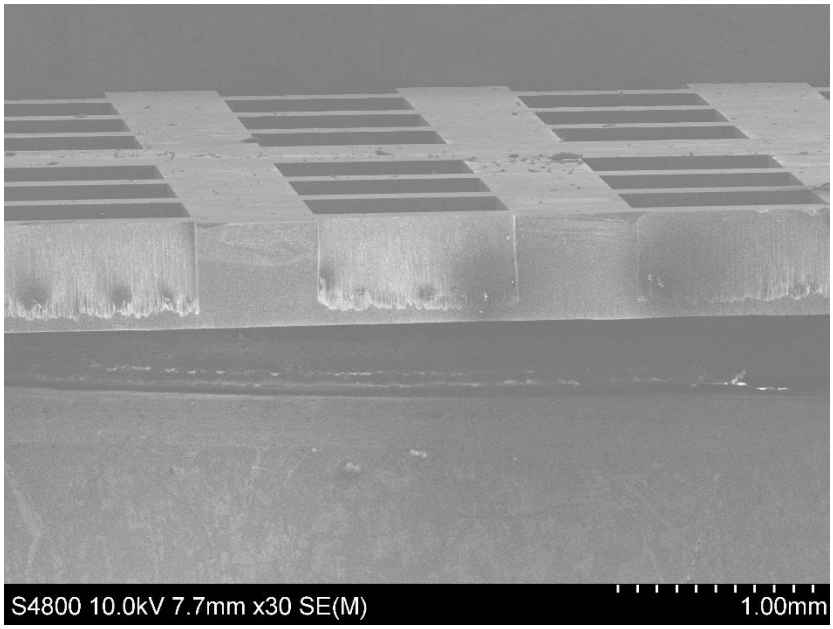

Figure 74: Cross-sectional image showing the etch depth of the silicon wafer after the Bosch process of etching

The dry etch was able to produce windows of depth of 490µm on the wafer as seen in Figure 74. The Bosch process produced an average etch depth of 471µm on the 572µm silicon wafer substrate.

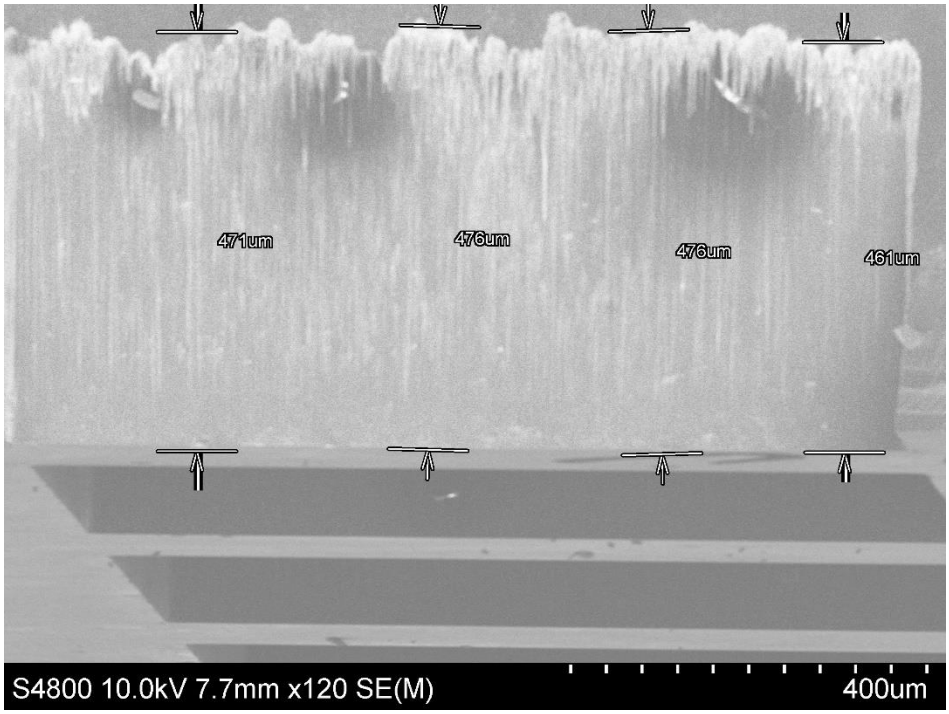

Figure 75: Cross-sectional image showing the dimensions of the etch depth of the silicon wafer after the Bosch process of etching.

Higher magnification images of the etched substrate are shown in Figure 76

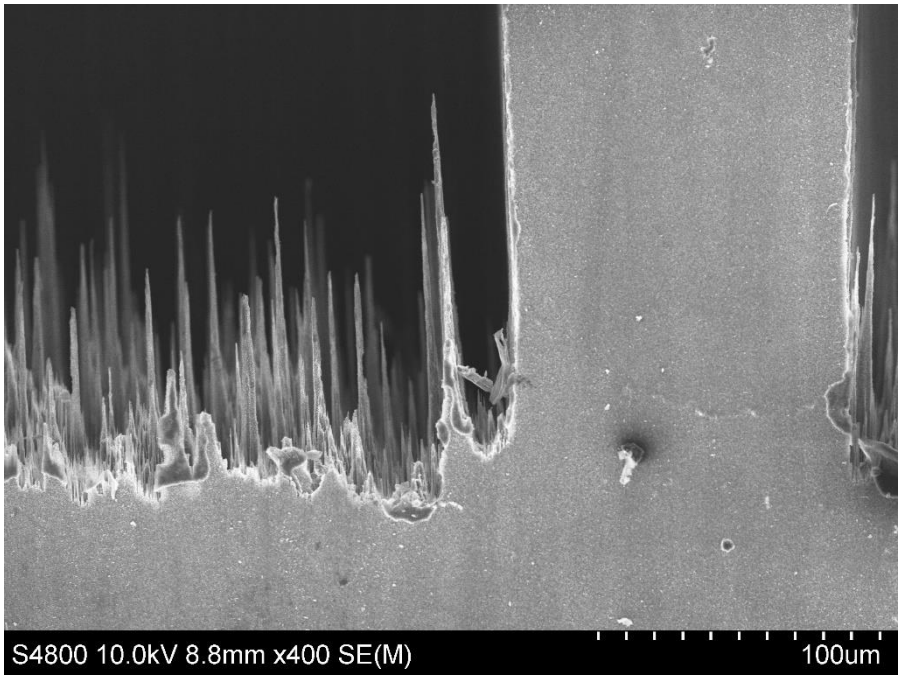

Figure 76: Higher magnification cross-sectional image showing the etch depth (grass) of the silicon wafer after the Bosch process of etching

The Bosch process was successfully used to reduce the thickness of the silicon wafer. The resultant wafer from the process was more fragile than the original wafer.

Having been able to reduce the wafer thickness by about 82% through the Bosh process, the wet etch was then used to create pores on the other side of the wafer, and the image is shown (Fig. 77). A 4-hour wet etch process was used to create pores on the other side of the wafer.

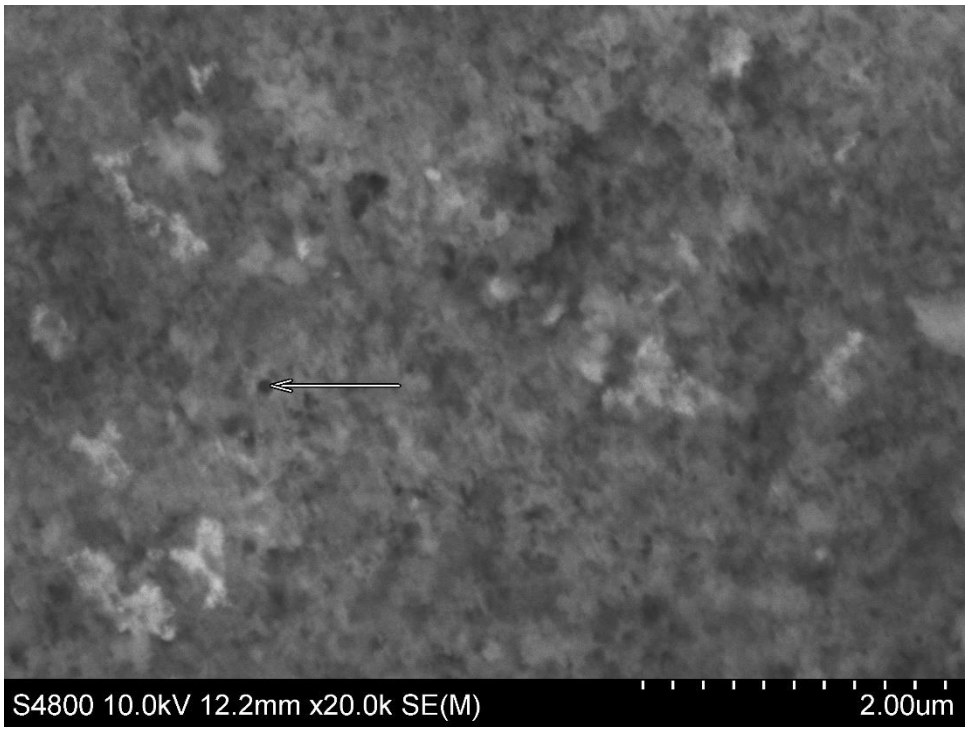

Figure 77: Cross-sectional image of the porous silicon showing pores created by the wet etch through the wafer

Higher magnification images showed higher pore density on the surface of the substrate (Fig. 78)

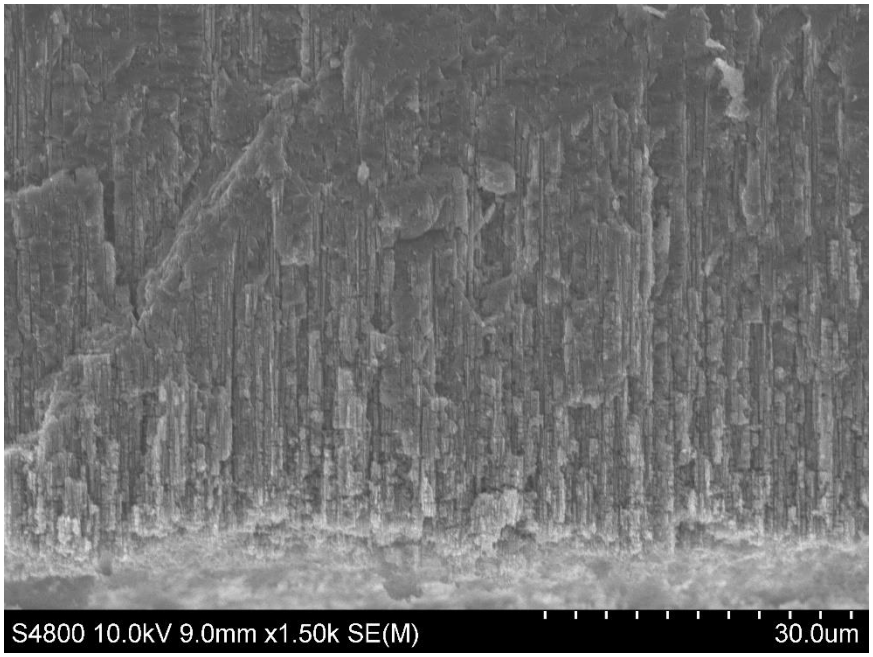

*Figure 78: 11C*ross-sectional image of the porous silicon showing pores created through the wet etch process on the etched silicon substrate

The pores went through the silicon down to the base of the dry etch (Fig. 79)

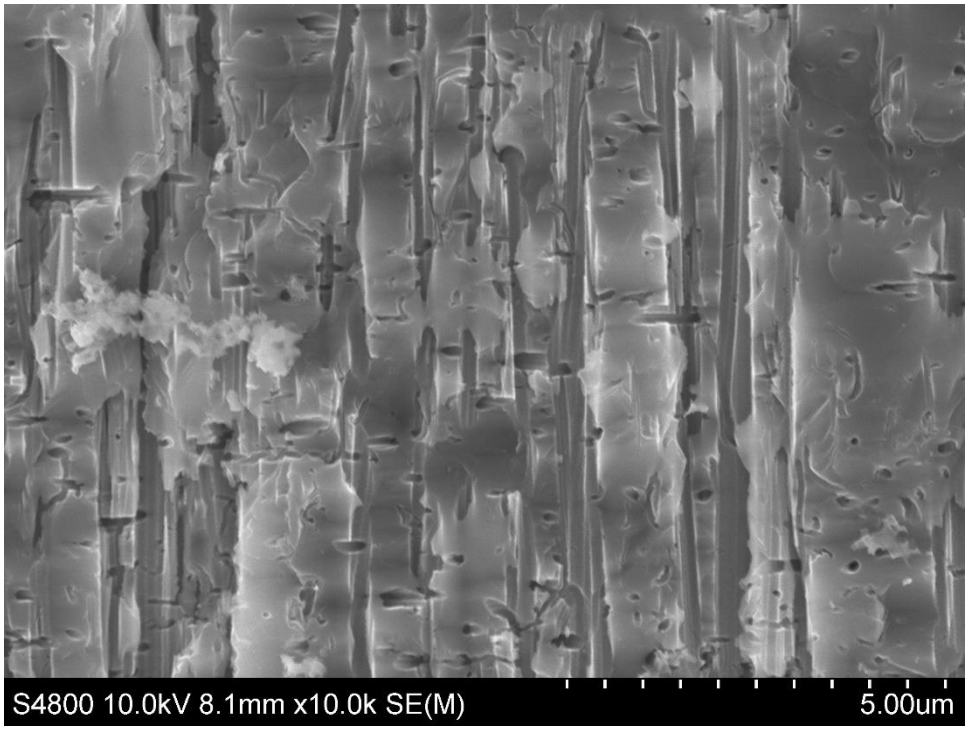

Figure 79: Cross-sectional image of the porous silicon showing pores going through the wafer into the wells produced by the dry etch process

From observations, the pore orientations are not uniform. Some of the pores are vertically oriented, others are diagonally buried deep in the wafer. The size of the pores varies. The pores have an average pore size of about 100nm, were created (Fig. 80)

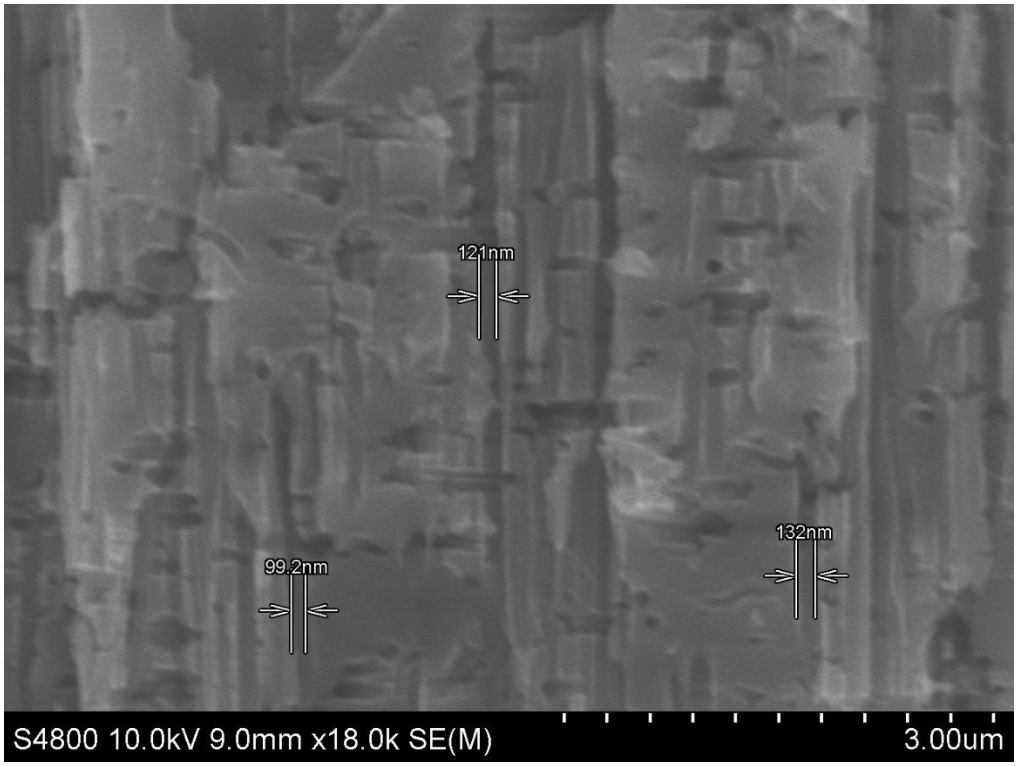

Figure 80: Cross-sectional image of the porous silicon showing the size of the pores created. Pores created are around 100nm.

7.4. Future Experiments using the porous silicon

The silicon membrane produced had an average pore size of 100nm. Filtration experiments showed that water is able to pass through the produced membrane.

This will be most suitable for microfiltration operations. Microfiltration is widely used in concentrating, purifying, as well as separating macromolecules, colloids, and suspended particles from a feed solution. MF membranes typically have pore sizes around 0.1–1.0μm. This silicon membrane thus created has an average pore size of about 0.1μm.

Silicon MF membrane can be used in the food industry for applications such as wine, juice, and beer clarification.

Silicon MF membranes can also be used for wastewater treatment as a pre-treatment method and plasma separation from the blood for therapeutic and commercial uses. It can also be

applied in biotechnology industries as well as applications such as cell recycling, harvesting, separation of recombinant proteins from cell debris, and purification of process streams. It is low-cost and abundant.

Future research might focus on the fabrication of smaller pore sizes to create nanopores. This might be an alternative to polymer membranes.

Synthesis and characterization of porous silicon membranes of different pore sizes – 5nm, 10nm, 15nm, 20nm using SEM, AFM, FTIR.

Surface Modification of Porous Silicon Membrane of various pore sizes – 5nm, 10nm, 15nm, 20nm. This is with a view to optimizing the performance of the membranes.

Recent developments in wafer-scale porous silicon (pSi) fabrication have significantly strengthened its potential for filtration applications. Gries et al. [200] developed a scalable technique that combines metal-assisted chemical etching (MACE) with photolithographic patterning to produce hierarchically porous silicon membranes exhibiting dual porosity—1 µm macropores and ~60 nm mesopores—over entire silicon wafers. This approach not only enhances mass transport and surface area but also supports conversion to silica while retaining pore architecture, reinforcing reproducibility and industrial scalability Complementing this, Zhumabay et al. [201] demonstrated that combining MACE with electrochemical etching yields pSi structures with improved thermophysical properties—such as higher activation energy for water-splitting reactions—suggesting better thermal stability in membrane operations. From an application standpoint, Lee et al. [202] introduced an adaptive cavitation ultrasonication method for the large-scale production of porous silicon nanoparticles (~170 nm), achieving good yield (59%) and reproducibility, implying potential translation to bulk membrane fabrication. Furthermore, silicon nanomembrane filters have recently been shown to efficaciously isolate micro- and nano-particles (sub-20 µm) from municipal water supplies, underscoring their precise separation capability and suitability for real-world water treatment systems [203].

Together, these studies present a compelling evidence base: scalable fabrication, favourable thermophysical attributes, and demonstrated filtration performance—all pointing to porous silicon as a viable material for next-generation desalination and microfiltration applications.

7.5. Potential Applications of a 100 nm Pore Size Membrane

1. Water & Wastewater Treatment

Bacteria Removal:

- Microfiltration membranes with 100 nm pores can effectively remove bacteria (typically 200–500 nm) but not viruses (which are often <100 nm).
- Used in pre-treatment for reverse osmosis (RO) and ultrafiltration (UF) systems.

Turbidity Reduction:

- Can remove suspended solids, algae, and colloidal particles, improving water clarity.

Industrial Wastewater Filtration:

- Removes particulates before further treatment with finer membranes.

2. Food & Beverage Industry

Dairy Processing (Milk Filtration):

- Used to separate fat, bacteria, and spores from milk.
- Helps in whey protein concentration.

Juice & Wine Clarification:

- Removes yeasts, sediments, and microorganisms while retaining colour and flavour.

Beer Filtration:

- Used instead of pasteurization to remove yeasts and spoilage bacteria while maintaining taste.

3. Pharmaceutical & Biotech Applications

Sterile Filtration (without Heat):

- Used for filtering protein solutions, cell culture media, and enzymes to remove bacterial contamination.

Separation of Microorganisms:

- It can be used in labs to filter out bacteria from samples.

4. Air & Gas Filtration

Particulate & Bacterial Filtration in Ventilation Systems:

- Used in clean rooms, hospitals, and biosafety labs to remove airborne contaminants.
- Found in face masks & respirators (e.g., N95 filters have similar pore sizes ~100 nm).

Sterilization of Compressed Air:

- Removes bacterial contamination in the pharmaceutical and food industries.

5. Electronics & Semiconductor Industry

Ultrapure Water Filtration:

- Used in semiconductor manufacturing to remove sub-micron contaminants from water used in chip fabrication.

Inkjet & Paint Filtration:

- Prevents nozzle clogging in inkjet printers by removing aggregates & impurities.

6. Biomedical & Medical Applications (Limited)

Some Blood Filtration Applications (But NOT Dialysis)

- It can be used for removing larger debris or cells from blood samples.
- Not suitable for artificial kidneys (dialysis), as it would allow essential proteins to pass through.

7.6 . Scalability and Cost-Effectiveness of Porous Silicon Membranes

Porous silicon membranes offer unique advantages, such as precise pore size control (1–100 nm) and high thermal/chemical stability, making them suitable for harsh environments like organic solvent filtration or high-temperature processes [202]. However, their scalability is limited by fabrication challenges. The electrochemical etching process is slow, often requiring hours to produce small wafers, and the membranes' inherent brittleness makes large-area production difficult. Additionally, manufacturing typically demands cleanroom facilities, increasing costs. Current estimates suggest fabrication costs range from 500–1,000 USD/m², significantly higher than polymer membranes, which cost around 50–200 USD/m² [203].

Durability is another concern, as porous silicon membranes are prone to cracking under mechanical stress and may degrade in extreme pH conditions [204,205]. While they outperform polymers in thermal stability (withstanding >400°C) and solvent resistance, their operational lifespan (2–5 years) is shorter than that of conventional polymeric membranes (5–10 years). This shorter lifespan, combined with high production costs, limits their economic feasibility for large-scale water treatment applications [203].

Despite these challenges, porous silicon membranes excel in niche applications where polymer membranes fail, such as in aggressive chemical environments or high-precision separations. Their high flux rates (>50 LMH/bar) and tunable surface chemistry make them attractive for specialized industries (e.g., pharmaceuticals, aerospace) [206]. Future advancements in wafer-scale manufacturing or hybrid designs (e.g., silicon-polymer composites) could improve scalability and reduce costs [199]. For now, their adoption remains restricted to high-value applications where performance justifies the expense.

While polymer membranes dominate the market due to their low cost, flexibility, and established roll-to-roll manufacturing, porous silicon membranes fill critical gaps in extreme-condition separations. However, unless production costs decrease or durability improves, their widespread use in conventional desalination or water treatment remains unlikely in the near term. Emerging technologies, such as 3D-printed supports or optimized etching techniques, may eventually bridge this gap, but further research is needed to make them cost-competitive at scale [207,208].

7.7. Conclusion

Investigation of low-cost porous silicon as a means of desalination was conducted. Nanometre Pores were created in a 517µm reclaimed polished silicon wafer through the metal-assisted etching procedure. This procedure involved the sputtering of gold nanoparticles on the silicon wafer.

The sputtered wafer was etched with a solution of Hydrofluoric acid and hydrogen peroxide. SEM images showed that nanometre pores were created in the silicon wafer. However, the depth of the pores created depended on the etch time.

The dry etch or Bosch process was used to optimise the etching operation. Through this process, over 400µm of the silicon wafer was etched. This allowed pores to go through the wafer, as seen from the SEM images.

Pores of about 100nm created in the wafer allowed water to pass through at the rate of 23l/hr.

However, the silicon membrane could be useful in the removal of larger particles such as colloids, turbidity, and microorganisms.

CHAPTER EIGHT

CONCLUSIONS AND RECOMMENDATIONS

This work focused on investigating nanofiltration as a means of seawater desalination and comparing its performance with other electrodialysis and surface-modified membranes.

8.1 Conclusion

NF membrane is a pressure-driven liquid membrane process, which has successful applications in various industries. It is primarily used for water softening. It can remove 85% of calcium and 93% of magnesium ions in seawater. NF technology is also capable of removing turbidity, organic carbon, and microorganisms from seawater. However, its rejection of monovalent ions such as sodium ions is just 30%. For this reason, it is not capable of sufficiently desalinating seawater, which contains 70% of monovalent ions (sodium and potassium). The achieved rejection of seawater with the NF membrane was 30%. Fouling is one of the major challenges of the NF technology.

Surface modification of NF membranes was carried out to improve the flow rate of the membrane, tackle fouling, and consequently reduce running costs in the long run. Surface modification of NF membrane with oxygen plasma was used to improve hydrophilicity through the introduction of polar functional groups, such as carbonyl and hydroxyl groups, to the surface of the membrane. This consequently improved permeate flux. Longer treatment times were found to further reduce the water contact angle of the membranes, thus making the membrane more hydrophilic. However, rejection of divalent ions was reduced because of the surface modification. The observed rejection was 60% of divalent ions.

Hydrophobic recovery occurred on the NF membrane that was treated for 50 seconds with ammonia plasma. The water contact angle of the treated membrane was found to have reduced. However, upon water immersion, the treated membrane exhibited similar behaviour to the untreated membrane. It has similar water flow rates as well as rejection rates to the untreated membrane. Hydrophobic recovery was found to have occurred as a result of the instability of the hydrophilic-inducing surface bonds that were formed during the treatment. Treatment time plays a vital role in the stability of surface bonds formed as a result of the plasma treatment. Longer treatment time could mitigate hydrophobic recovery. Electrodialysis as a means of seawater desalination was also investigated. it is a multi-functional process that could remove a vast variety of ions from a solution. It is more energy efficient than RO for the desalination of brackish water. It could remove 90% of ions in seawater after an hour. However, the output

flow rate of 20ml/min is considered low. Again, ED performance, like other membrane processes, is dependent on the concentration of the feed.

Novel use of porous silicon for water desalination presented a new approach to water treatment. Through metal-assisted etching, pores of about 100nm in size were formed in a polished silicon wafer. For the etching process, gold nanoparticles were sputtered on the polished silicon surface, after which it was etched with a mixture of HF and hydrogen peroxide. Pores formed in the wafer ranged from 90nm to 140nm. Filtration experiments showed that water was able to pass through the pores of the porous silicon with a good flow rate of 22 l/hr. However, the pores were too big to retain any ions. The size of the Au nanoparticles used for the etch determines the pore size. Therefore, smaller metal particles could result in smaller pore sizes.

The table below summarises the key results from the experimental work conducted in this study:

Parameter	**Nanofiltration (NF)**	**Electrodialysis (ED)**	**Membrane Modification (O_2 & NH_3 Plasma)**
Ion Types Targeted	Mainly divalent (Ca^{2+}, Mg^{2+}); limited monovalent (Na^{+}) rejection	Both monovalent and divalent	Divalent (Ca^{2+}, Mg^{2+}); evaluated post-modification
Ion Rejection (%)	Ca^{2+}: ~85%, Mg^{2+}: ~93%, Na^{+}: <20%	Ca^{2+}/Mg^{2+}/Na^{+}: >90% over 75 min	reduced rejection vs unmodified membranes
Water Flux	Moderate flux (e.g., 15–30 $L/m^2 \cdot h$)	N/A (ion exchange process, not direct water flow)	Enhanced flux post-treatment (O_2 > NH_3)
Energy Requirement	Moderate to high pressure (~4–10 bar)	High electrical energy input	Same as NF; no direct change in energy input
Advantages	Effective for divalent ions, scalable	High ion selectivity; effective desalination	Improved hydrophilicity and flux

Parameter	Nanofiltration (NF)	Electrodialysis (ED)	Membrane Modification (O_2 & NH_3 Plasma)
Limitations	Poor Na^+ rejection; requires pre-treatment	High energy use; organic removal is poor	Trade-off in rejection performance

Table 10: Comparison of NF, ED, and NF Membrane Modifications results

8.2. Recommendations for future research

This work presented surface modification and porous silicon as novel methods of seawater desalination. It can be further developed by allowing longer treatment times and higher power for ammonia plasma treatment of NF membranes. Increasing plasma treatment time and power could improve the chemical stability of the surface of the ammonia plasma-treated membrane. Permeate flux will be improved without compromising rejection.

Another interesting area for further research is the development of the porous silicon membrane. Silicon is a low-cost and earth-abundant material. This work demonstrated that water can pass through the silicon membrane. Given its pore size of 100nm, it could be capable of removing organic carbon, turbidity, and microorganisms from seawater. This feature makes it competitive with some membrane processes like ultrafiltration and microfiltration. Again, the low cost of silicon could give it a comparative economic advantage over microfiltration and ultrafiltration.

Its ability to remove solids from water could also make it useful in medicine and biological sciences for the removal of large waste substances from the human body. Porous silicon has a prospective future in the development of artificial kidneys, which could be used to separate waste products in the blood before sending the blood back to the heart.

In seawater desalination, modifications in features such as pore size and surface chemistry can be useful in developing the material into a useful nanosized filter that can favourably compete with nanofiltration membranes. Pore size can be adjusted by introducing polymers into the pores to block some parts of the pores. Smaller gold nanoparticles (e.g, 3-5nm) could be used to etch pores of similar size on the silicon. Surface modification could also be used to introduce hydrophobic properties to the porous silicon for enhanced separation.

Finally, this research work improved the knowledge and understanding of the behaviour of nanofiltration membranes as well as processes aimed at optimising and improving its performance by modifying some of their characteristics. This work also unveiled porous silicon as a novel water treatment technique.

References

[1] UNESCO, 2024. Ocean Literacy for All: A Toolkit. United Nations Educational, Scientific and Cultural Organization.

[2] U.S. Geological Survey, 2023. How Much Water is There on Earth?

[3] P. H. Gleick (ed.), 1993. Water in Crisis: A Guide to the World's Fresh Water Resources. New York: Oxford University Press.

[4] NESCO, 2024. The United Nations World Water Development Report 2024: Water for Prosperity and Peace. Paris: UNESCO.

[5] P. Rogers, R. Bhatia & A. Huber, 1998. Water as a Social and Economic Good: How to Put the Principle into Practice. Stockholm: Global Water Partnership.

[6] M. T. Islam, F. Karim, M. Mainuddin & J. M. Kirby, 2023. Impacts of climate change on groundwater level and irrigation cost in a groundwater-dependent irrigated region. Agricultural Water Management, 253, p.106944

[7] A. E. Kabeel, El-S. A. Agouz, & R. Sathyamurthy, 2016. Performance of the modified tubular solar still integrated with cylindrical parabolic concentrators. Solar Energy, 134, pp.94–106

[8] U. Yermiyahu, A. Tal, Ben-A. Gal, Bar-A. Tal, J. Tarchitzky, & O. Lahav, 2007. Rethinking Desalinated Water Quality and Agriculture. Science, 3185852, pp.920–921

[9] R. Ullah, M. A. Khan, & A. H. Malik, 2013. Desalination: A Sustainable Solution to Water Scarcity in Pakistan. Journal of Independent Studies and Research-Management, Social Sciences and Economics, 11(1), pp.17–24.

[10] M. Kumar, A. Puri, & R. Singh, 2014. Desalination for Sustainable Water Supply. International Journal of Environmental Science and Development, 5(3), pp.251–255

[11] E. Jones, M. Qadir, van M. T. VlietH., V. Smakhtin, & S. M. Kang, 2019. The state of desalination and brine production: A global outlook. Science of The Total Environment, 657, pp.1343–1356.

[12] N. Ghaffour, T. M. Missimer, & G. L. Amy, 2013. Technical review and evaluation of the economics of water desalination: Current and future challenges for better water supply sustainability. Desalination, 309, pp.197–207

[13] El-H. T. Dessouky and H. M. Ettouney, 2002. Fundamentals of Salt Water Desalination. Elsevier

[14] A. Alkaisi, R. Mossad and Sharifian-A. Barforoush, 2017. A review of the water desalination systems integrated with renewable energy. Energy Procedia, 110, pp.268–274

[15] T. Michels, Recent achievements of low-temperature multiple effect desalination in the western area of Abu Dhabi, UAE, Desalination, 93 1993 111–118

[16] A. A. Ophir Gendel and G. Kronenberg, The LT-MED process for SW Cogen Plants, Desal. Water Reuse, 4 (1) 1994 28–31

[17] A.D. T. Khawaji Khan and J.M. Wie, Gas Turbine Operating Experience in a Power/Seawater Desalination Cogeneration Mode, ASME ASIA '97 Congress & Exhibition, Paper Reprint No 97-AA-120, Singapore, September 30–October 2, 1997.

[18] B.A. S. Kamaluddin Khan and B.M. Ahmed, Selection of optimally matched cogeneration plants, Desalination, 93 1993 311–321

[19] A.M. El-Nashar, Cogeneration for power and desalination-state of the art review, Desalination, 134 2001 7–28

[20] A.M. Al Mudaiheem and H. Miyamura, Construction and Commissioning of Al Jobail Phase II Desalination Plant, in: Proceedings of the Second IDA World Congress on Desalination and Water Re-use, Bermuda, Vol. II, November 17–22, 1985, pp. 1–11.

[21] M.F. Al C. H. Ghamdi Hughes and S. Kotake, The Makkah-Taif MSF desalination plant, Desalination, 66 1987 3–10.

[22] M.A.K. Al-M. A. Sofi Al-A. A. HussainZ. Al-Omran and K.M. Farran, A Full Decade of Operating Experience on Al-Khobar-II Multi Stage Flash (MSF) Evaporators (1982–1992), in: Proceedings of the IDA and WRPC World Conference on Desalination and Water Treatment, Yokohama, Japan, November 3–6, 1993, pp. 271–279.

[23] The 12 MIGD Multistage Flash Desalination Units, Mod. Power Sys., 15 (7) 1995 11–14.

[24] C. Sommariva, The 72 MIGD multi-stage flash distillation plant at Al Taweelah, Abu Dhabi, UAE, Desal. Water Reuse, 6 (1) 1996 30–36

[25] A.D. J. M. Khawaji Wie and T. Khan, Operating Experience of the Royal Commission Acid-Dosed MSF Seawater Desalination Plant, in: Proceedings of IDA World Congress on Desalination and Water Reuse, Vol. II, Madrid, Spain, October 6–9, 1997, pp. 3–19.

[26] A. Harris, Seawater Chemistry and Scale Control, Desalination Technology Development and Practice, in: A. Porteous (Ed.), Applied Science Publishers, London, UK, 1983, 31–56.

[27] S.A. Al-Saleh and A.R. Khan, Evaluation of Belgard EV 2000 as Antiscalant Control Additive in MSF Plant, in: Proceedings of the IDA and WRPC World Conference on Desalination and Water Treatment, Yokohama, Japan, November 3–6, 1993, pp. 483–490.

[28] F. Y. Pujadas Fukumoto and K. Isobe, Performance Test of Antiscalant AQUAKREEN KC-550 under a Wide Range of Temperature Conditions at the MSF Desalination Plant in

Abu-Dhabi, in: Proceedings of IDA World Congress on Desalination and Water Reuse, Vol. II, Washington, DC, August 1991, pp. 25–29.

[29] American Cyanamid Company, Performance of CYANAMER P-80 on an MSF Seawater Distillation Unit Operating at 112°C Top Temperature, Ras Abu Fontas Power and Water Station, Qatar, 29 October 1986–24 January 1987, 1987

[30] G.F. Casini, The application of a high temperature scale control additive in a Middle East MSF plant, Desalination, 47 1983 19–22.

[31] J.C. Bernard and E. Demolins, Scale Control Additive-Practical Experiences in Multistage Flash Plants, in: Proceedings of the Second IDA World Congress on Desalination and Water Re-use, Vol. I, Bermuda, November 17–22, 1985, pp. 301–305.

[32] H.G. Heitmann, Chemical Problems and Chemical Conditioning in Seawater Desalination, Saline Water Processing, in: H.G. Heitmann (Ed.), VCH Verlagsgesellschaft, Germany, 1990, pp. 55–66.

[33] M. Al-Ahmad and F.A.A. Aleem, Scale formation and fouling problems effect on the performance of MSF and RO desalination plants in Saudi Arabia, Desalination, 93 (1–3) 1993 287–310.

[34] I. Barthelmes and H. Bohmer, Fouling and scaling control in MSF desalination units by on-load tube cleaning, Desal. Water Reuse, 7 (2) 1997, 27–33.

[35] S. Patel and M.A. Finan, New antifoulants for deposit control in MSF and MED plants, Desal. Water Reuse, 9 (2) 1999 61–69.

[36] D.P. Logan and S.P. Rey, Scale Control in Multi Stage Flash Evaporators, Materials Performance, June 1986, pp. 38–44.

[37] IDA Desalination Yearbook 2006–2007, Water Desalination Report, Global Water Intelligence and International Desalination Association, Topsfield, MA, USA

[38] O.K. Buros, The Desalting ABC, International Desalination Association, Topsfield, MA, USA, 1990.

[39] W.E. Johnson, The story of freeze desalting, Desal. Water Reuse, 3 (4) 1993 20–27

[40] Takht Ravanchi et al. 2009, A. Application of membrane separation processes in petrochemical industry: A review. Desalination 235, 199–244.

[41] J. Crittenden C., R. Trussell R., D. Hand W., K. Howe J., & G. Tchobanoglous 2012. MWH's Water Treatment: Principles and Design (3rd ed.). Wiley.

[42] Obotey E. Ezugbe and S. Rathilal 2020. Membrane Technologies in Wastewater Treatment: A Review. Membranes, 10(5), p.89.

[43] R. Singh; N. Hankins Emerging Membrane Technology for Sustainable Water Treatment; Elsevier: Amsterdam, The Netherlands, 2016.

[44] Muro, et al. 2012 Membrane separation process in wastewater treatment of food industry. In Food Industrial Processes–Methods and Equipment; InTech, Rijeka: Rijeka, Croatia, pp. 253–280

[45] "Desalination" (definition), The American Heritage Science Dictionary, Houghton Mifflin Company, via dictionary.com. Retrieved August 19, 2007.

[46] Hari J Krishna. Introduction to Desalination Technologies. Texas water development board

[47] O. K. Buros, "The ABCs of Desalting", International Desalination Association, 2000

[48] K.P. T. C. Lee D. Arnot Mattia, A review of reverse osmosis membrane materials for desalination—development to date and future potential, J. Membr. Sci. 370 2011 1–22,

[49] M.A. M. J. Ashraf A. K. Maah M. Qureshi I. Gharibreza Yusoff, Synthetic polymer composite membrane for the desalination of saline water, Desalin. Water Treat. 51 2013 3650–3661, http://dx.doi.org/10.1080/19443994.2012.751152.

[50] M.R. J. L. Esfahani H. A. Tyler M. J. StretzM. Wells, Effects of a dual nanofiller, nanoTiO2 and MWCNT, for polysulfone-based nanocomposite membranes for water purification, Desalination 372 2015 47–56, http://dx.doi.org/10.1016/j.desal. 2015.06.014

[51] S. J. Daer A. Kharraz S. W. Giwa Hasan, Recent applications of nanomaterials in water desalination: a critical review and future opportunities, Desalination 367 2015 37–48,

[52] G.M. D. R. Geise B. D. Paul Freeman, Fundamental water and salt transport properties of polymeric materials, Prog. Polym. Sci. 39 2014 1–42, http://dx.doi.org/10. 1016/j.progpolymsci.2013.07.001.

[53] K. Z. Cao X. Jiang Y. Zhang J. Zhang R. Zhao Xing, et al., Highly water-selective hybrid membrane by incorporating g-C3N4 nanosheets into polymer matrix, J. Membr. Sci. 490 2015 72–83, http://dx.doi.org/10.1016/j.memsci.2015.04.050.

[54] H.Z. A. Shafi Z. Matin A. Khan K. K. Khalil Gleason, Surface modification of reverse osmosis membranes with zwitterionic coatings: a potential strategy for control of biofouling, Surf. Coat. Technol. 279 2015 171–179, http://dx.doi.org/10.1016/j. surfcoat.2015.08.037

[55] L. W. S. ZhaoW. Ho, Novel reverse osmosis membranes incorporated with a hydrophilic additive for seawater desalination, J. Membr. Sci. 455 2014 44–54, http:// dx.doi.org/10.1016/j.memsci.2013.12.066.

[56] J. L. Xu X. Zhang H. Gao Y. Bie C. Fu Gao, constructing antimicrobial membrane surfaces with polycation–copper(II) complex assembly for efficient seawater softening treatment, J. Membr. Sci. 491 2015 28–36,

[57] M.B. F. Ghandashtani Zokaee M. Ashtiani A. Karimi Fouladitajar, A novel approach to fabricate high performance nano-SiO2 embedded PES membranes for microfiltration of oil-in-water emulsion, Appl. Surf. Sci. 349 2015 393–402,

[58] V. S. S. VatanpourA. R. Madaeni E. Khataee S. Salehi H. A. Zinadini Monfared, TiO2-embedded mixed matrix PES nanocomposite membranes: influence of different sizes and types of nanoparticles on antifouling and performance, Desalination 292 201219–29,

[59] L.Y. A. W. Ng C. P. Mohammad N. Leo Hilal, Polymeric membranes incorporated with metal/metal oxide nanoparticles: a comprehensive review, Desalination 308 2013 15–33,

[60] E. Bet-moushoul, Y.K. Mansourpanah M. Farhadi Tabatabaei, TiO2 nanocomposite based polymeric membranes: a review on performance improvement for various applications in chemical engineering processes, Chem. Eng. J. 283 2016 29–46,

[61] S.-R. E. M. Chae M. R. Hotze Wiesner, Possible Applications of Fullerene Nanomaterials in Water Treatment and Reuse, Second Edi Elsevier Inc., 2014

[62] P.S. A. F. Goh Ismail, Graphene-based nanomaterial: the state-of-the-art material for cutting edge desalination technology, Desalination 356 2014 115–128,

[63] V. M. Vatanpour M. H. EsmaeiliD.A. Farahani, Fouling reduction and retention increment of polyethersulfone nanofiltration membranes embedded by amine-functionalized multi-walled carbon nanotubes, J. Membr. Sci. 466 2014 70–81,

[64] R. Valladares Z. Linares V. Li Yangali-Q. Quintanilla G. Li Amy, Cleaning protocol for a FO membrane fouled in wastewater reuse, Desalin. Water Treat. 51 2013 4821–4824,

[65] K. L. Goh L. Setiawan R. Wei A. G. Si R. Fane Wang, et al., Graphene oxide as effective selective barriers on a hollow fiber membrane for water treatment process J. Membr. Sci. 474 2015 244–253,

[66] D. Cohen-J. C. Tanugi Grossman, Water desalination across nanoporous graphene, Nano Lett. 12 2012 3602–3608,

[67] C. Z. Tang I. Wang Petrinić, A.G. C. Fane Hélix-Nielsen, Biomimetic aquaporin membranes coming of age, Desalination 368 2015 89–105, http://dx.doi.org/10.1016/j.desal.2015.04.026.

[68] C.Y. Y. Tang R. W. Zhaoang, C. Hélix-A. G. Nielsen Fane, Desalination by biomimetic aquaporin membranes: review of status and prospects, Desalination 308 2013 34–40,

[69] J.E. Cadotte, Interfacially synthesized reverse osmosis membrane, U.S. Patent 4,277,344, 1981.

[70] A. A. Altaee Sharif, Pressure retarded osmosis: advancement in the process applications for power generation and desalination, Desalination 356 2015 31–46, http://dx.doi.org/10.1016/j.desal.2014.09.028.

[71] J.H. E. J. Kim C. K. Moon Kim Composite membranes prepared from poly(m-aminostyrene-co-vinyl alcohol) copolymers for the reverse osmosis process J. Membr. Sci., 216 2003, pp. 107–120

[72] A.D. J. M. Khawaji Wie and A.A. Al-Mutairi, Technical and Economic Evaluation of Seawater MSF and RO Desalination Processes for Madinat Yanbu Al-Sinaiyah, in: Proceedings of the IDA World Congress on Desalination and Water Reuse, Manama, Bahrain, March 8–13, 2002.

[73] M.A. M. A. Darwish Jawad and G.S. Aly, Technical and economic comparison between large capacity MSF and RO desalting plants, Desalination, 76 1989 281–304.

[74] G.F. Leitner, Water Desalination, What are today's costs? Desal. Water Reuse, 2 (1) 1992 39–43

[75] F.H. Kiand, Supply of desalinated water by the private sector: 30 MGD Singapore seawater desalination plant, in: MEDRC International Conference on Desalination Costing, Conference proceeding, Lemesos, Cyprus, December 2004

[76] Van der M. Bruggen, Mänttäri, M., Nyström, M. 2008 Drawbacks of applying nanofiltration and how to avoid them: a review. Separation and Purification Technology, 63, pp.251–263.

[77] N. Hilal, Al-H. Zoubi, N. Darwish, A. Mohammad 2005 Nanofiltration of Magnesium Chloride, Sodium Carbonate, and Calcium Sulphate in Salt Solutions. Separation Science and Technology, 40(16), pp.3299–3321.

[78] L.P. M. Raman Cheryan and N. Rajagopalan, Consider nanofiltration for membrane separation. Chem. Eng. Prog., 90 1994 68–74

[79] P. Eriksson, Nanofiltartion extends the range of membrane filtration. Environ Prog., 7 1988 58–61

[80] A. Mohammad, Y. Teow, W. Ang, Y. Chung, Oatley-D. Radcliffe and N. Hilal 2015. Nanofiltration membranes review: Recent advances and future prospects. Desalination, 356, pp.226-254.

[81] C. Zhang, K. Wei, W. Zhang, Y. Bai, Y. Sun, & J. Gu 2017. Graphene oxide quantum dots incorporated into a thin film nanocomposite membrane with high flux and antifouling properties for low-pressure nanofiltration. ACS Applied Materials & Interfaces

[82] H. Lee, & J. Kim 2023. Recent advancements in antifouling strategies for nanofiltration membranes: A comprehensive review. Desalination, 549, 116277.

[83] W. Chen, H. Zhang, J. Gao, & Q. Li 2021. Zwitterionic modification of polyamide nanofiltration membranes for improved fouling resistance and chlorine tolerance. Separation and Purification Technology, 258, 118018. https://doi.org/10.1016/j.seppur.2020.118018

[84] Al-Y. Gamal, A. Hassan, & El-M. Aassar 2023. Plasma-treated nanofiltration membranes for organic fouling reduction and flux recovery improvement. Membranes, 13(2), 187. https://doi.org/10.3390/membranes13020187

[85] S. Patel, S. Ankit, & S. Kulkarni 2024. Influence of membrane surface roughness and hydrophilicity on ion rejection in nanofiltration. Journal of Water Process Engineering, 58, 104121.

[86] N. H. Hilal Al-N. A. Zoubi A. W. Darwish M. Mohammad Abu Arabi, A comprehensive review of nanofiltration membranes: treatment, pretreatment, modelling, and atomic force microscopy, Desalination 170 2004 281–308. (Smith et al., 2023) B.

[87] Van der M. Bruggen Mänttäri, M. Nyström, Drawbacks of applying nanofiltration and how to avoid them: a review, Sep. Purif. Technol. 63 2008 251–263.

[88] H. Yacubowicz and J. J. Yacubowicz 2005 'Nanofiltration: Properties and uses', Filtration & Separation, 42(7), pp. 16–21. (05)70617-0.

[89] M. A. Ernst J. Bismarck M. Springer Jekel, Zeta-potential and rejection rates of a polyethersulfone nanofiltration membrane in single salt solutions, J. Membr. Sci. 165 2000 251–259.

[90] G. R. Hagmeyer Gimbel, Modelling the salt rejection of nanofiltration membranes for ternary ion mixtures and for single salts at different pH values, Desalination 117 1998 247–256.

[91] M.S. D. R. Hall V. M. Lloyd Starov, Reverse osmosis of multicomponent electrolyte solutions. Part II. Experimental verification, J. Membr. Sci. 128 1997 39–53

[92] A.E. M. Childress Elimelech, Effect of solution chemistry on the surface charge of polymeric reverse osmosis and nanofiltration membranes, J. Membr. Sci. 119 1996 253–268

[93] M.D. G. Afonso R. Hagmeyer Gimbel, Streaming potential measurements to assess the variation of nanofiltration membranes surface charge with the concentration of salt solutions, Sep. Purif. Technol. 22–23 2001 529–541.

[94] J. C. Schaep Vandecasteele, Evaluating the charge of nanofiltration membranes, J. Membr. Sci. 188 2001 129–136

[95] Iowa State University, Membranes – Chemical Engineering Separations: A Handbook for Students. Iowa State University Pressbooks.

[96] J. Schaep, Van der B. Bruggen, S. Uytterhoeven and C. Vandecasteele, 1998. Characteristics and retention properties of a mesoporous γ-alumina nanofiltration membrane. Journal of Membrane Science, 163(2), pp.229–237

[97] Y. Boussouga A., & A. Lhassani 2017. Study of mass transfer mechanisms for reverse osmosis and nanofiltration membranes intended for desalination. Journal of Materials and Environmental Sciences, 8(4), 1266–1276.

[98] R. W. Baker, 2012. Membrane Technology and Applications. 3rd ed. Hoboken: Wiley

[99] A.I. Schäfer, A.G. T. D. Fane Waite, Nanofiltration-principles and Applications, 1st edition Elsevier Advanced Technology, Kidlington, UK, 2005

[100] D.L. L. Oatley R. Llenas Pérez, P.M. X. Williams Martínez-Lladó, M. Rovira, Review of the dielectric properties of nanofiltration membranes and verification of the single oriented layer approximation, Adv. Colloid Interface 173 2012 1–11.

[101] Y. L. Fang Q. Bian Q. Bi X. Li Wang, Evaluation of the pore size distribution of a forward osmosis membrane in three different ways, J. Membr. Sci. 454 2014 390–397.

[102] H. J. Qian S. Zheng Zhang, Preparation of microporous polyamide networks for carbon dioxide capture and nanofiltration, Polymer 54 2013 557–564

[103] T. Y. Wang J. Yang Q. Zheng S. Zhang Zhang, A novel highly permeable positively charged nanofiltration membrane based on a nanoporous hyper-crosslinked polyamide barrier layer, J. Membr. Sci. 448 2013 180–189.

[104] A.L. F. Carvalho V. Maugeri A. Silva Hernández, L. P. Palacio Pradanos, AFM analysis of the surface of nanoporous membranes: application to the nanofiltration of potassium clavulanate, J. Membr. Sci. 46 2011 3356–3369.

[105] D.J. S. A. Johnson Al B. A. MalekM. Al-N. Rashdi Hilal, Atomic force microscopy of nanofiltration membranes: effect of imaging mode and environment, J. Membr. Sci. 389 2012 486–498. A.W. Mohammad et al. / Desalination 356 2015 226–254 249

[106] N. W. J. Misdan A. F. Lau T. Ismail D. Matsuura Rana, Study on the thin film composite poly(piperazine-amide) nanofiltration membrane: Impacts of physicochemical properties of substrate on interfacial polymerization formation, Desalination 344 2014 198–205.

[107] J. A. G. Stawikowska Livingston, Assessment of atomic force microscopy for characterisation of nanofiltration membranes, J. Membr. Sci. 425–426 2013 58–70.

[108] N. García-Martín, V. F. J. Silva L. Carmona A. Palacio Hernández, P. Prádanos, Pore size analysis from retention of neutral solutes through nanofiltration membranes. The contribution of concentration–polarization, Desalination 344 2014 1–11.

[109] Y. K. Kiso T. Muroshige M. Oguchi T. Hirose T. Ohara Shintani, Pore radius estimation based on organic solute molecular shape and effects of pressure on pore radius for a reverse osmosis membrane, J. Membr. Sci. 369 2011 290–298.

[110] L. W. Jye, & A. F. Ismail 2016. Nanofiltration Membranes: Synthesis, Characterization, and Applications (1st ed.). CRC Press. https://doi.org/10.1201/9781315181479

[111] D.L. L. Oatley N. H. LlenasM. P. M. Aljohani X. Williams Martínez-Lladó, M. J. Rovira de Pablo, Investigation of the dielectric properties of nanofiltration membranes, Desalination 315 2013 100–106.

[112] J. A. G. Stawikowska Livingston, Nanoprobe imaging molecular scale pores in polymeric membranes, J. Membr. Sci. 413–414 2012 1–16.

[113] T. S. Tsuru T. Sasaki T. Kamada T. Shintani H. Ohara K. Nagasawa M. Nishida T. Kanezashi Yoshioka, Multilayered polyamide membranes by spray-assisted 2-step interfacial polymerization for increased performance of trimesoyl chloride (TMC)/m-phenylenediamine (MPD)-derived polyamide membranes, J. Membr. Sci. 446 2013 504–512.

[114] M.N. Abu M. Seman N. Khayet Hilal, Development of antifouling properties and performance of nanofiltration membranes modified by interfacial polymerisation, Desalination 273 2011 36–47.

[115] M.N.A.N.A. M. Seman N. Khayet Hilal, Nanofiltration thin-film composite polyester polyethersulfone-based membranes prepared by interfacial polymerization, J. Membr. Sci. 348 2010 109–116.

[116] Y. Y. Li Y. Su X. Dong Z. Zhao R. Jiang J. Zhang Zhao, Separation performance of thin- film composite nanofiltration membrane through interfacial polymerization using different amine monomers, Desalination 333 2014 59–65

[117] X. Y. Fan Y. Dong X. Su Y. Zhao J. Li Z. Liu Jiang, Improved performance of composite nanofiltration membranes by adding calcium chloride in aqueous phase during interfacial polymerization process, J. Membr. Sci. 452 2014 90–96

[118] C. A. Kong koushima, T. T. Kamada M. Shintani T. Kanezashi T. Yoshioka Tsuru, Enhanced performance of inorganic-polyamide nanocomposite membranes prepared by metal-alkoxide-assisted interfacial polymerization, J. Membr. Sci. 366 2011 382–388

[119] M. N. M. Zuthi A. Ngo, and H. Zhang, “A Comprehensive Review on Membrane Fouling: Types, Causes, and Control Strategies,” Water, vol. 13, no. 9, p. 1327, Apr. 2021,

[120] E.-S. Q. Kim B. Yu Deng, Plasma surface modification of nanofiltration (NF) thin-film composite (TFC) membranes to improve anti organic fouling, Appl. Surf. Sci. 257 2011 9863–9871

[121] M.G. L. C. Buonomenna M. Lopez P. Davoli R. Favia d' E. Agostino Drioli, Polymeric membranes modified via plasma for nanofiltration of aqueous solution containing organic compounds, Microporous Mesoporous Mater. 120 2009 147–153

[122] K. Kim, K. Lee, K. Cho and C. Park 2002. Surface modification of polysulfone ultrafiltration membrane by oxygen plasma treatment. Journal of Membrane Science, 199(1-2), pp.135-145.

[123] S. D. J. Mok A. Worsfold T. Fouda Matsuura, Surface modification of polyethersulfone hollow fiber membranes by γ -ray irradiation, J. Appl. Polym. Sci. 51 1994 193.

[124] M. Mulder, Basic Principle of Membrane Technology, Kluwer Academic Publishers, Dordrecht, 1996

[125] K.J. A. C. Kim C. J. FaneD. D. C. Fell Joy, Fouling mechanisms of membranes during protein ultrafiltration, J. Membr. Sci. 68 1992 79.

[126] A. V. A. Hamza T. Pham J. P. Matsuura Santerre, Development of membranes with low surface energy to reduce the fouling in ultrafiltration applications. Journal of Membrane Science, 131(1–2), 217–227.

[127] N. Hilal, Al-H. Zoubi, N. Darwish A., & A. Mohammad W. 2005. Modification of membrane surface properties using low-pressure plasma treatment. Desalination, 172(3), 279–286.

[128] M. Sadrzadeh and T. Mohammadi 2008. Sea water desalination using electrodialysis. Desalination, 221(1-3), pp.440-447.

[129] AWWA, Electrodialysis and Electrodialysis Reversal, American Water Works Association, Denver 1995

[130] S.K. P. K. Thampy W. P. Narayanan K. P. Harkare Govindan, Seawater desalination by electrodialysis. Part II: a novel approach to combat scaling in seawater desalination by electrodialysis, Desalination 69 1988 261–273.

[131] T. L. Seto R. Ehara A. Komori T. Yamaguchi Miwa, Seawater desalination by electrodialysis, Desalination 25 1978 1–7

[132] M. Turek, Dual-purpose desalination-salt production electrodialysis, Desalination 153 2003 377–381

[133]] M. T. Sadrzadeh Mohammadi, Sea water desalination using electrodialysis, Desalination 221 2008 440–447.

[134] M. Mulder, ed., Basic Principles of Membrane Technology, 2nd ed., Kluwer Academic, Dordrecht, 1997.

[135] J.M.M. Peeters, Characterization of nanofiltration membranes. PhD Thesis, Twente University, Ensehede, the Netherlands, 1997.

[136] K. Linde and Jönsson, A. 1995. Nanofiltration of salt solutions and landfill leachate. Desalination, 103(3), pp.223-232.

[137] M. G. Afonso Hagmeyer, and R. Gimbel, “On nanofiltration Desal-5 DK performances with calcium chloride–water solutions,” Separation and Purification Technology, vol. 22–23, pp. 123–132, 2001

[138] N. Hilal, Al-H. Zoubi, N. Darwish and A. Mohammad 2005. Nanofiltration of Magnesium Chloride, Sodium Carbonate, and Calcium Sulphate in Salt Solutions. Separation Science and Technology, 40(16), pp.3299-3321.

[139] B. Tansel 2012. Significance of thermodynamic and physical characteristics on permeation of ions during membrane separation: Hydrated radius, hydration free energy and viscous effects. Separation and Purification Technology, 86, pp.119-126.

[140] M.F.A. S. S. Goosen S. S. Sablani Al-R. H. Maskari Al-Belushi, and M. Wilf, Effect of feed temperature on permeate flux and mass transfer coefficient in spiral-wound reverse osmosis systems. Desalination, 144 2002: p. 367-372. 12

[141] J. B. Schaep Van der S. Bruggen R. Uytterhoeven C. Croux D. Vandecasteele E. Wilms Van Houtte, and F. Vanlerberghe, Removal of hardness from groundwater by nanofiltration. Desalination, 119(1-3) 1998: p. 295-302.

[142] X. Y. Jian G. Dai He, and G. Chen, Preparation of UF and NF poly (phthalazine ether sulfone ketone) membranes for high temperature application. J. Membr. Sci., 161(1-2) 1999: p. 185- 191.

[143] Lyman J. and Fleming R.H. 1940 Composition of sea water. Journal of marine Research, 3, 134-146

[144] R.R. R. Sharma Agrawal, and S. Chellam, Temperature effects on sieving characteristics of thin-film composite nanofiltration membranes: pore size distributions and transport parameters. J. Membr. Sci., 223 2003: p. 69-87

[145] H. Dang, W. Price and L. Nghiem 2014. The effects of feed solution temperature on pore size and trace organic contaminant rejection by the nanofiltration membrane NF270. Separation and Purification Technology, 125, pp.43-51.

[146] L. Banasiak, T. Kruttschnitt and Schäfer, A. 2007. Desalination using electrodialysis as a function of voltage and salt concentration. Desalination, 205(1-3), pp.38-46.

[147] G Saracco, Transport properties of monovalent-ion permselective membranes, Chem.Eng.Sci., 52 1997, 3019-3031.

[148] Y. Tanaka 2015. Ion Exchange Membranes: Fundamentals and Applications. Elsevier. ISBN: 978-0-444-63319-4.

[149] J. Ryu, S. Kim, H. Lee & J. Park, 2022. Development of a coupled electrodialysis–capacitive deionization (ED-CDI) system for enhanced energy efficiency in brackish water desalination. Journal of Membrane Science, 650, p.120500.

[150] Gomez-L. Montano, A. Torres, Martínez, F. & Sánchez, D., 2023. Custom-designed 3D-printed spacers for improved fluid dynamics and ion transport in electrodialysis membrane stacks. Desalination, 540, p.116430.

[151] J. Tian, X. Zhao, S. Gao, X. Wang, & R. Zhang 2021. Progress in Research and Application of Nanofiltration (NF) Technology for Brackish Water Treatment.

[152] Al-S. Amshawee, Mohd M. Yunus Y., Mohd A. Azoddein A., D. Hassell G., I. Dakhil H., & Abu H. Hasan 2020. Electrodialysis desalination for water and wastewater: A review. Chemical Engineering Journal, 380, 122231

[153] N. Nady, M. Franssen, H. Zuilhof, M. Eldin, R. Boom and Schroën, K. 2011. Modification methods for poly(arylsulfone) membranes: A mini-review focusing on surface modification. Desalination, 275(1-3), pp.1-9.

[154] Y. K. Tsujii S. Ohno A. Yamamoto T. Goto Fukuda, Structure and properties of high-density polymer brushes prepared by surface-initiated living radical polymerization, Adv. Polm. Sci. 197 2006 1–45.

[155] T. A. Vrlinic V. Vesel M. Cvelbar M. Krajnc Mozetic, Rapid surface functionalization of poly(ethersulphone) foils using a highly reactive oxygen-plasma treatment, Surf. Interface Anal. 39 2007 476–481.

[156] K.R. M. L. Kull E. R. Steen Fisher, Surface modification with nitrogen-containing plasmas to produce hydrophilic, low-fouling membranes, J. Membr. Sci. 246 2005 203–215.

[157] D.S. E. R. Wavhal Fisher, Membrane surface modification by plasma-induced polymerization of acrylamide for improved surface properties and reduced protein fouling, Langmuir 19 2003 79–85.

[158] I. G. Gancarz Poźniak, M. Bryjak, Modification of polysulfone membranes 1. CO2 Plasma treatment, Eur. Polym. J. 35 1999 1419–1428.

[159] P. Gröning, M.C. O. M. Coen Küttel, L. Schlapbach, Influence of gas pressure on the plasma polyethersulphone, Appl. Surf. Sci. 103 1996 79–89 J.

[160] D.S. E. R. Wavhal Fisher, Hydrophilic modification of polyethersulfone membranes by low temperature plasma-induced graft polymerization, J. Membr. Sci. 209 2002 255–269.

[161] H. Wolf G. Steinhauser Ellinghorst, Tailoring of ultrafiltration membranes by plasma treatment and their application for the desalination and concentration of water-soluble organic substances, J. Membr. Sci. 36 1988 207–214.

[162] L. M. L. Michelle L. Steen E. D. Hymasa N. E. Havey D. G. Capps E. R. Castner Fisher, Low temperature plasma treatment of asymmetric polysulfone membranes for permanent hydrophilic surface modification, J. Membr. Sci. 188 2001 97–114.

[163] M.L. A. C. Steen E. R. Jordan Fisher, Hydrophilic modification of polymeric membranes by low temperature H2O plasma treatment, J. Membr. Sci. 204 2002 341–357.

[164] M. Mulder, Basic Principle of Membrane Technology, Kluwer Academic Publishers, Dordrecht, 1996.

[165] W.J. H. S. Feast Munro (Ed.), Polymer Surfaces and Interfaces, Wiley, Chichester, 1987.

[166] J.N. Iaraelachvili, Intermolecular and Surface Forces, Academic Press, London, 1985.

[167] A.G. C. J. FaneD. A. Fell Suki The effect of pH and ionic environment on the ultrafiltration of protein solutions with retentive membranes J. Membr. Sci., 16 1983, p. 195

[168] H. Y. Yuet al. 2008 Surface modification of poly (propylene) microporous membrane to improve its antifouling characteristics in an SMBR: O2 plasma treatment. Plasma Process. Polym.5, 84–90.

[169] A.D. P. A. Marshall G. Munro Tragardh The effect of protein fouling in microfiltration and ultrafiltration on permeate flux, protein retention and selectivity: a literature review Desalination, 91 1993, p. 65

[170] S. Wu, Polymer Interface and Adhesion, Chapman and Hall, London, 1987.

[171] C.-M. Chan, Polymer Surface Modification and Characterization, Hanser Publishers, NY, 1993.

[172] M. I. Bryjak Gancarz Plasma treatment of polyethylene ultrafiltration membranes Die Angew. Makromol. Chem., 219 1994, p. 117

[173] J. Kim, & B. Deng 2011. Surface modification of nanofiltration membranes by oxygen plasma treatment for improved water flux and antifouling properties. Journal of Membrane Science, 378(1–2), 73–81.

[174] M. Gryta, & W. Tomczak 2021. Stability of Ar/O_2 plasma-treated polypropylene membranes applied for membrane distillation. Membranes, 11(7), 531.

[175] C. Tsai-Y., R. Juang-S., & C. Huang 2011. Surface modification of polypropylene membrane by RF methane/oxygen mixture plasma treatment. Japanese Journal of Applied Physics, 50(8), 08KA02

[176] A. Maan M., A. Alpatova, & M. Tarr A. 2020. Plasma surface modification of reverse osmosis membranes to improve fouling resistance. Water Research, 170, 115351.

[177] M. Hyder N., J. Kim, & S. Wickramasinghe R. 2019. Plasma modification of membranes for improved performance in wastewater treatment. Membranes, 9(9), 111.

[178] N. C. Saxena S. Prabhavathy S. De DasGupta, Flux enhancement by argon–oxygen plasma treatment of polyethersulfone membranes, Sep. Purif. Technol. 70 2009 160–165.

[179] H.-Y. X. Yu-C. L. He-Q. J. Liu-S. X. Gu-W. Wei, Surface modification of polypropylene microporous membrane to improve its antifouling characteristics in an SMBR: N2 plasma treatment, Water Res. 41 2007 4703–4709.

[180] H.-Y. M. Yu-X. Z. Hu-K. J. Xu-L. S. Wang-Y. Wang, Surface modification of polypropylene microporous membranes to improve their antifouling property in MBR: NH3 plasma treatment, Sep. Purif. Technol. 45 2005 8–15.

[181] E. Kim and B. Deng 2013. Effect of NH3 plasma on thin-film composite membrane: Relationship of membrane and plasma properties. Membrane Water Treatment, 4(2), pp.109-126.

[182] E. Kim, Q. Yu and B. Deng 2011. Plasma surface modification of nanofiltration (NF) thin-film composite (TFC) membranes to improve anti organic fouling. Applied Surface Science, 257(23), pp.9863-9871.

[183] G. Primc, & Mozetič, M. 2022. Hydrophobic recovery of plasma-hydrophilized polyethylene terephthalate polymers. Polymers, 14(12), 2496

[184] H. Yasuda 2005. Luminous chemical vapor deposition and interface engineering. Marcel Dekker. ISBN: 9780824757885

[185] D. S. Wavhal; E. R. Fisher2002 Hydrophilic modification of polyethersulfone membranes by low temperature plasma-induced graft polymerization. J. Membr. Sci. 2002, 209, 255–269.

[186] Castro E. F. Vidaurre, C. A. Achete, R. A. Simao and A. C. Habert 2001, “Surface modification of porous polymeric membranes by RF-plasma treatment”, Nucl. Instrum. Methods Phys. Res., Sect. B, 175-177, 732-736

[187] I. Gancarz; Po´zniak, G.; M. Bryjak Modification of polysulfone membranes: 3. Effect of nitrogen plasma. Eur. Polym. J. 2000, 36, 1563–1569

[188] D. S. Wavhal and E. R. Fisher 2003, “Membrane surface modification by plasma-induced polymerization of acrylamide for improved surface properties and reduced protein fouling”, Langmuir, 19(1), 79-85

[189] I. Karagiannis C. & P. Soldatos G. 2008 Water desalination cost literature: review and assessment. Desalination 223, 448–456.

[190] N. Wade M. 2001 Distillation plant development and cost update. Desalination 136, 3–12.

[191] R. Borsani & S. Rebagliati 2005 Fundamentals and costing of MSF desalination plants and comparison with other technologies. Desalination 182, 29–37

[192] , L., J. Guo, Y. Tang & L. Cao 2005 A historical opportunity: economic competitiveness of seawater desalination project between nuclear and fossil fuel while the world oil price over $50 per boe—part A: MSF. Desalination 183, 317–325

[193] J. Miller E. 2003 Review of water resources and desalination technologies. Sandia National Labs Unlimited Release Report SAND - 2003–0800 2003.

[194] M. Darwish, Al F. Asfour & Al-N. Najem 2003 Energy consumption in equivalent work by different desalting methods: case study for Kuwait. Desalination 152, 83–92.

[195] AlF. Marzooqi A., Al A. Ghaferi A., I. Saadat & N. Hilal Application of Capacitive Deionisation in water desalination: A review. Desalination 342, 3–15 2014

[196] Peñate, B. & García-Rodríguez, L. 2012 Current trends and future prospects in the design of seawater reverse osmosis desalination technology. Desalination 284, 1–8

[197] G. Kang-d. & Y. Cao-m. 2012 Development of antifouling reverse osmosis membranes for water treatment: a review. Water Res. 46, 584–600

[198] E. Kim and B. Deng 2013. Effect of NH3-plasma on thin-film composite membrane: Relationship of membrane and plasma properties. Membrane Water Treatment, 4(2), pp.109-126.

[199] H. Park, et al. 2007. Porous silicon membranes for desalination. Nano Letters, 7(9), 3105–3111.

[200] T. Gries, H. Xu, J. Lee-H., C. Iliescu, & S. Baek Y. 2023. Wafer-scale hierarchical porous silicon membranes via MACE and photolithography. Micromachines, 14(1), 98.

[201] B. Zhumabay, A. Nurpeisova, S. Tungatarova, B. Sarsenbayev, & D. Dosmagambetov 2023. Thermophysical properties of porous silicon synthesized by hybrid etching. arXiv preprint, arXiv:2303.07113.

[202] S. Lee Y., H. Um-J., M. Sailor J., S. Kim, & H. Jeong H. 2024. Large-scale production of porous silicon nanoparticles via adaptive cavitation ultrasonication for biomedical applications. ACS Applied Nano Materials, 7(1), 1234–1242.

[203] Dastgheib-A. Shirazi, J. Song, V. Kalra, & O'D. Carroll M. 2023. Silicon nanomembranes for water treatment: Removal of microplastics and colloidal matter. Separation and Purification Technology, 320, 124213.

[204] D. J. Papadimitriou J. Bitsakis M. Lopez-J. Villegas Samitier, and J. R. Morante, "Depth dependence of stress and porosity in porous silicon: a micro-Raman study," Thin Solid Films, vol. 349, no. 1, pp. 293–297, 1999.

[205] L. Canham 2018. Mechanical properties of porous silicon. In Handbook of Porous Silicon (pp. 309–318). Springer.

[206] R. Guider, C. Traversa, & P. Bettotti 2015. Mechanical stress relief in porous silicon free-standing membranes. Optical Society of America.

[207] Xifré-Pérez, E., Ferré-J. Borrull, Pallarés, J., & L. Marsal F. 2015. Methods, properties and applications of porous silicon. In Electrochemically Engineered Nanoporous Materials (pp. 37–63). Springer.

[208] S. Bastide, et al. 2019. 3D patterning of Si by contact etching with nanoporous metals. Frontiers in Chemistry, 7, 256.